EFFECTIVE ALLOCATION OF ELECTRIC VEHICLE CHARGING STATIONS AND POWER MANAGEMENT IN A DISTRIBUTION NETWORK

A THESIS SUBMITTED IN PARTIAL FULFILLMENT OF THE REQUIREMENTS FOR THE DEGREE OF DOCTOR OF PHILOSOPHY

DEBAPARNA SENGUPTA
MZU REGN. NO. 1800055
PH.D. REGN. NO. MZU/PH.D./1294 OF 08.08.2018

DEPARTMENT OF ELECTRICAL ENGINEERING
SCHOOL OF ENGINEERING AND TECHNOLOGY
FEBRUARY 2022

EFFECTIVE ALLOCATION OF ELECTRIC VEHICLE CHARGING STATIONS AND POWER MANAGEMENT IN A DISTRIBUTION NETWORK

BY

Debaparna Sengupta
Department of Electrical Engineering

Supervisor: Prof. Asim Datta

Submitted

In partial fulfillment of the requirements for the degree of Doctor of Philosophy in Electrical Engineering of Mizoram University, Aizawl

Department of Electrical Engineering
School of Engineering and Technology

MIZORAM UNIVERSITY

(*A Central University*)

Tanhril**,** Aizawl – 796 004, Mizoram

Dr. Asim Datta
Professor
Department of Electrical Engineering
Mizoram University
Mizoram, Aizawl, Tanhril-796004

Phones: +91-389-2330654/642(O)
FAX: +91-389-2330834

Email: mzut224@mzu.edu.in

CERTIFICATE

This is to certify that the thesis entitled **"Effective Allocation of Electric Vehicle Charging Stations and Power Management in a Distribution Network"** submitted by **Debaparna Sengupta**, Ph.D. Registration No. **MZU/Ph.D./1294 of 08.08.2018**, for the degree of **Doctor of Philosophy in Electrical Engineering**, of Mizoram University: Aizawl, India, embodies the record of original investigations carried out by her under my supervision. She has been duly registered, and the thesis presented is worthy of being considered for the award of Ph.D. degree. This research work has not been submitted for any degree of any other university.

Prof. Asim Datta

Professor
Dept. of Electrical Engineering
MIZORAM UNIVERSITY, AIZAWL

Date: 16th February, 2022

(Supervisor)

DECLARATION

MIZORAM UNIVERSITY

February 2022

I, **Debaparna Sengupta,** hereby declare that the subject matter of this thesis is the record of work done by me, that the contents of this thesis did not form basis of the award of any previous degree to me or to the best of my knowledge to anybody else, and that the thesis has not been submitted by me for any research degree in any other University/Institute.

This is being submitted to the Mizoram University for the degree of ***Doctor of Philosophy*** in Electrical Engineering.

Date: 16th February, 2022

(Candidate)

Prof. Asim Datta

(Supervisor)

(Head)

Acknowledgement

First and foremost, I would like to express my gratitude to my supervisor, **Dr. Asim Datta**, Associate Professor, Department of Electrical Engineering, school of science, for his support and deep insights. His colossal support, endless ideas and high spirits encouraged me during the entire period of the study. I am very grateful to him for introducing me to the recent industry trends in electrical engineering and steering me towards the right direction until this thesis was completed.

I would like to express my gratitude to the other faculty members of the department, **Dr. Amarendra Matsa, Dr. Subir Datta**, **Dr. Sadhan Gope**, **Dr. Subhasish Deb** and **Dr. Dileep G.** for their positive criticism and valuable suggestions, which directed me into the right direction. I would like to express my gratitude to our Dean sir **Prof. Dr. L. Lolit Kumar Singh**, **Dr. N. P. Maity** and **Dr. Reshmi Maity** of Electronics and Communication Engineering Department, for their constant help, support and kind co-operation at the time of coursework completion.

I would like to thank my brother, **Mr. Rishiraj Sarker**, an Ex-research fellow of the Electrical Engineering Department, MZU for always suggesting and motivating me in the field of research. I would like to take the opportunity to thank my fellow mates and juniors, who helped me in various ways.

I would like to thank all faculty members as well as non-teaching staffs of the Department of Electrical Engineering for helping me whenever required.

As a final thought, I am lucky to have a wonderful family having very supportive children, **Anushka** and **Prantik**. I can never give enough thanks to my parents, without whom, I could not reach to this position. Credit goes to my maternal uncles and aunts for constantly motivating me during the entire duration of work. It is their love, affection, endless support, and encouragement, that made this work possible.

I like to convey my earnest gratitude to all for motivating me to work hard with dedication, patience and keep the right attitude for lifelong learning.

Most importantly, I would like to thank **Almighty God** for giving me good health, strength, and support to be able to complete my research work.

Date: 16th February, 2022

(**DEBAPARNA SENGUPTA**)
Department of Electrical Engineering
Mizoram University
Aizawl, Mizoram

Dedication

To my parents and children

CONTENTS

LIST OF FIGURES

LIST OF TABLES

ABBREVIATIONS

BFSM	Backward forward sweep method
BOL	Beginning of life
BPSO	Binary PSO
CVD	Cumulative voltage deviation
DE	Differential evolution
DEMATEL	Decision-making trial and evaluation laboratory
DG	Distributed generation
DOD	Depth of discharge
DSO	Distribution system operator
EDF	Earliest deadline first
ER	Evidential reasoning
ESU	Energy storage unit
EV	Electric vehicle
EVCS	Electric vehicle charging station
EVCS2G	EVCS to grid
FAME	Faster adoption and manufacturing of (hybrid and) electric vehicle
GA	Genetic algorithm
GIS	Geographic information system
G2V	Grid to vehicle
HHO	Harris' hawk's optimization
IEEE	Institute of electrical and electronics engineers
IES	Integrated energy system
IGBT	Insulated gate bipolar junction transistor
INBPSO	Improved new binary particle swarm optimization
LSI	Loss sensitivity index
MAS	Multi-agent system
MATLAB	Matrix Laboratory

MPC	Model predictive control
MPP	Maximum power point
PEV	Plug-in-electric-vehicle
PHEV	Plug-in-hybrid-electric-vehicle
PID	Proportional-integral-derivative
PLL	Phase locked loop
PPSO	Powell particle swarm optimization
PSO	Particle swarm optimization
PV	Photovoltaic
RE-EVCS	Renewable energy based EVCS
RER	Renewable energy resource
RMS	Root-mean-square
RS	Rank selection
RWS	Roulette wheel selection
SOC	State of charge
SPV-EVCS	Solar PV powered EVCS
STC	Standard test conditions
SUS	Stochastic universal sampling
SVC	Static VAR compensator
SVPWM	Space vector pulse width modulation
UL-MULTIMOORA	Uncertain linguistic multi-objective optimization by ratio analysis plus full multiplicative form
VSI	Voltage sensitivity index
V2G	Vehicle to grid
V2V	Vehicle to vehicle

CHAPTER -1

GENERAL INTRODUCTION

1. GENERAL INTRODUCTION

1.1 Background of the Research

The swelling electricity demand all over the world along with decaying reserve of conventional energy resources has compelled the researchers for exploring new innovative technologies to extract electrical energy from different renewable energy resources (RERs) available abundantly in nature [Mohtasham, 2015]. Consequently, renewable energy based distributed generations (DGs) and micro grids are being developed as the option to come out from the future energy crisis [Alonso et al., 2012; Al-Shetwi et al., 2020]. Power transmission and distribution systems are being unified with renewable energy-based generations to meet the increased electricity demand due to urbanization and modernization and, to create a provision for replacement of the conventional energy driven generating stations [Khatod et al., 2012]. On the other hand, transportation sector has started embracing renewable energy due to causes such as excessive price hike of conventional fuels, detrimental environmental effects, etc. [Amin et al., 2020; Gielen et al., 2019]. Many developed countries like USA, Germany, Japan, etc., have already travelled a long journey in the direction of plug-in-electric-vehicles (PEVs) and plug-in-hybrid-electric-vehicles (PHEVs) to shift from the conventional internal combustion engine-based vehicles [Wirasingha et al., 2008; Ahmad et al., 2018]. In developing countries like India, the progress in the electric vehicle (EV) is being accelerated [Vidhi and Shrivastava, 2018; Goel et al., 2021]. Therefore, production of energy efficient EVs is the key area of investigation now-a-days. The EVs are being recommended by the governments of all countries. Down the line, the top-class car producing companies worldwide have moved forward to embrace it ambitiously [Xu et al., 2015; Du et al., 2017]. Many leading car manufacturing companies like Mahindra, Hyundai, etc., have already launched their EVs in Indian market. Indian government has been trying to promote EVs by providing subsidies to buyers through various promotional schemes. The Faster Adoption and Manufacturing of (Hybrid and) Electric Vehicle

(FAME) scheme has been introduced by the Indian government in the year 2019 for increasing the sales of EVs. The first phase of this scheme will be ended up by 2022 In order to achieve major paradigm shift in transportation sector, the development of EV charging stations (EVCSs) [Mishra et al., 2021] and their integration with the existing power distribution system in a skillful manner are quite important. In the line, EVCS integration with the distribution network is a thought-provoking task as optimal EVCS location identification is essential for ensuring quality and consistent power output without hampering the existing network operations [Lam et al., 2014]. Literature survey reveals that much research has been accomplished in the sphere of optimal size and location allocation of EVCSs. Numerous optimization techniques like differential evolution algorithm, delphi and hybrid multi-criteria decision-making approach, game theoretical approach, particle swarm optimization, genetic algorithm, etc., have already been utilized for the purpose. But, in most of the previous studies, EVCSs have been taken as simple load points considering unidirectional power flow from the network to EVCSs. This is the first drawback identified from the literature survey. However, bi-directional mode of operation of the renewable energy based EVCSs (RE-EVCSs) can bring a new revolution in the domain of distribution network connected EVCS system in near future. Bi-directional RE-EVCSs with the grid can be beneficial for both the RE-EVCS, and the power network as it would keep a backup option for the RE-EVCSs to draw power from distribution system under low generation from RERs and could deliver surplus power to the power distribution network to meet the peak load demand. Thus, the need of installing large battery backup systems or peak load generating stations can be eliminated. This kind of bi-directional energy flow scheme has not been considered seriously in most of the reported studies. Among different kinds of renewable energy resources, solar energy [Srivastava and Srivastava, 2013] is abundantly available in tropical countries like India. Therefore, the design and installation of solar photovoltaic (PV) powered EVCSs (SPV-EVCSs) is very prospective in Indian scenario [Fathabadi, 2017; Ji et al., 2020]. Much research has been performed to find-out the optimum location as well as size of EVCSs. But sometimes it is not practically feasible or beneficial to install EVCSs of the optimum

sizes at the optimum locations as per the simulation results due to involvement of several socio-economic factors like geographical constraints, required charging capacity, etc. This is the second drawback. This problem can be solved by selecting the required sizes of the EVCSs at first considering the associated socio-economic factors and then proceeding for optimum allocation of EVCSs for better power management in the integrated system. The third drawback to be pointed out from the survey is, in most of the previous studies, the total number of EVCSs to be optimally allocated and integrated with the distribution network/grid was fixed beforehand with/without their size optimization. The identification of optimum number of EVCSs of stipulated sizes, along with their optimum locations has not been practiced. The fourth and last shortfall to be noticed is that, in most of the earlier research, voltage and loss sensitivity analyses have not been performed, though it is very important for confirming the stability of the power integrated system. Hence, to address the afore-mentioned shortcomings of the existing practices in the field of EVCS integrated distribution network, a profound optimization technique collaborated with dynamic power flow analysis need to be applied and, also, the stability analyses need to be performed.

After the optimum allocation of the EVCSs, power flow management of the RE-EVCS integrated system is another crucial area to be focused. The bi-directional power transfer, i.e., grid to vehicle (G2V) and EVCS to grid (EVCS2G) are bringing a new revolution in the field of grid-integration of EVCSs [Rodrigues et al., 2018]. Recently, vehicle to vehicle (V2V) energy transfer technique [Sousa et al., 2018] and battery swapping technique [Xu et al., 2015] at charging stations are being proposed for efficient energy management and reliable operation of EVs. With the integration of EVCSs into the power network, an important aspect is the development of an efficient power flow management technique to take care of the operation and power flow control in the integrated system.

1.2 Scope of Study

From the background study, it is observed that the scope of EV charging infrastructure development is widespread. A lot of exploration can be done in the domain of EVCS design, installation, and their optimum integration with the power distribution network. Installation of bi-directional RE-EVCS integrated network, and the design of smart and cost-effective power management system is very demanding to enhance the utilization of EVs. Very less research was conducted in the province of optimum allocation of bi-directional RE-EVCS considering their effective integration with the distribution system for achieving better power management in terms of voltage profile improvement and/or line loss minimization. Thus, in this proposed research, optimum allocation of bi-directional RE-EVCS for network voltage profile improvement with/without line loss minimization is chosen as the province of study. Additionally, the integration of multiple EVCSs with the distribution network is investigated in MATLAB/Simulink environment concerning the power flow management and voltage profile improvement.

The proposed work has been accomplished in two phases. During the first phase, optimum allocation of the different EVCSs has been carried out considering unidirectional/bidirectional mode of operation. Four case studies are conducted using different optimization techniques collaborated with efficient power flow analysis algorithms. In *Case Study 1*, the particle swarm optimization (PSO) technique is adopted in compliance with an efficient dynamic power flow analysis method for optimal allocation of optimum number of EVCSs to maintain the voltage profile of a distribution network. The EVCSs are with the specified identical capacities. The IEEE 15-bus system is taken as a test bed system for the study. The optimum results obtained from the case study are substantiated with the voltage sensitivity analysis. A comparison of the system voltage profiles with EVCS and without EVCS is presented to show the effectiveness of the optimal allocation of EVCSs. In *Case Study 2*, optimal allocation of bi-directional SPV-EVCSs is carried out in an efficient manner by using backward forward sweep method (BFSM) collaborated powell's particle swarm optimization (PPSO) technique. Firstly, voltage sensitivity analysis is

performed to find out the strong and weak nodes of the test network in terms of power injection. Afterwards, the proposed BFSM collaborated PPSO method is applied for optimum location and number identification of the identical capacity SPV-EVCSs in power injection mode (injecting power into the distribution network). The IEEE 69-bus test system is chosen as the test bed to validate and exemplify the usefulness of the proposed methodology. Thereafter, the effect of such integration on the network profile in load point mode (taking power from the distribution network) of operation is observed. A comparison of the system voltage profiles with EVCS and without EVCS is presented to show the effectiveness of the optimal allocation of EVCSs. It has been assumed that SPV-EVCSs are situated nearby the industrial belt and the local PV generations are coupled with the SPV-EVCSs. During the peak loading hours, SPV-EVCSs are streaming the collected surplus electrical energy directly into the distribution network thus avoiding the need of costly energy storage systems (ESUs). During the adverse weather condition, the SPV-EVCSs are capable for drawing power from the distribution network instead of receiving from the ESUs. *Case Study 3* presents an improved new binary particle swarm optimization (INBPSO) approach in conjunction with dynamic power flow analysis for optimal allotment of bi-directional RE-EVCSs in a distribution network. For optimization, the power injection mode of the EVCSs is considered to minimize the line power losses and voltage deviations. Finally, the maximum number and acceptable capacities of such EVCSs along with their optimum locations are decided utilizing maximum EVCS penetration level. Thereafter, the consequence of EVCS integration on the system performance is studied considering the EVCSs working in load point mode. A comparison of the network voltage profiles under different modes of operation is carried out to investigate their effects on the network. Simulation study is carried out on the IEEE 15-bus test system. Voltage and loss sensitivity analyses of network nodes are accomplished to cross-check the acceptability of the optimum locations obtained by the computation approach. *Case Study 4* is conducted taking fixed number of identical EVCSs of optimum capacities integrated into the distribution network in power injection mode. The optimum allocation of these

EVCSs has been carried out by genetic algorithm (GA) optimization technique collaborated with BFSM algorithm.

During the second phase of the proposed work, a MATLAB/Simulink model of a multiple SPV-EVCS integrated distribution network is developed to investigate power flow. The voltages, currents, active and reactive powers at different points of the SPV-EVCS integrated system are observed as a power management study. A comparison of the voltage profiles of EVCS unintegrated and integrated systems is performed to verify the effectiveness of the integration.

While carrying out mentioned studies, few assumptions may be followed. These are: a) EVs are charged at night-time at their allotted residential parking areas. b) the night-time tariff is comparatively less than daytime. c) the RE-EVCSs situated nearby the industrial area can deliver the surplus amount of power into the distribution network at peak loading hours.

1.3 Literature Survey

Keeping the recent nonrenewable energy scarcity, their price inflation and ecological problems like global warming, air quality degradation, etc. in mind, both the power industries and conveyance sector are putting massive effort for augmented exploitation of naturally available RERs. Most of the countries are gradually ratifying renewable energy-powered distributed electricity production and its amalgamation with the existing power distribution networks. Extensive research was accomplished in this field, and the research is still going on to invent more efficient energy extraction techniques and more effective optimization techniques for optimum allocation of RER powered distributed generators with the grid. Alonso et al., (2012) presented an evolutionary optimization technique for RER integration with the smart grid. Al-Shetwi et al., (2020) discussed the difficulties encountered during RER integration with the grid and presented the integration necessities and control approaches used for effectual integration in interconnected system. Muñoz-Aguilar et al., (2017) presented the downsides of harmonic resonance developed in the long distribution lines and technique of eradicating these drawbacks by

renewable energy integration (wind energy driven alternators). Cowell et al., (2011) highlighted the gradual increase in wind -energy powered generations which are swiftly growing worldwide. Keskin and Soykan, (2017) showed the technique of lessening the peak power ingestion of the grid by assimilating PV powered generation with the distribution network. The solar PV energy is the apparent choice in renewable energy applications for its prevalent availability and reduced installation cost [Strzalka et al., 2012]. Following the tracks of power generation and distribution industries; there is a corresponding archetype shift from traditional internal combustion-based vehicles to EVs in the transportation sector [Xu et al., 2015; Du et al., 2017]. With the upsurge in the number of EVs, there is an equivalent compulsion to facilitate the EV charging requirements. In this standpoint, a massive infrastructure development is obligatory for the installation of EVCSs at large scale. Yao et al., (2014); Wang et al., (2017) and Mehrjerdi, (2020) projected several planning of grid integrated EVCSs. Gong et al., (2019) emphasized the importance of optimal allocation of EVCSs in the power distribution network by establishing the fact that unplanned integration can cause severe problems to the network like voltage sags, swells, increased line losses, etc. During the literature survey, two important objectives in optimum EVCS allocation-based research were noticed. One objective was to minimize line losses and to improve voltage profile in conjunction with retention of voltage stability. Another objective was focused on optimum EVCS allocation concerning socio-economic factors like optimizing the charging time, EV travel time to EVCS, owners' profit, etc. Very few researches were found which considered the aforesaid two objectives together. Lam et al., (2014) utilized greedy algorithm along with three other optimization techniques for capitalizing the availability of EVCS to the EV owners. Moghaddam et al., (2017) presented an ant colony optimization technique for finding the optimum EVCS location concerning the charging time and cost. The EVCSs may be equipped with numerous charging options, like AC level 2 charging, DC fast charging, and battery exchange amenities. Xiong et al., (2017) proposed optimal assignment of fast charging facility EVCSs with the charging price minimization using game theoretical approach. Faddel et al., (2018) introduced a multi-objective bilayer pareto search optimization procedure for

maximizing EV parking garage turnover and minimizing voltage fluctuation as well as line losses. Jiang et al., (2018) utilized a multi-agent system (MAS) simulation background in alliance with evidential reasoning (ER) technique for minimization of the charging cost, charging waiting time and the travel time to reach EVCS. Gong et al., (2019) accomplished optimal allocation of EVCSs for charging level enhancement and total charging distance minimization. Liu et al., (2012) explored an adaptive PSO technique for finding the optimum size and location of EVCSs while minimizing the set up and running costs. Sadeghi-Barzani et al., (2014) developed a geographic information system (GIS) based GA optimization technique to minimize EVCS installation cost and system losses. Zhao and Li, (2016) developed a fuzzy delphi technique combined with hybrid multi-criteria decision-making method to optimally allocate EVCSs considering several economic, societal, environmental, and technical constraints. Mozafar et al., (2017) employed a GA based PSO technique for optimal size and location identification of EVCSs and, also, described a compatible optimum vehicle charging procedure for minimizing voltage fluctuations, active power loss, and vehicle's battery expenses. Liu et al., (2018) manifested a gray decision-making trial and evaluation laboratory (DEMATEL) coordinated with the uncertain linguistic multi-objective optimization by ratio analysis plus full multiplicative form (UL-MULTIMOORA) for optimum EVCS allocation minimizing EVCS installation and maintenance costs. Ponnam and Swarnasri, (2020) developed a teaching learning-based algorithm for optimum allocation of EVCSs to minimize the node voltage errors along with line losses. Yao et al., (2014) developed a multi-objective collaborative planning for optimum EVCS allocation in a radial distribution system for voltage deviation, system loss and establishment cost minimization, considering service radius and environmental factors. Pal et al., (2021) proposed optimum EVCS allocation for voltage profile improvement along with grid energy loss and EVCS establishment cost minimization by means of differential evolution (DE) and Harris' hawk's optimization (HHO) methods. Moradi et al., (2015) proposed DE algorithm based optimum size and site allocation of RER powered EVCSs for enhanced voltage stability, reduced power loss and EV charging cost. Yazdi et al., (2019) presented the optimum allocation of

static number and sizes of EVCSs to maximize the monthly profit by using mixed integer linear model.

The expansion of generation and energy storage facilities is a great concern of power industries to accommodate voluminous EVCSs [Mehrjerdi, 2020]. The generation expansion may be unified with the vast energy storage systems, but can be inhibited by numerous aspects like incorporation of sporadic natured renewable energy, rating of prevailing transmission/distribution lines, venture cost, long-term forecasting, etc. The installation of SPV-EVCSs has become one of the significant zones of emphasis in power industry. The SPV-EVCSs can be nearly self-sustainable in view of energy availability [Mohtasham, 2015]. The problem arises due to irregular nature in power generation from SPV. There should be a battery back-up system to facilitate the SPV-EVCSs. But building a vast energy storage is a costly affair along with periodic maintenance. Faisal et al., (2018) discussed the problems associated with energy storage units. Zhang et al., (2018) and Ren et al., (2015) discoursed the diverse issues related to energy storage systems. The interconnection of SPV-EVCSs with the power grid is a viable option to guarantee power output in adverse weather conditions also [Luo et al., 2020]. The development of SPV-EVCSs in diverse forms and dimensions is being modernized in distribution network planning [Gong et al., 2019]. A GIS based technique for the location analysis and evaluation of the SPV-EVCSs was presented. Various research works for optimum site selection have considered several usual, financial, methodological, and communal criteria. Two-fold sensitivity study and relative scrutiny were accomplished to verify the stability and trustworthiness of a system [Zhou et al. 2020].

SPV-EVCS amalgamation with the power distribution system can deliver profit to EVCS owners as well as power utility companies [Ji et al., 2020]. Grid integrated SP-EVCSs can be used in bi-directional mode, i.e., power injection and load point, and can be utilized significantly for voltage profile enhancement and power loss minimization of distribution networks [Luo et al., 2020]. The effects of bi-operational SPV-EVCS placement on peak power shaving, voltage profile

improvement and spinning reserve, etc. were studied thoroughly by linearized distflow equations along with second order conic relaxation technique [Luo et al., 2020]. Despite the paybacks offered by SPV-EVCSs, several technical glitches may ascend due to inappropriate placement of them in an existing distribution system [Luo et al., 2020]. To exploit profits from SPV-EVCSs while retaining the stability of the distribution grid, the optimum allocation of SPV-EVCSs is crucial [Pal et al., 2021].

Literature review reveals that though a considerable amount of work was accomplished in the province of EVCS and RE-EVCS allocation in view of voltage profile retention and minimization of line losses, one of the major shortfalls identified is the absence of bi-directional energy transfer mechanism. Most of the previous researches considered the EVCSs as simple load points and very less work was carried out in the province of bi-directional power transfer while tackling the power quality and voltage profile improvement concerns. The second drawback is found in the optimum size and site allocation-based studies, where the optimum sizes and sites obtained from the optimization results are not always feasible to be materialized due to several socio-economic factors. The third drawback noticed is the number of EVCSs to be allocated optimally was assumed constant. Firstly, study with the gradually augmented numbers of EVCSs that a distribution network can accommodate, and thereafter the optimum allocation of the selected number of EVCSs for better power management had not yet been exploited systematically. The last general deficit of these earlier researches identified is the absence of voltage and loss sensitivity analyses which are essential to verify the appropriateness of the nodes for power injection/absorption to hold the system stability.

To perform the optimum integration of RE-EVCSs in power injection mode, a comprehensive literature review in the field of optimum DG allocation with/without their size optimization was accomplished. The effect of renewable energy entrenched generation on the performance of a power distribution network was studied [Motyka et al., 2018]. There may be a good or bad effect of this integration on the distribution network. Thus, thoughtful integration is obligatory for

sustaining the standard power quality throughout. The economic influences of different capacities on self-sufficient PV and wind energy unified hybrid energy constructions were studied in Celik, 2003. Zhou et al., (2010) presented an investigation regarding the optimum sizing of stand-alone solar and wind power-based hybrid DGs. Georgilakis and Hatziargyriou, (2013) presented a widespread review on diverse optimal DG sizing and allocation models. Viral and Khatod, (2012) accomplished an extensive review on optimal planning of DG integrated system. Kaabeche et al., (2011) developed an optimization algorithm for integrated PV/wind energy driven systems to optimize the power flow and different economic factors. A multi-objective DG planning and optimization was attained by impact indices and trade-off method [Singh and Goswami, 2011]. Optimum sizing of hybrid PV/wind-based generation units utilizing different techniques were presented [Diaf et al., 2007; Yang et al. 2007]. Different optimization techniques for optimum allocation of DGs with/without their size optimization were discoursed [Abri et al., 2012; Khatod, et al., 2012; Sanjay et al., 2017]. Savić and Đurišić, (2014) presented a GA-based optimization method for optimum size and allocation identification of static VAR compensator (SVC) devices in dispersed wind and PV generator integrated network. Sudabattula and Kowsalya, (2016) exploited bat algorithm optimization method to optimally place the solar PV powered DGs in the distribution network for minimizing the network active power loss. The optimum site and size allocation of several micro gas turbine driven DGs was accomplished for minimization of power loss of the distribution system [Ghanbari et al., 2017]. El-Fergany, (2015) presented a backtracking search optimization technique based optimal allocation of multi-class DGs. Su, et al., (2011) proposed wind powered DG placement by utilizing binary particle swarm optimization (BPSO) technique to maintain voltage profile.

For the power management study, an extensive literature survey in the domain of power management in grid integrated EVCSs was accomplished. Wang et al., (2020) projected an optimum dispersed energy transaction strategy for an integrated energy system (IES) developed for delivering power into the grid connected EVCSs. IES has been considered as separate entity to deliver power to

EVCSs at a lower cost than the grid. The unidirectional i.e., load point mode of operation of the EVCSs was presumed in the study. Goli and Shireen, (2014) proposed a PV powered grid-integrated smart charging station with ESU backup. The charging controller of the EVCS efficiently controlled the power injection at peak loading hours to retain the grid in a healthy condition. The bidirectional mode operation of EVCS was considered. The drawbacks of the scheme are a) The control strategy was designed by taking only one EV into consideration. b) V2G/V2V functionalities are not included. Sortomme and El-Sharkawi, (2010) proposed an aggregator-based V2G energy supply mechanism to deliver energy into the grid for aggregator revenue maximization while reducing system load effects and consumer costs. The result was validated hypothetically with 10,000 customer EVs in the system entity. Only power injection node was considered, but the EV charging mode was not considered. Di Giorgio et al., (2014) presented a bi-directional (i.e., G2V and V2G) operation of EVs controlled by an incident motivated model predictive control (MPC) strategy. The strategy was implemented with mixed integer linear programming for minimizing energy ingestion cost while facilitating EV drivers' proclivities. Nguyen and Song, (2012) considered a bi-directional mode of EVCS operation. A smart charging and discharging technique for numerous PHEVs situated in a building's garage was developed to compensate the peak load demand of the building. Both centralized and decentralized controllers have been developed. Karfopoulos and Hatziargyriou, (2012) proposed a disseminated, multi-agent EV charging regulator mechanism based on the nash inevitability likeness principle for an urban distribution network to maintain the network profile. He et al., (2018) presented a smart charging/discharging scheme for multiple smart electrical car parking zones networked together facilitating G2V, V2G and V2V operations to improve the grid power quality. Different control schemes for generation cost or overall system cost minimization such as simulated annealing [Valentine et al., 2011]; multi period optimal power flow algorithm [Vayá and Andersson, 2012]; bender’s decomposition along with fuzzy control [Zakariazadeh et al., 2014]; maximum sensitivities selection technique [Deilami et al., 2011] and price signal scheme [Zhang et al., 2018] were proposed. Moreover, several strategies focusing the

grid voltage stabilization using techniques like artificial immune system [Oliveira et al., 2013]; fuzzy logic [Singh et al., 2013] and gradient based optimization method [Wu et al.,2011] were presented.

Different control techniques for optimum utilization of electric power with the minimization of electric power loss viz. EV aggregator and distribution system operator (DSO) [Soares et al., 2014]; maximum sensitivities selection [Deilami et al., 2011]; monte-carlo simulation method followed by forward backward sweep method [Sortomme et al., 2010]; open-source linear optimization model [Fattori et al., 2014]; self-developed real time control algorithms along with linear programming [Van Der Kam and van Sark, 2015]; fuzzy logic control [Berthold et al.,2015] and adaptive proportional-integral-derivative (PID) control [Mumtaz et al., 2017] were explored. Jian et al., (2014); Kang et al., (2013) and Tan and Wang, (2015) presented various control strategies like double layer optimal charging technique, earliest deadline first (EDF) and double layer game theory for load variance minimization, load leveling by valley filling and off-peak charging, respectively. Vagropoulos et al., (2015) proposed a smart EV charging technique keeping prime focus on less battery degradation. García-Villalobos et al., (2014) carried out an extensive survey where different types of charging schemes as well as multiple charging facilities have been discussed elaborately. Gupta et al., (2020) proposed a cooperative multi aggregator-based EV charge scheduling algorithm for a PV- assisted EVCS under inconsistent solar profiles in view of charging station's profit maximization. From the extensive literature survey, it can be inferred that many research works were conducted in the domain of PV- assisted EVCS considering unidirectional/bidirectional power flow using different centralized and decentralized control algorithms. But very few research works have been noticed in bidirectional mode of operation taking EV charging benefits as well as grid profile enhancement into consideration. Figure 1 presents a pictorial representation of the literature survey.

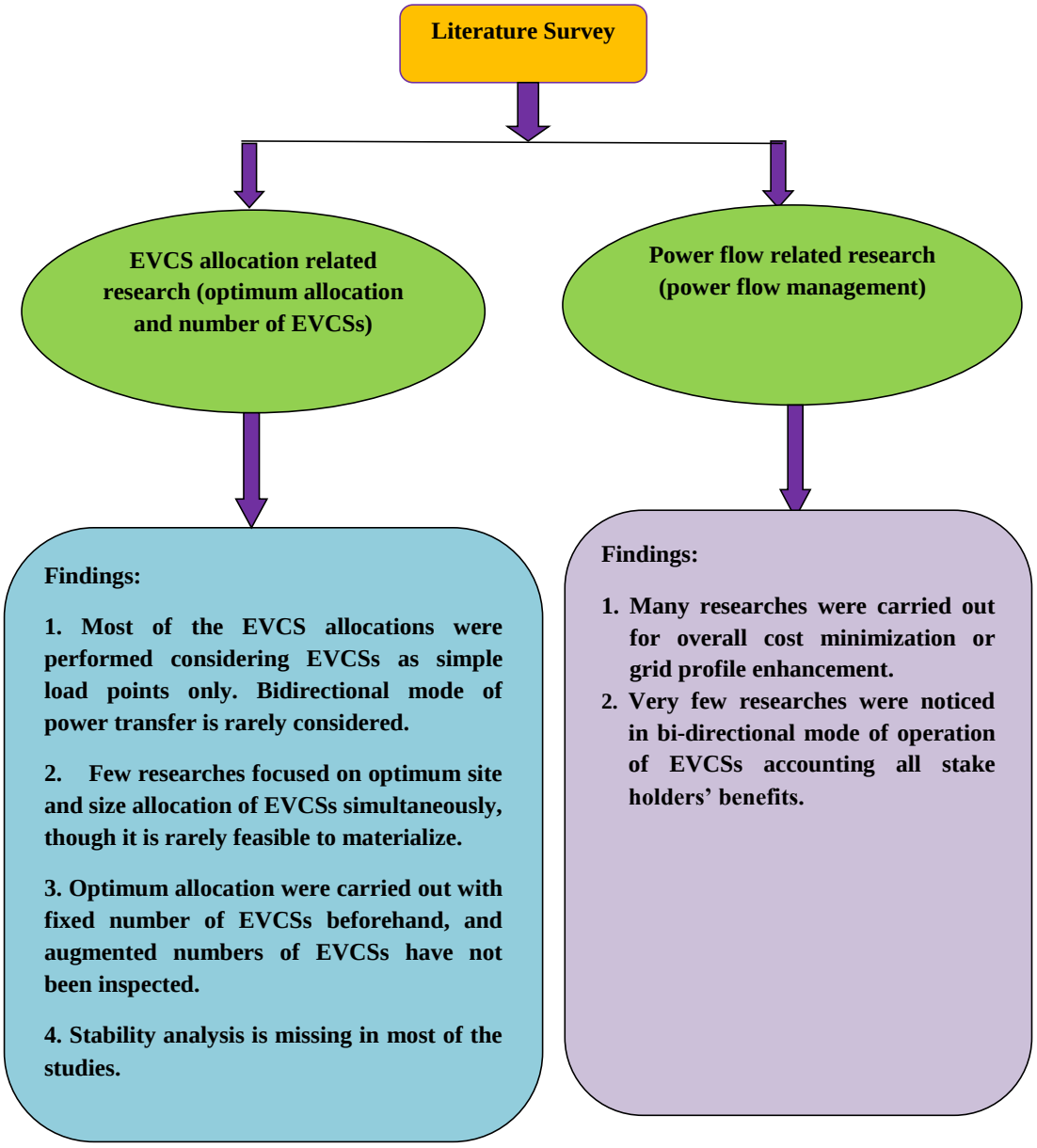

Figure 1. Pictorial representation of the literature survey

1.4 Phases of the Research Work

The total research work is accomplished in two phases:

Phase 1: Optimum allocation of EVCSs in power distribution network for better power interaction and maintaining system stability.
Phase 2: Power flow management of a multiple SPV-EVCS integrated distribution network and study on voltage profiles.

1.5 Thesis Organization

The thesis consists of five chapters including the conclusion and future scope. The **Chapter 1** discusses the background of the research, scope of study, literature survey and phases of the work. **Chapter 2** presents the problem formulation required for performing optimization in finding the appropriate EVCS locations with/without their optimum numbers in different case studies. Objective function, decision variables, different optimization constraints and their boundaries are presented in detail. **Chapter 3** elaborately presents all mathematical and computational models used for multiple EVCS location optimization with/without their number optimization. Also, the model of power management of the multiple SPV-EVCS integrated network is developed. Different power flow analysis and optimization techniques used are explained in detail. MATLAB/Simulink model of multiple SPV-EVCSs, integrated with the distribution system is presented. **Chapter 4** presents system validation with results. Different case studies on optimum allocation of EVCSs considering unidirectional/bidirectional power flow of EVCSs are carried-out and their results are presented. Simulation results on power flow management are also presented. **Chapter 5** presents the conclusion and future scope conceivable in this paradigm.

CHAPTER -2

PROBLEM FORMULATION

2. PROBLEM FORMULATION

2.1 Introduction

Effective allocation of EVCSs in power distribution network can be considered as an optimization problem. For implementing an optimization technique, objective function formation is essential. Another important factor is to take care of all the constraints and system parameters, so that they persist within the prescribed boundaries. The objective functions used in different case studies along with different associated parameters and boundaries have been discussed in this chapter in detail.

2.2 Objective Function

The amalgamation of numerous EVCSs with a distribution network can give unwanted voltage deviations as well as upsurge of line losses. Consequently, optimum capacity, number, and location identification of such EVCSs are indispensable to preserve the voltage deviation and line losses within the standard boundary. During the first phase of the proposed work, effective allocation of EVCSs is accomplished using different optimization techniques. The first phase work is accomplished with four case studies. In *Case Studies* 1 and 2, concentration have been given only on the network voltage profile improvement, whereas in *Case Studies* 3 and 4, concentration is given on both the voltage profile improvement as well as line loss minimization. Two separate objective functions are constructed and utilized in these case studies. For the first fragment of phase one study, the first objective function is formulated to minimize the highest voltage upsurge and drip with respect to the reference voltage.

The first objective function is defined as:

$$Minimize\ E_{devihighest} = Minimize|\{(V_{ref} - V_1), \dots, (V_{ref} - V_n), \dots, (V_{ref} - V_{N_B})\}| \quad (1)$$

where, N_B signifies the total number of network nodes. V_n is the n^{th} node voltage. $1 \leq n \leq N_B$

Two different power flow analysis methods are utilized in the case studies. The first objective function is utilized in power flow algorithms in two different forms. For an efficient power flow algorithm, the objective function in equation (1) is transformed as:

$$Minimize\ E_{devihighest}$$

$$= Minimize|\{(V_{ref} - V[F_N(i,1)]),\ (V_{ref} - V[F_N(i,j+1)])\}|$$

$$= Minimize\{\ (|V_{ref}| - |V[F_N(i,1)]|), \left(|V_{ref}| - \left\{|V[F_N(i,j)]| - \frac{\sqrt{(P_S[F_B(i,\ j)])^2 + (Q_S[F_B(i,\ j)])^2}}{|V[F_N(i,j)]|} . |Z[F_B(i,j)]|\right\}\right)\} \quad (2)$$

where, $i = 1, \ldots, T_N$ and $j = 1, \ldots, N(i) - 1$

- $E_{devihighest}$ is the array for holding the maximum voltage (over and under voltage) errors.
- V_{ref} represents the reference bus voltage; the value of which is reserved as $(1 + \hat{j}.0)$ pu.
- $V[F_N(1,1)]$ $(= 1 + \hat{j}.0$ pu) represents first node voltage of the main feeder, which is considered as the reference node.
- $V[F_N(i,1)]$ denotes the first node voltage of the i^{th} path.
- i^{th} path represents any path associated with main feeder, laterals, and sub-laterals.
- $|V[F_N(i,j+1)]|$ $(= |V[F_N(i,j)]| - \frac{\sqrt{(P_S[F_B(i,\ j)])^2 + (Q_S[F_B(i,\ j)])^2}}{|V[F_N(i,j)]|} . |Z[F_B(i,j)]|)$ denotes the $(j + 1)^{th}$ node voltage of the i^{th} path.
- $V[F_N(i,j)]$ is the j^{th} node voltage of the i^{th} path.
- $Z[F_B(i,j)]$ represents the j^{th} branch impedance of the i^{th} path.
- $P_S[F_B(i,j)]$ and $Q_S[F_B(i,j)]$ are the active and reactive power flows of the $[F_B(i,j)]$ branch.

For another dynamic power flow algorithm named BFSM, the first objective function transforms into:

$$Minimize\ E_{devihighest} = Minimize|\left\{\left(V_{ref}\ - V_1\right), (V_{ref} - \left\{V_m - z_{mn}.\left[\left\{\frac{(P_n + \hat{\jmath}.Q_n)}{\widehat{V_n}}\right\}^* + \sum_{r=r_1}^{r_k} I_{nr}\right]\right\})\right\}| \quad (3)$$

where, $1 \leq m \leq (N_B - 1)$ and $2 \leq n \leq N_B$. m and n denote the preceding and succeeding nodes, respectively.

- $\mathbf{V_{ref}}$ is the reference voltage.
- $\boldsymbol{V_1}$ is the voltage of the first node. Here the first node is taken as the reference node and its value is considered as $(\mathbf{1} + \hat{\boldsymbol{\jmath}}.\mathbf{0})$ pu.
- $\boldsymbol{V_m}$ and $\boldsymbol{V_n}$ are the m^{th} and n^{th} node voltages, respectively.
- $\widehat{\boldsymbol{V_n}}$ is the n^{th} node voltage achieved in previous ($(\boldsymbol{t_{max}} - \mathbf{1})^{\boldsymbol{th}}$ iteration, where, $\boldsymbol{t_{max}}$ is the highest iteration number of the BFSM algorithm.
- $\boldsymbol{z_{mn}}$ is the impedance of the branch situated in between the m^{th} and n^{th} nodes.
- $\boldsymbol{P_n}$ and $\boldsymbol{Q_n}$ are the load active and reactive powers, respectively.
- $\sum_{\boldsymbol{r=r_1}}^{\boldsymbol{r_k}} \boldsymbol{I_{nr}}$ is the summation of the currents coming out of the n^{th} node.

For the second fragment of phase one study, a bi-objective function is formulated targeting the decrease of node voltage errors and the total line loss. A weighting factor (ω) is reserved to apportion the required share among the two sections of the bi-objective function. The two sections are named as the cumulative voltage deviation (CVD) and the total active line loss (P_{LOSS}). CVD is correlated to the voltage profile. The mathematical expression of CVD is being given as:

$$CVD = 0 \qquad \text{for} \quad |V_{min}| \leq |V_n| \leq |V_{max}|$$

$$= \sum_{n=1}^{N_B} |1 - V_n| \qquad \text{else} \quad (4)$$

where, n signifies the network node under consideration. $1 \leq n \leq N_B$

N_B signifies the total number of network nodes. V_n is the n^{th} node voltage. V_{min} and V_{max} are the minimum and maximum permissible values of V_n.

The weighted bi-objective function (objective function 2) formed for both the voltage deviation as well as line loss minimization is expressed as:

$$obj_{fn} = Minimize\{w.\frac{\sum_{b=1}^{n_{br}} P_{LOSS}(b)|_{W-EVCS}}{\sum_{b=1}^{n_{br}} P_{LOSS}(b)|_{WO-EVCS}} + (1-w).\frac{CVD|_{W-EVCS}}{CVD|_{WO-EVCS}} \quad (5)$$

where, $1 \leq b \leq n_{br}$

The indices n and b represent any node and line of the network, respectively. $\sum_{b=1}^{n_{br}} P_{LOSS}(b)|_{W-EVCS}$ and $\sum_{b=1}^{n_{br}} P_{LOSS}(b)|_{WO-EVCS}$ present the total active power loss of the RE-EVCS integrated and unintegrated networks, correspondingly. $CVD|_{W-EVCS}$ and $CVD|_{WO-EVCS}$ are the CVD values of the EVCS integrated and unintegrated networks. w is the weighting factor.

2.3 Decision Variables

EVCS (renewable energy integrated, or unintegrated) locations are the decision variables chosen for the optimization study.

An array named $EVCSLOCS$ is assigned to store the decision variables of the proposed optimization problem, i.e., the randomly generated EVCS locations.

$$EVCSLOCS = [EVCSLOCS_1, \dots, EVCSLOCS_k, \dots, EVCSLOCS_p] \quad (6)$$

where, p numbers of EVCSs are to be allocated. $EVCSLOCS_k$ denotes the k^{th} EVCS location among total p numbers of locations. The operating range of $EVCSLOCS_K$ is restricted to $F_N(i,j)$; where, for $i = 1$, $j = 2, \dots, N(i)$ and for $i = 2, \dots, T_N$, $j = 1, \dots, N(i)$ as per the proposed efficient power flow analysis method. The range is restricted to $2 \leq EVCSLOCS_k \leq N_B$ for the BFSM algorithm. The range is same for both power flow analysis methods (only the notations differ). The total number of EVCSs (p) varies based on the requirements in different case studies.

2.4 Power Balance Criterion

For sustaining the stability in an integrated system, the active and reactive power balances are indispensable. The active and reactive power balance equations are represented by equations (7) and (8), correspondingly considering power injection mode of the EVCSs.

$$P_{Slack} + \sum_{k=1}^{p} P_{EVCS}(k) = \sum_{c=1}^{N_L} P_D(c) + \sum_{b=1}^{n_{br}} P_{LOSS}(b) \quad (7)$$

$$Q_{Slack} + \sum_{k=1}^{p} Q_{EVCS}(k) = \sum_{c=1}^{N_L} Q_D(c) + \sum_{j=1}^{n_{br}} Q_{LOSS}(b) \quad (8)$$

where, k, c and b are the indices representing the number of EVCSs, loads and branches.

$1 \leq k \leq p$, $1 \leq c \leq N_L$ and $1 \leq b \leq n_{br}$

P_{Slack}, Q_{Slack}; $\sum_{k=1}^{p} P_{EVCS}(k)$, $\sum_{k=1}^{p} Q_{EVCS}(k)$; $\sum_{c=1}^{N_L} P_D(c)$, $\sum_{c=1}^{N_L} Q_D(c)$; $\sum_{b=1}^{n_{br}} P_{LOSS}(b)$, $\sum_{b=1}^{n_{br}} Q_{LOSS}(b)$ are the pairs representing the total active and reactive powers of slack bus; active and reactive powers of EVCSs working in power injection mode; active and reactive powers of loads and active and reactive line losses; respectively.

The equations are modified in load point mode of EVCSs as:

$$P_{Slack} = \sum_{k=1}^{p} P_{EVCS}(k) + \sum_{c=1}^{N_L} P_D(c) + \sum_{b=1}^{n_{br}} P_{LOSS}(b) \quad (9)$$

and

$$Q_{Slack} = \sum_{k=1}^{p} Q_{EVCS}(k) + \sum_{c=1}^{N_L} Q_D(c) + \sum_{j=1}^{n_{br}} Q_{LOSS}(b) \quad (10)$$

2.5 EVCS Sizing Restrictions

The maximum permissible capacity assortments of the EVCSs in power injection mode depend on numerous factors like total load demand, minimum essential power factor and maximum admissible EVCS diffusion level. The disparity ranges of active power, power factor and reactive power of k^{th} EVCS are epitomized by the equations (11) to (13), respectively.

$$P_{EVCSmin} \leq P_{EVCS}(k) \leq P_{EVCSmax} \quad (11)$$

$$PF_{EVCSmin} \leq PF_{EVCS}(k) \leq PF_{EVCSmax} \quad (12)$$

$$Q_{EVCS}(k) = P_{EVCS}(k).\tan(cos^{-1}PF_{EVCS}(k)) \quad (13)$$

where, $P_{EVCS}(k)$ and $Q_{EVCS}(k)$ are the active and reactive powers injected by the k^{th} EVCS. $P_{EVCSmin}$ and $P_{EVCSmax}$ are the minimum and maximum active power injection limits of k^{th} EVCS. $PF_{EVCSmin}$ is the minimum tolerable power factor and $PF_{EVCSmax}$ is the maximum viable power factor of the network. $PF_{EVCS}(k)$ implies the presently accessible power factor of the k^{th} EVCS.

2.6 The EVCS Diffusion Level and Capacity

The eminence as well as trustworthiness of the EVCS integrated network in power injection mode depends on its diffusion level (μ). For consistent operation of the overall integrated network, the following condition should be fulfilled:

$$\sum_{k=1}^{p} P_{EVCS}(k) \leq \mu \sum_{c=1}^{N_L} P_D(c) \quad (14)$$

The diffusion level μ can be calculated by the equation (15) if the total active power delivered by the EVCSs and the load power demand are known.

$$\mu = \frac{\sum_{k=1}^{p} P_{EVCS}(k)}{\sum_{c=1}^{N_L} P_D(c)} \quad (15)$$

where, $\mu_{min} \leq \mu \leq \mu_{max}$. μ_{min} and μ_{max} are the minimum and maximum tolerable values of μ.

If the maximum EVCS diffusion level μ_{max} and the peak load demand $\sum_{c=1}^{N_L} P_D(c)$ are known, then the maximum permissible EVCS capacity, $\sum_{k=1}^{p} P_{EVCS}(k)$ can be evaluated and, based on the capacity, the optimal (maximum) numbers and sizes of such EVCSs can be calculated without any filth in network performance.

The capacities and numbers of the EVCSs in load point mode should also follow EVCS size restrictions.

The arrays for holding the maximum active and reactive power capacities of the EVCSs are P_{EVCS} and Q_{EVCS}, respectively.

$$P_{EVCS} = [P_{EVCS1}, \dots, P_{EVCSk}, \dots, P_{EVCSp}] \quad (16)$$

and

$$Q_{EVCS} = [Q_{EVCS1}, \dots, Q_{EVCSk}, \dots, Q_{EVCSp}] \quad (17)$$

The active and reactive power capacities of k^{th} EVCS (EVCS$_k$) are P_{EVCSk} and Q_{EVCSk}, respectively.

2.7 Bus Voltage Constraints

For steady operation of the total system, the feeder voltages should persist within the stipulated boundaries, defined as:

$$V_{min} \leq V[F_N(i,j)] \leq V_{max} \text{ or } V_{min} \leq V_n \leq V_{max} \quad (18)$$

where, $V[F_N(i,j)]$ or V_n represents the node voltages of the distribution network. The V_{min} and V_{max} are their minimum and maximum permissible values, respectively. For the proposed study, these values are taken as 0.9 pu and 1.1 pu, respectively (considering primary distribution).

2.8 Total Active Power Loss Limit

For the power performance preservation in power injection mode, equation (19) should be fulfilled:

$$\sum_{b=1}^{n_{br}} P_{LOSS}(b)\,|_{W-EVCS} < \sum_{b=1}^{n_{br}} P_{LOSS}(b)\,|_{WO-EVCS} \quad (19)$$

2.9 Conclusion

Objective functions have been formulated aiming to reduce the node voltage errors and/or the total line loss in the network while integrating EVCSs. A detailed discussion about the objective functions, the related parameters, and constraints along with their boundaries for the optimum allocation of unidirectional/bidirectional EVCSs in power distribution network have been given in this chapter.

CHAPTER -3

MODELS AND METHODS

3. MODELS AND METHODS

3.1 Introduction

After the formulation of the objective functions specifying related parameters, constraints, and their boundaries, it is to be presented the different models and methods. The different techniques utilized for the optimum allotment of EVCSs are described in detail. Voltage and loss sensitivity analyses for verifying the feasibility of the network nodes in view of EVCS integration are explained. Henceforth, two popular power flow analysis methods developed especially for the distribution network are presented elaborately. Thereafter, several useful optimization techniques namely PSO, PPSO, INBPSO and GA are explored. Lastly, a MATLAB/Simulink model of multiple SPV-EVCS integrated distribution network is developed for the power management study.

3.2 Voltage Sensitivity Analysis

Voltage sensitivity analysis is generally measured by investigating the changes in voltage with corresponding changes in active and reactive powers. It is the investigation regarding the sensitivities of the system node voltages subjected to the incremental changes in load reactive power at the nodes for decoupled systems. This technique is used to identify the potential nodes for injecting or extracting reactive power to/from the distribution network as unplanned reactive power injection/extraction at any node may lead to instability. Thus, for integrating the EVCS in reactive power injection/extraction mode, it is fundamental to investigate the suitability of the system nodes. To find out the voltage sensitivity of the network nodes [Popović et al., 2005; Chakrabarti et al., 2010; Roy et al., 2013], the nodal differential equation intended for calculating bus active and reactive powers in matrix form is given by:

$$\begin{bmatrix}\Delta P\\ \Delta Q\end{bmatrix} = \begin{bmatrix}\frac{\partial P}{\partial \delta} & \frac{\partial P}{\partial V}\\ \frac{\partial Q}{\partial \delta} & \frac{\partial Q}{\partial V}\end{bmatrix}\begin{bmatrix}\Delta \delta\\ \Delta V\end{bmatrix} \tag{20}$$

For decoupled load flow, the $\frac{\partial P}{\partial V}$ and $\frac{\partial Q}{\partial \delta}$ terms are zero. Henceforward, the equation (20) is further reduced to:

$$[\Delta P] = \left[\frac{\partial P}{\partial \delta}\right].[\Delta \delta] \tag{21}$$

and

$$[\Delta Q] = \left[\frac{\partial Q}{\partial V}\right].[\Delta V] \tag{22}$$

Equation (22) can be reorganized to compute $\left[\frac{\partial V}{\partial Q}\right]$ by considering the incremental change in node voltage ΔV, ensuing from an incremental change in load reactive power ΔQ. The revised equation is:

$$\left[\frac{\Delta V}{\Delta Q}\right] = \left[\frac{\partial V}{\partial Q}\right] \tag{23}$$

$\left[\frac{\partial V}{\partial Q}\right]$ is the matrix demonstrative of node voltage sensitivities. There are two reasons of node voltage disparity: reactive power injection/extraction in the same node or other nodes of the network. Among them, the most prevalent deviation occurs due to change in reactive power to/from the same node. That's why, the diagonal elements of the $\left[\frac{\partial V}{\partial Q}\right]$ matrix, i.e., $(\frac{\partial V_n}{\partial Q_n})$ for all the network nodes are the best predictors of node voltage sensitivities. The voltage sensitivity index (VSI) of the n^{th} node is formulated as:

$$VSI|_n = (\frac{\partial V_n}{\partial Q_n}) \tag{24}$$

VSI of a node is defined as the incremental change in node voltage ∂V_n due to an incremental change in load reactive power ∂Q_n at that node. So far, the power extraction is concerned, high positive VSI is not desirable. Hence, the nodes having high positive VSI are unsuitable for reactive power extraction. On the contrary, nodes having higher positive VSIs are more suitable for reactive power injection. The negative VSI at any node indicates instability in view of reactive power extraction/injection. The positive VSI of node indicates stability within boundaries.

3.3 Loss Sensitivity Analysis

Like the voltage sensitivity analysis, loss sensitivity analysis is another kind of analysis to inspect the consequence of variation in active power extraction at the network nodes upon the total system active power loss [Popović et al., 2005; El-Fergany, 2015]. The active power losses (P_{LOSS}) of a network depend on the power flow through the transformers and lines. Hereafter, P_{LOSS} is reliant on active and reactive power flows P_S and Q_S, which are the functions of V and δ. The loss sensitivity index (LSI) of any node n is defined as:

$$LSI|_n = \left(\frac{\partial P_{LOSS}}{\partial P_D(n)}\right) \tag{25}$$

If LSI is more positive, the total incremental line loss ∂P_{LOSS} is more subjected to a small change in active power extraction $\partial P_D(n)$. Thus, nodes having high positive LSIs are the weak nodes for active power extraction. However, in the case of active power injection, the effect is contrary. The nodes having more positive LSI values are the more appropriate nodes for power injection. Negative LSI leads to instability. Hence, the nodes having negative LSI values are the unsuitable nodes for both power extraction and injection. It has been observed that the nodes closer to the substation have smaller LSI values. Gradually with the progression towards the end nodes, the LSI values increase. The reason behind that is, when heavy loads are coupled at the nodes closer to the substation, the high line current voyages less distance.

3.4 Backward Forward Sweep Method (BFSM)

3.4.1 Constructional description of radial distribution system

As the physical constructional features of transmission and distribution systems are different from each other, their power flow equations are also dissimilar [Grainger and Lee, 1982; Shirmohammadi et al., 1988; Baran and Wu, 1989]. BFSM is a renowned power flow analysis method used for the power distribution network. Before discussing the BFSM method, the basic constructional features of a radial distribution network are demonstrated in this sub-section. The network under consideration is assumed to be a balanced three-phase network for simplicity. For brevity, initially a case has been considered with only one main feeder. The practical

configuration of a radial distribution system with laterals (branches) is presented and discussed later.

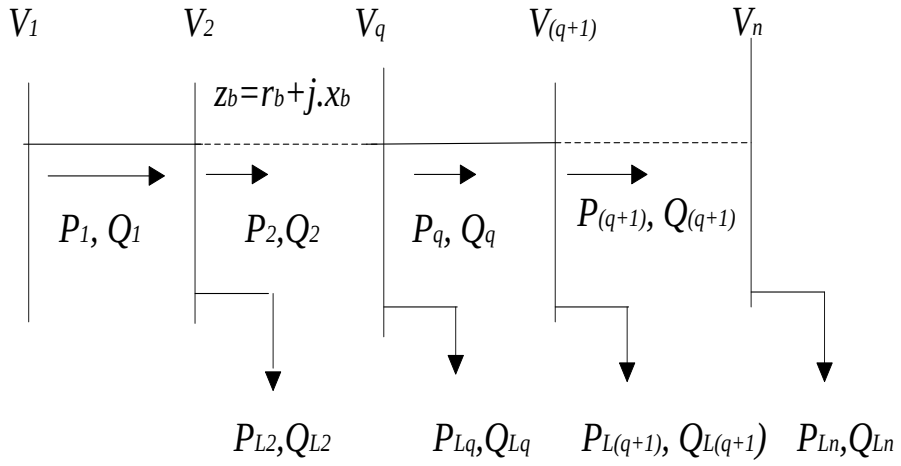

Figure 2. Single-line diagram of the radial distribution network with main feeder

Figure 2 shows a distribution system consisting of only the radial main feeder. $|V_1|$ represents the magnitude of substation bus voltage which is assumed to be constant. The voltage of the q^{th} node is V_q. The total load demand at q^{th} node is $S_{Lq} = P_{Lq} + \hat{j}.Q_{Lq}$. The power flow from the q^{th} node is denoted by P_q and Q_q.The line b of the distribution system has a series impedance $z_b = r_b + \hat{j}.x_b$.

System with main feeder and laterals:

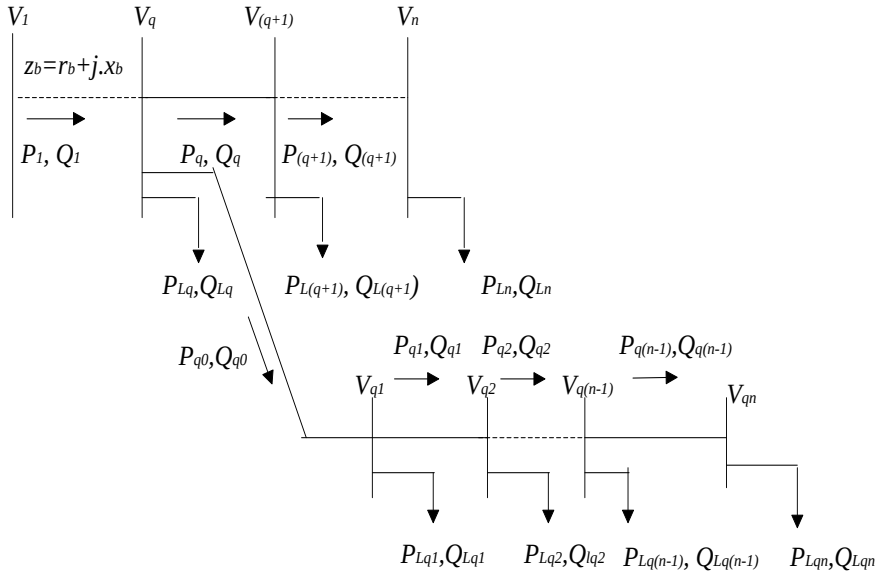

Figure 3. Single-line diagram of the radial distribution network with main feeder and laterals

Figure 3 presents a radial distribution system with a main feeder along with laterals. $|V_1|$ represents the magnitude of substation bus voltage. The load demand of main feeder's q^{th} node is $S_{Lq} = P_{Lq} + \hat{j}.Q_{Lq}$. The active and reactive powers flowing out from the q^{th} node are denoted by P_q and Q_q, respectively. The parameters of lateral coming out of the q^{th} node are represented mainly by the notation q. The nodes of this lateral are denoted by q_1, q_2, …,q_n. The node voltages are V_{q_1}, V_{q_2}, …, V_{q_n}. (P_{Lq_1},Q_{Lq_1}), (P_{Lq_2},Q_{Lq_2}), …, (P_{Lq_n},Q_{Lq_n}) are the load active and reactive power demands at these nodes. (P_{q_1},Q_{q_1}), (P_{q_2},Q_{q_2}), …, ($P_{q_{(n-1)}}$,$Q_{q_{(n-1)}}$) are the power flows of the lateral nodes q_1, q_2, …,$q_{(n-1)}$. The b^{th} line impedance of the distribution system is $z_b = r_b + \hat{j}.x_b$.

3.4.2 Mathematical modelling for development of BFSM algorithm

Backward forward sweep method is a widespread power flow analysis method used for the distribution network. This is a competent, fast, accurate and derivative free modest method for the power flow resolution of a grid-connected radial distribution network. Unlike the conventional load flow analysis methods adopted for transmission systems, it directly evaluates the currents flowing through the entire system by means of simple system equations. The network configuration for the development of the mathematical model to execute the BFSM algorithm is presented below.

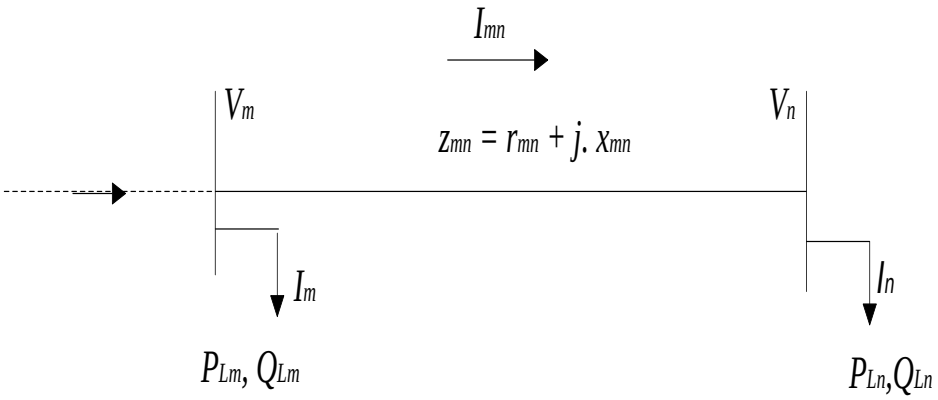

Figure 4. Line connected with end nodes of main feeder, laterals, or sub-laterals

Figure 4 represents the line coupled with the end node of main feeder, laterals, or sub-laterals. The symbolizations of node voltages and load powers are same as that of previous sub-section. I_n is the load current flowing from the end node (n^{th} node). I_{mn} is the line current flowing through the line connected with the end node. It is situated in between the m^{th} and n^{th} nodes.

In this case, $I_{mn} = I_n$ (26)

as n^{th} node is the end node.

z_{mn} is the impedance of the line in between the nodes, represented as:

$z_{mn} = r_{mn} + \hat{j}.x_{mn}$ (27)

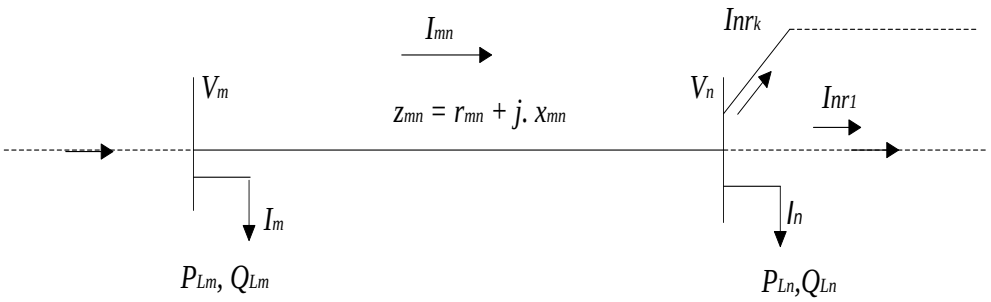

Figure 5. Line connected in between the intermediate nodes of main feeder, laterals, or sub-laterals

Figure 5 demonstrates the line linked in between the intermediate nodes of main feeder, laterals, or sub-laterals. The symbolizations of node voltages, load powers, line impedances, load currents and line currents are same as that of the previously discussed annotations. But the difference lies in the calculation of I_{mn}. In the occasion of end node connective lines as in Figure 4, I_{mn} is equal to I_n as n^{th} node is the termination node of the network and m^{th} node is the node just before the n^{th} node. On contrary, in this case, I_{mn} is the line current flowing in between the intermediate nodes *m* and *n*. The n^{th} node denotes the subsequent node of the main feeder, laterals, or sub-laterals with/without connection with the other succeeding nodes. In this condition:

$$I_{mn} = I_n + \sum_{r=r_1}^{r_k} I_{nr} \tag{28}$$

$\sum_{r=r_1}^{r_k} I_{nr}$ is the summation of all currents flowing out from the n^{th} node to the other nodes of the network. I_n is the n^{th} node load current.

3.4.3 The steps involving BFSM algorithm

The BFSM algorithm [Díaz et al., 2015] comprises of two parts: backward sweep and forward sweep. In backward sweep, currents of the entire network (all line and load currents) are calculated. After evaluation of all currents, the forward sweep

is initiated to compute all the node voltages. The detailed steps for employing this algorithm are given below [Teng and Chang, 2007]:

A) Initialization of parameters:

Before starting the power flow analysis, some arrays must be taken and initialized.

The active and reactive powers of the system nodes are stored inside the *P* and *Q* arrays for holding the load active and reactive power data.

$$P = [P_1, P_2, \dots, P_n, \dots, P_{N_B}] \tag{29}$$

and

$$Q = [Q_1, Q_2, \dots, Q_n, \dots, Q_{N_B}] \tag{30}$$

where, P_n and Q_n $(1 \leq n \leq N_B)$ represent the active and reactive load powers associated with the n^{th} bus.

Impedance of a line connected in between nodes *m* and *n* is articulated as, $z_{mn} = r_{mn} + \hat{j}.x_{mn}$ as per equation (27).
where, $1 \leq m \leq N_B$ and $1 \leq n \leq N_B$.
N_B stands for the total number of network nodes. If there is no physical linking or line in between any two nodes of the system under speculation, then the conforming z_{mn} value is $(0 + \hat{j}.0)$ pu. $\boldsymbol{Z}$ matrix holds the line impedance data.

$$\boldsymbol{Z}_{(\boldsymbol{N_B \times N_B})} = \begin{bmatrix} z_{(1,1)} & \cdots & z_{(1,N_B)} \\ \vdots & \dots & \vdots \\ z_{(N_B,1)} & \cdots & z_{(N_B,N_B)} \end{bmatrix} \tag{31}$$

where, $z_{(m,n)}$ is an element of the $\boldsymbol{Z}$ matrix, which holds the line impedance z_{mn}.

Two three-dimensional matrices $\boldsymbol{V}$ and $\boldsymbol{I}$ are formed to hold the voltage and current data generated in successive iterations of the proposed power flow algorithm. The t denotes the current iteration number. The range of t is, $1 \leq t \leq t_{max}$, where t_{max} signifies the maximum iteration number of the proposed algorithm.

Initialization of $\boldsymbol{V}$ is accomplished by:

$$\boldsymbol{V}_{(\mathbf{1}\times \boldsymbol{N_B}\times(\boldsymbol{t_{imax}}))} = \left[V_{(1,1,t_i)} V_{(1,2,t_i)} \dots V_{(1,n,t_i)} \dots V_{(1,N_B,t_i)}\right] \ddots$$
$$= [(1 + \hat{\jmath}.0)(1 + \hat{\jmath}.0) \dots (0 + \hat{\jmath}.0) \dots (0 + \hat{\jmath}.0)] \ddots \quad (32)$$

The first dimension of the $\boldsymbol{V}$ matrix is 1. The ranges of the second and third dimensions are as $1 \leq n \leq N_B$ and $1 \leq t_i \leq t_{imax}$.

The relation between the indices t and t_i is $t_i = t + 1$, where t_i denotes the current third dimensional index of the $\boldsymbol{V}$ matrix and t index implies the current iteration number of the proposed power flow algorithm. As $1 \leq t \leq t_{max}$, $t = 0$ indicates the 0^{th} iteration of the power flow. Since, $1 \leq t_i \leq t_{imax}$ and $t_i = t + 1$; hence, at $t = 0$, $t_i = 1$. Subsequently at $t = t_{max}$, $t_i = (t_{max} + 1)$, which is the maximum value of t_i i.e., t_{imax}. Henceforth, the relationship between the maximum values of t_i and t is $t_{imax} = (t_{max} + 1)$.

$\left[V_{(1,1,1)} V_{(1,2,1)} \dots V_{(1,N_B,1)}\right]$ stores the 0^{th} iteration values of the node voltages (initial node voltage values). Similarly, $\left[V_{(1,1,t_{imax})} V_{(1,2,t_{imax})} \dots V_{(1,N_B,t_{imax})}\right]$ holds the maximum iteration $(t_{max})^{\text{th}}$ values of node voltages.

Similarly, $\boldsymbol{I}$ matrix is initialized by:

$$\boldsymbol{I}_{(\boldsymbol{N_B}\times \boldsymbol{N_B}\times(\boldsymbol{t_{imax}}))} = \begin{bmatrix} I_{(1,1,t_i)} & \cdots & I_{(1,N_B,t_i)} \\ \vdots & I_{(m,n,t_i)} & \vdots \\ I_{(N_B,1,t_i)} & \cdots & I_{(N_B,N_B,t_i)} \end{bmatrix} \ddots$$

$$= \begin{bmatrix} (0 + \hat{\jmath}.0) & \cdots & (0 + \hat{\jmath}.0) \\ \vdots & (0 + \hat{\jmath}.0) & \vdots \\ (0 + \hat{\jmath}.0) & \cdots & (0 + \hat{\jmath}.0) \end{bmatrix} \ddots \quad (33)$$

where, $I_{(m,n,t_i)}$ epitomizes line current flowing in between two nodes m and n at power flow iteration number t, where $t_i = t + 1$. $1 \leq m \leq N_B$ and $1 \leq n \leq N_B$. The elements $I_{(1,1,t_i)}$, $I_{(2,2,t_i)}, \dots, I_{(N_B,N_B,t_i)}$ designate the load currents flowing from the specific nodes of the network. In general, $I_{(n,n,t_i)}$indicates n^{th} node's load current at iteration number t.

B) Backward sweep:

After initialization of the arrays and matrices vital for running the anticipated algorithm, the backward sweep is started. The backward sweep came from the concept of backward propagation as the process proceeds towards the backward direction while calculating the line and load currents of the network. The current evaluation starts from the end nodes and gradually proceeds towards the starting nodes.

The syntax used for calculating the load currents is shown in Figure 6.

```
.
.
for t = 1: t_max
                    t_i = t + 1
for n = N_B : 2
            I_(n,n,t_i) = [(P_n + ĵ.Q_n) / V_(1,n,(t_i−1))]*
            n = n − 1
end
end
.
.
```

Figure 6. Syntax for calculating the load currents

where, $2 \leq n \leq N_B$. $I_{(n,n,t_i)}$, P_n and Q_n are the n^{th} node load current at current iteration, load active power and load reactive power respectively. $V_{(1,n,(t_i-1)}$ denotes the n^{th} node voltage obtained at previous iteration. After reception of all load currents

of the network, all the line currents of the distribution network are calculated by the syntax presented in Figure 7.

.
.

for $t = 1: t_{max}$

$$t_i = t + 1$$

for $m = 1: (N_B - 1)$

for $n = N_B: 2$

$$I_{(m,n,t_i)} = I_{(n,n,t_i)} + \sum_{r=r_1}^{r_k} I_{(n,r,t_i)}$$

$$n = n - 1$$

end

end

end

.
.

Figure 7. Syntax for calculating the line currents

where, m and n signify the prior and subsequent node numbers, respectively. $2 \leq n \leq N_B$ and $1 \leq m \leq (N_B - 1)$. $I_{(m,n,t_i)}$ is the line current flowing in between nodes m and n at current iteration. $I_{(n,n,t_i)}$ is the load current of node n at current iteration. r signifies all other nodes connected with the n^{th} node in the forward direction and $r_1 \leq r \leq r_k$. $\sum_{r=r_1}^{r_k} I_{(n,r,t_i)}$ is the summation of all current iteration values of the line currents for the lines connected with n^{th} node in forward direction of the distribution network. r_1 to r_k are discrete values taken by r, depending on the network arrangement. All calculated load and line currents are stored inside the ***I***

matrix. $I_{(m,n,t_i)}$ element of the three-dimensional current matrix will be updated if nodes *m* and *n* are physically coupled within the distribution network. Otherwise, its value will remain as it is [$(0 + \hat{j}.0)$, initialized value].

C) Forward sweep:

After the evaluation of all currents of the network by backward sweep, forward sweep is initiated for calculating all the node voltages. This process proceeds towards the forward path while evaluating the node voltages.

The syntax used for calculating the node voltages of the network is shown in Figure 8.

.
.

for $t = 1: t_{max}$

$$t_i = t + 1$$

for $m = 1: (N_B - 1)$

for $n = 2: N_B$

$$V_{(1,n,t_i)} = V_{(1,m,t_i)} - z_{(m,n)}.I_{(m,n,t_i)}$$

end

end

end

.
.

Figure 8. Syntax for calculating the node voltages

where, *m* and *n* denote the former and next node numbers as per network configuration; $2 \leq n \leq N_B$ and $1 \leq m \leq (N_B - 1)$.

After completion of the forward sweep process, all the network currents and node voltages are known for the current iteration. At that point, the stopping criterion for this iterative algorithm is verified and if it is not fulfilled, the next iteration begins. After accomplishment of the algorithm, the network active and reactive power losses, node voltage errors, and power flow from the nodes can be premeditated as per necessity. Figure 9 displays the flow chart of the proposed power flow analysis algorithm.

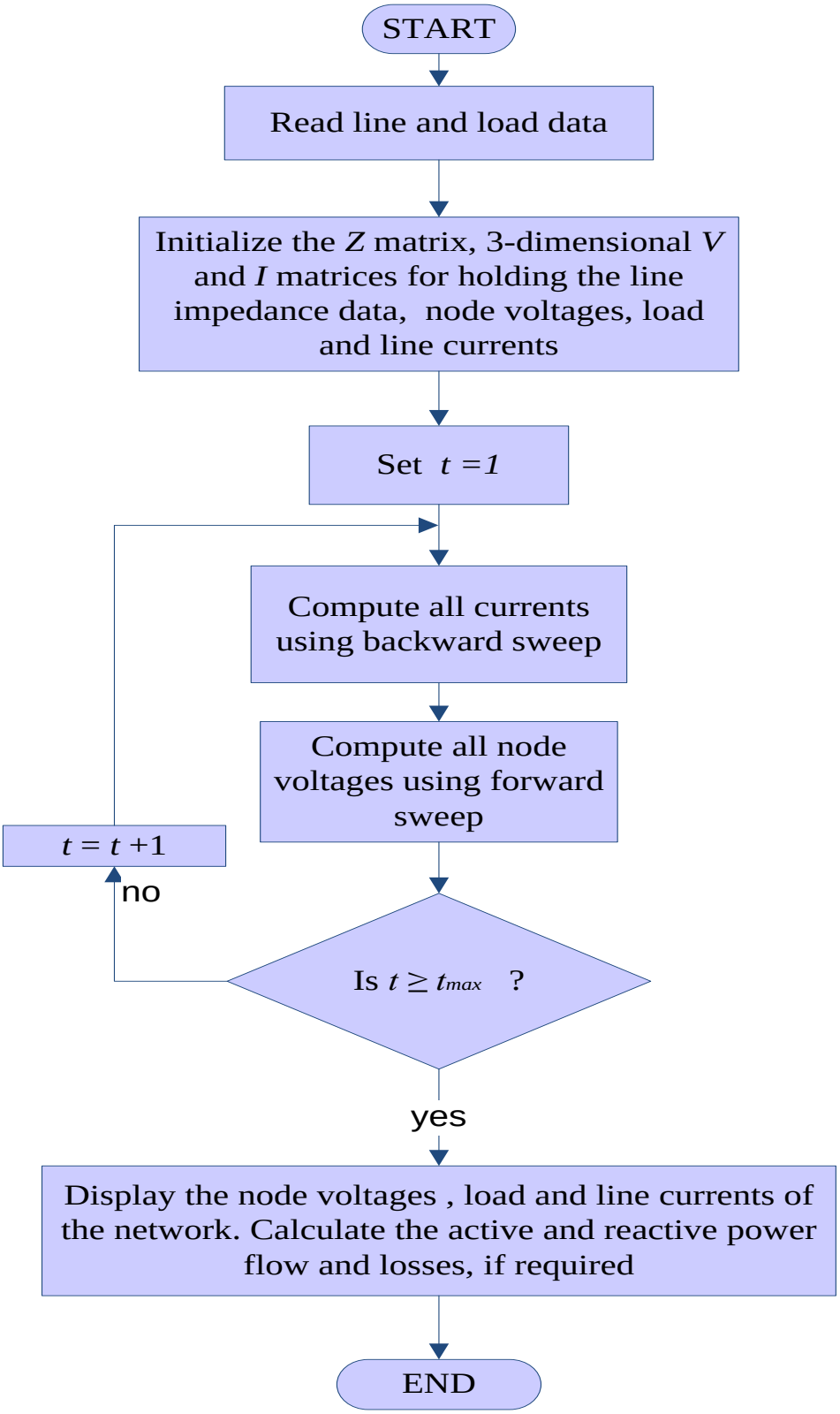

Figure 9. Flow chart of BFSM algorithm

3.5 An Efficient Power Flow Analysis Technique

3.5.1 Mathematical modelling and formation of node and branch sets

Before establishing the mathematical model of the proposed technique [Ghosh and Sherpa, 2008], a three-phase balanced radial distribution network is presumed as reference.

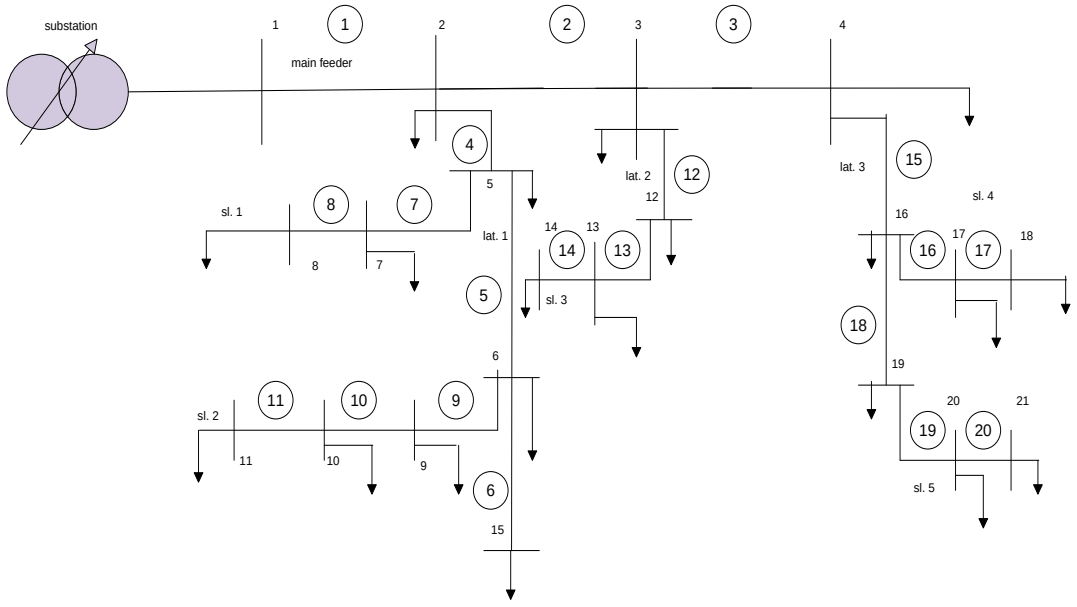

Figure 10. Single-line diagram of a radial distribution system with main feeder, laterals, and sub-laterals

Figure 10 illustrates the single-line diagram of a distribution network with main feeder, laterals, and sub-laterals with no charging capacitances in effect considering only one phase. A non-sequential numbering scheme is presented to validate the effectiveness of the proposed technique on any type of numbering scheme involved. From Figure 10, it is seen that apart from the main feeder, there are three laterals and five sub-laterals. In this method, at first, the sets of all main feeder, laterals and sub-lateral nodes and branches are formed. For this specific configuration depicted in Figure 10, the set of feeder nodes is {1, 2, 3, 4}. Sets of lateral nodes are {2, 5, 6, 15}, {3, 12} and {4, 16, 19}, respectively. {5, 7, 8}, {6, 9, 10, 11}, {12, 13, 14}, {16, 17, 18} and {19, 20, 21} are the sets of sub-lateral nodes. The set of branch

numbers of main feeder is {1, 2, 3}. The sets of branch numbers of the three laterals are {4, 5, 6}, {12} and {15, 18}. The sets of branch numbers of the five sub-laterals are {7, 8}, {9, 10, 11}, {13, 14}, {16, 17} and {19, 20}, respectively.

3.5.2 Formation of the array for storing the total node numbers of each feeder, laterals, and sub-laterals

After forming the sets of all main feeder, lateral and sub-lateral nodes and branches, the next step is to form the required arrays for storing the total node numbers of each feeder, laterals, and sub-laterals. The total number of feeders, laterals and sub-laterals of the entire network are denoted by *A*, *B* and *C*, respectively. For the network of Figure 10, $A = 1$, $B = 3$ and $C = 5$. The all-total number of feeders, laterals and sub-laterals is presented by T_N .

The general expression of T_N is:

$$T_N = A + B + C \tag{34}$$

Following Figure 10, T_N value is 9.

The total numbers of feeders, laterals and sub-laterals nodes are stockpiled in a one-dimensional array N. The number of columns of this array is T_N. Hereafter, the total number of columns of N array for the network embodied in Figure 10 is 9. Thus, as per the network of Figure 10, $N(1) = 4$, $N(2) = 4$, $N(3) = 2$, $\mathrm{N}(4) = 3$, $N(5) = 3$, $N(6) = 4$, $N(7) = 3$, $N(8) = 3$and $\mathrm{N}(9) = 3$.

3.5.3 Formation of node and branch data sets

For creating the data set of nodes and branches involving the feeder, laterals, and sub-laterals; two matrices $\boldsymbol{F_N}$ and $\boldsymbol{F_B}$ are taken: one for holding the node data and another for holding the branch data. Relating to the first index of these two matrices, feeder is represented by 1, laterals by (2, 3, 4) and sub-laterals by (5, 6, 7, 8, 9). The second index symbolize the order of the nodes or branches in a specific feeder, lateral or sub-lateral already indicated by the first index. At first, feeder data is stored, then comes the turn of laterals and sub-laterals. The formation of the $\boldsymbol{F_N}$ and $\boldsymbol{F_B}$ matrices are presented below:

The elements of the $\boldsymbol{F_N}$ matrix (two-dimensional) are:

$F_N(1,1) = 1, F_N(1,2) = 2,\ F_N(1,3) = 3$ and $F_N(1,4) = 4$ {presenting main feeder node data}

$F_N(2,1) = 2, F_N(2,2) = 5\ ,\ F_N(2,3) = 6$ and $F_N(2,4) = 15$ {presenting lateral 1 node data}

$F_N(3,1) = 3$ and $F_N(3,2) = 12$ {presenting lateral 2 node data}

$F_N(4,1) = 4, F_N(4,2) = 16$ and $F_N(4,3) = 19$ {presenting lateral 3 node data}

$F_N(5,1) = 5, F_N(5,2) = 7$ and $F_N(5,3) = 8$ {presenting sub-lateral 1 node data}

$F_N(6,1) = 6, F_N(6,2) = 9, F_N(6,3) = 10$ and $F_N(6,4) = 11$ {presenting sub-lateral 2 node data}

$F_N(7,1) = 12, F_N(7,2) = 13$ and $F_N(7,3) = 14$ {presenting sub-lateral 3 node data}

$F_N(8,1) = 16, F_N(8,2) = 17$ and $F_N(8,3) = 18$ {presenting sub-lateral 4 node data}

$F_N(9,1) = 19, F_N(9,2) = 20$ and $F_N(9,3) = 21$ {presenting sub-lateral 5 node data}

Consequently, the elements of the $\boldsymbol{F_B}$ matrix (two-dimensional) are:

$F_B(1,1) = 1,\ F_B(1,2) = 2$ and $F_B(1,3) = 3$ {presenting main feeder branch data}

$F_B(2,1) = 4, F_B(2,2) = 5$ and $F_B(2,3) = 6$ {presenting lateral 1 branch data}

$F_B(3,1) = 12$ {presenting lateral 2 branch data}

$F_B(4,1) = 15$ and $F_B(4,2) = 18$ {presenting lateral 3 branch data}

$F_B(5,1) = 7$ and $F_B(5,2) = 8$ {presenting sub-lateral 1 branch data}

$F_B(6,1) = 9, F_B(6,2) = 10$ and $F_B(6,3) = 11$ {presenting sub-lateral 2 branch data}

$F_B(7,1) = 13$ and $F_B(7,2) = 14$ {presenting sub-lateral 3 branch data}

$F_B(8,1) = 16$ and $F_B(8,2) = 17$ {presenting sub-lateral 4 branch data}

$F_B(9,1) = 19$ and $F_B(9,2) = 20$ {presenting sub-lateral 5 branch data}

In general, the elements of the $\boldsymbol{F_N}$ matrix are represented by $F_N(i,j)$, where $i = 1, 2, \dots, T_N$ and $j = 1, 2, \dots, N(i)$. The elements of the $\boldsymbol{F_B}$ matrix are represented by $F_B(i,j)$, where $i = 1, 2, \dots, T_N$ and $j = 1, 2, \dots, N(i) - 1$.

3.5.4 Formation of arrays for storing the common nodes of laterals and sub-laterals

An array named m_m is formed for storing the common nodes of laterals and sub-laterals. These common nodes are the first elements of the rows representing the sub-lateral data of the previously formed $\boldsymbol{F_N}$ matrix. A second array named m_n is premeditated for storing the associated sub-lateral numbers. The syntax used for storing the information into the m_m and m_n arrays is shown in Figure 11.

```
.
.
                    j = 0
for i = T_N : (T_N − C + 1)
                    j = j + 1
                    m_m(j) = F_N(i, 1)
                    m_n(j) = i
                    i = i − 1
end
.
.
```

Figure 11. Syntax for storing the common nodes of laterals and sub-laterals, and associated sub-lateral numbers

3.5.5 Storing the common nodes of main feeder and laterals

The same arrays used in sub-section 3.5.4 are utilized for storing information about the common nodes of main feeder and laterals. These common nodes are the first elements of the rows representing the lateral data of the previously formed $\boldsymbol{F_N}$ matrix. m_m array stores the common nodes of feeder and laterals whereas, m_n stores information about the associated lateral numbers. The syntax used for storing the information into the m_m and m_n arrays is shown in Figure 12.

```
.
.
for i = (T_N − C) : (T_N − C − B + 1)
                    j = j + 1
                    m_m(j) = F_N(i, 1)
                    m_n(j) = i
                    i = i − 1
end
.
.
```

Figure 12. Syntax for storing the common nodes of main feeder and laterals, and associated lateral numbers

3.5.6 Formation of matrices for storing the various system data

For storing the load active and reactive powers drawn from the system nodes, $\boldsymbol{P_L}$ and $\boldsymbol{Q_L}$ matrices are formed. $P_L[F_N(i,j)]$ and $Q_L[F_N(i,j)]$ represent the elements of these two matrices. Similarly, line resistance, reactance and impedance data are stored inside the newly formed $\boldsymbol{R}$, $\boldsymbol{X}$ and $\boldsymbol{Z}$ matrices. $R[F_B(i,j)]$, $X[F_B(i,j)]$ and $Z[F_B(i,j)]$ display the elements of these three matrices.

3.5.7 Formation, initialization and retention of V and I matrices

For calculating the active and reactive line losses of the network, the initial values of the node voltages and line currents are to be stored inside voltage and current matrices formed. The initial values of all elements $V[F_N(i,j)]$ of the $\boldsymbol{V}$ matrix are set to $(1+\hat{j}.0)$ pu whereas all elements $I[F_B(i,j)]$ of the $\boldsymbol{I}$ matrix are taken as $(0+\hat{j}.0)$ pu. The dimensional ranges of $V[F_N(i,j)]$ elements are $i = 1, 2, \dots, T_N$ and $j = 1, 2, \dots, N(i)$. The $\boldsymbol{I}$ matrix elements $I[F_B(i,j)]$ are stored for $i = 1, 2, \dots, T_N$ and $j = 1, 2, \dots, N(i)-1$. Apart from holding the initial values, the $\boldsymbol{V}$ and $\boldsymbol{I}$ matrices hold the previous iteration values to be used for the current iteration.

3.5.8 Calculating the active and reactive line losses

$\boldsymbol{L_P}$ and $\boldsymbol{L_Q}$ matrices are formed to store the values of calculated active and reactive power line losses, respectively. $L_P[F_B(i,j)]$ and $L_Q[F_B(i,j)]$ represents the elements of the two matrices. The step-by-step procedure for calculating the active and reactive line losses of the network are presented by the following equations:

$$|\, I[F_B(i,j)]| = \frac{|V[F_N(i,j)]| - |\, V[F_N(i,j+1)]|}{|Z[F_B(i,j)]|} \tag{35}$$

$$L_P[F_B(i,j)] = |\, I[F_B(i,j)]|^{2\cdot}.R[F_B(i,j)] \tag{36}$$

$$L_Q[F_B(i,j)] = |\, I[F_B(i,j)]|^{2}.X[F_B(i,j)] \tag{37}$$

After finding out the active and reactive power line losses, the elements of the node voltage matrix are preserved for further use into $\boldsymbol{V_1}$ matrix. $V_1[F_N(i,j)]$ is presenting the element of V_1.

$$V_1[F_N(i,j)] = V[F_N(i,j)] \tag{38}$$

3.5.9 Calculating the active and reactive power flows

For calculating the active and reactive power flows from the sub-lateral nodes, the syntax used is shown in Figure 13.

.
.

for $i = T_N : (T_N - C + 1)$

for $j = (N(i) - 1) : 1$

if $j == N(i) - 1$

$$P_S[F_B(i,j)] = P_L[F_N(i,j+1)] + L_P[F_B(i,j)]$$

$$Q_S[F_B(i,j)] = Q_L[F_N(i,j+1)] + L_Q[F_B(i,j)]$$

else

$$P_S[F_B(i,j)] = P_L[F_N(i,j+1)] + L_P[F_B(i,j)] + P_S[F_B(i,j+1)]$$

$$Q_S[F_B(i,j)] = Q_L[F_N(i,j+1)] + L_Q[F_B(i,j)] + Q_S[F_B(i,j+1)]$$

end

$$j = j - 1$$

end

$$i = i - 1$$

end

.
.

Figure 13. Syntax for calculating the active and reactive power flows of sub-lateral nodes

For finding out the active and reactive power flows from the lateral and feeder nodes, the syntax is castoff as shown in Figure 14.

.
.

for $i = (T_N - C)$: 1

for $j = (N(i) - 1) : 1$

for $k = 1$: $(T_N - 1)$

if $F_N(i, j+1) == m_m(k)$

if $j + 1 == N(i)$

$$P_S[F_B(i,j)] = P_L[F_N(i,j+1)] + L_P[F_B(i,j)] + P_S[F_B(m_n(k),1)]$$

$$Q_S[F_B(i,j)] = Q_L[F_N(i,j+1)] + L_Q[F_B(i,j)] + Q_S[F_B(m_n(k),1)]$$

else

$$P_S[F_B(i,j)] = P_L[F_N(i,j+1)] + L_P[F_B(i,j)] + P_S[F_B(m_n(k),1)] + P_S[F_B(i,j+1)]$$

$$Q_S[F_B(i,j)] = Q_L[F_N(i,j+1)] + L_Q[F_B(i,j)] + Q_S[F_B(m_n(k),1)] + Q_S[F_B(i,j+1)]$$

end
end

k=k+1

end

$j = j - 1$

end

$i = i - 1$

end

.
.

Figure 14. Syntax for calculating the active and reactive power flows of lateral and feeder nodes

These active and reactive power flows are stored inside the $\boldsymbol{P_S}$ and $\boldsymbol{Q_S}$ matrices formed. $P_S[F_B(i,j)]$ and $Q_S[F_B(i,j)]$ represent the elements of these two matrices, respectively.

3.5.10 Calculating the node voltages, associated parameters, and checking criteria

For the first iteration; after initializing the voltage and current matrices, retaining the initial voltages, calculating the initial values of the active and reactive line losses as well as active and reactive power flows of the lines (following sub-sections 3.5.7, 3.5.8 and 3.5.9); the iteration value is set to 1, i.e., $T = 1$

For other iterations, the T value for the current iteration is already set to $(T + 1)$ in the previous iteration and therefore at this position, current iteration number needs not to be updated. Henceforth, for other iterations, the steps depicted in sub-sections 3.5.8 and 3.5.9 are followed for retaining the previous iteration values of node voltages in V_1 matrix, calculating the active and reactive line losses and power flows of the lines in current iteration.

For calculating the node voltages and associated voltage errors for the current iteration, the following equations are used:

$$V[F_N(i,j+1)] = V[F_N(i,j)] - \frac{\sqrt{(P_S[F_B(i,j)])^2 + (Q_S[F_B(i,j)])^2}}{|V[F_N(i,j)]|} . Z[F_B(i,j)] \quad (39)$$

$$|\Delta V[F_N(i,j)]| = |V_1[F_N(i,j)]| - |V[F_N(i,j)]| \quad (40)$$

where, $i = 1, 2, \ldots, T_N$; $j = 1, 2, \ldots, N(i)$ for the $\boldsymbol{F_N}$ and $j = 1, 2, \ldots, N(i) - 1$ for the $\boldsymbol{F_B}$ matrix elements. $\boldsymbol{V_1}$ matrix retains the initial node voltages and $\boldsymbol{V}$ matrix holds the first iteration values of the node voltages during the first iteration. For the other iterations, $\boldsymbol{V_1}$ and $\boldsymbol{V}$ matrices retain the previous and the current iteration values of node voltages, respectively.

Then, the maximum node voltage error is calculated by using the equation:

$$\Delta V_{max} = \max([\,|\Delta V[F_N(i,j)]|]) \quad (41)$$

After obtaining the maximum network voltage error, the next step is to verify whether the optimum voltage error criterion is met or not. If the optimum voltage error criterion is met, the iteration process terminates and the node voltages, line losses and power flows obtained are the optimum results corresponding to the optimum voltage error criterion.

If the optimum voltage error criterion is not satisfied, then T should be set to $(T+1)$, i.e., $T = T + 1$. At that moment, inspection of maximum iteration criterion is accomplished.

If $T < T_{max}$, then the next iteration begins, and the control goes to sub-section 3.5.8 and subsequently to sub-sections 3.5.9 and 3.5.10, where preservation of node voltages attained from previous iteration is accomplished. The calculation and retention of the active and reactive line losses, line power flows, node voltages, node voltage errors and maximum node voltage error in current iteration are calculated and the optimum voltage error as well as maximum iteration criteria are checked. If the maximum iteration criterion is met (i.e., $T = T_{max}$), then the process stops without any convergence i.e., convergence is not achieved.

The governing equations of this method are:

$$|I[F_B(i,j)]_{new}| = \frac{|V[F_N(i,j)]_{old}| - |V[F_N(i,j+1)]_{old}|}{|Z[F_B(i,j)]|} \tag{42}$$

$$L_P[F_B(i,j)]_{new} = |I[F_B(i,j)]_{new}|^2 . R[F_B(i,j)] \tag{43}$$

$$L_Q[F_B(i,j)]_{new} = |I[F_B(i,j)]_{new}|^2 . X[F_B(i,j)] \tag{44}$$

$$|V[F_N(i,j+1)]_{new}| = |V[F_N(i,j)]_{new}| - \frac{\sqrt{(P_S[F_B(i,j)])_{new}{}^2 + (Q_S[F_B(i,j)])_{new}{}^2}}{|V[F_N(i,j)]_{new}|} . Z[F_B(i,j)] \tag{45}$$

where, $i = 1, 2, \dots, T_N$ and $j = 1, 2, \dots, N(i) - 1$ for $\boldsymbol{F_B}$ matrix elements and $i = 1, 2, \dots, T_N$ and $j = 1, 2, \dots, N(i)$ for $\boldsymbol{F_N}$ matrix elements.

$V[F_N(i,j)]$, $I[F_B(i,j)]$, $L_P[F_B(i,j)]$ and $L_Q[F_B(i,j)]$ are the relevant node voltage, line current, line active and reactive power losses, respectively. The active and reactive power flows from the $[F_B(i,j)]$ branch are $P_S[F_B(i,j)]$ and $Q_S[F_B(i,j)]$, respectively, which are dependent upon the values of $L_P[F_B(i,j)]$, $L_Q[F_B(i,j)]$, $P_L[F_N(i,j)]$, $Q_L[F_N(i,j)]$ and the system configuration. $P_L[F_N(i,j)]$ and $Q_L[F_N(i,j)]$ are the load active and reactive powers connected to the $[F_N(i,j)]$ node. The subscript $'new'$ represents the running iteration of power flow, whereas subscript $'old'$ denotes the previous iteration.

3.6 Particle Swarm Optimization (PSO) Technique

PSO [Asadi and Kouhsari,2009] is a populace motivated process which has a good similarity with the actions of the flight of birds searching for nutrition in a search space. The entire populace is called the swarm and distinct members of the swarm are called particles. In contrast to the conventional optimization techniques, PSO gives quicker convergence, identification of global optima in presence of local optima along with the features of easiness in programming and flexibility for the constrained problems [Qian et al., 2007; Qu et al., 2020].

The governing equations for PSO algorithm are:

$$V_e(i_t) = \omega(i_t).V_e(i_t - 1) + c_1.r_1.\big(P_e(i_t - 1) - X_e(i_t - 1)\big) + c_2.r_2.\big(G(i_t - 1) - X_e(i_t - 1)\big) \quad (46)$$

and

$$X_e(i_t) = X_e(i_t - 1) + V_e(i_t) \quad (47)$$

where, X_e and V_e signify the position and velocity of the e^{th} particle, respectively. They are presented by $X_e = [x_{e1}, \dots, x_{ep}]$ and $V_e = [v_{e1}, \dots, v_{ep}]$, respectively. These are the arrays containing the position and velocity of the e^{th} particle. P_e and G are the

arrays encompassing the local best position of the e^{th} particle and global best position of the swarm ever visited in each iteration, respectively. i_t signifies the current iteration number and $(i_t - 1)$ indicates the previous iteration number. $1 \leq i_t \leq i_{tmax}$. i_{tmax} is the maximum iteration number. When $i_t = 1$, the $V_e(i_t - 1)$, $X_e(i_t - 1)$, $P_e(i_t - 1)$ and $G(i_t - 1)$ present $V_e(0)$, $X_e(0)$, $P_e(0)$ and $G(0)$, respectively. These are the 0^{th} iteration (initial) values of velocity, position, best position of e^{th} particle and global best position of the entire swarm. Before starting the iteration process, initialization of all the particles' position, velocity, particles' best position and global best position of the entire swarm is accomplished. The entire swarm size or population of all the particles is denoted by n_{pop}. Therefore, $1 \leq e \leq n_{pop}$. At first, x_{e1} to x_{ep} (the positions of p numbers of decision variables) of all the particles are initialized by generating random values in p dimensional search space. Velocities (V_e values) of all the particles are initialized by storing zeros. After initialization of particles' position and velocity arrays, the objective (or fitness) function values for all particles are calculated. Particle's best position P_e is initialized by assigning the same initial random values stored inside the X_e array for all particles. Particle's initial objective function value is stored inside the particle's best objective function array for initialization. Global best objective function is initialized by taking (0) or (inf) for the maximization and minimization problems, respectively. Gradually, with the initialization of each particle's best values; continuous updating of global best values (global best position G and global best objective function value) for the entire swarm is completed to achieve the final initialized global best values. ω is the inertia coefficient. At first iteration, usually its value is taken as 1 for the entire swarm and gradually at successive iterations, its value decreases to almost zero if damping inertia coefficient, ω_{damp} is introduced. $\omega(i_t) = \omega(i_t - 1).\omega_{damp}$. c_1 and c_2 are the cognitive and social parameters, respectively. $r_1$and r_2 denote random numbers. Figure 15 presents the flow chart of the PSO algorithm utilized in the proposed work.

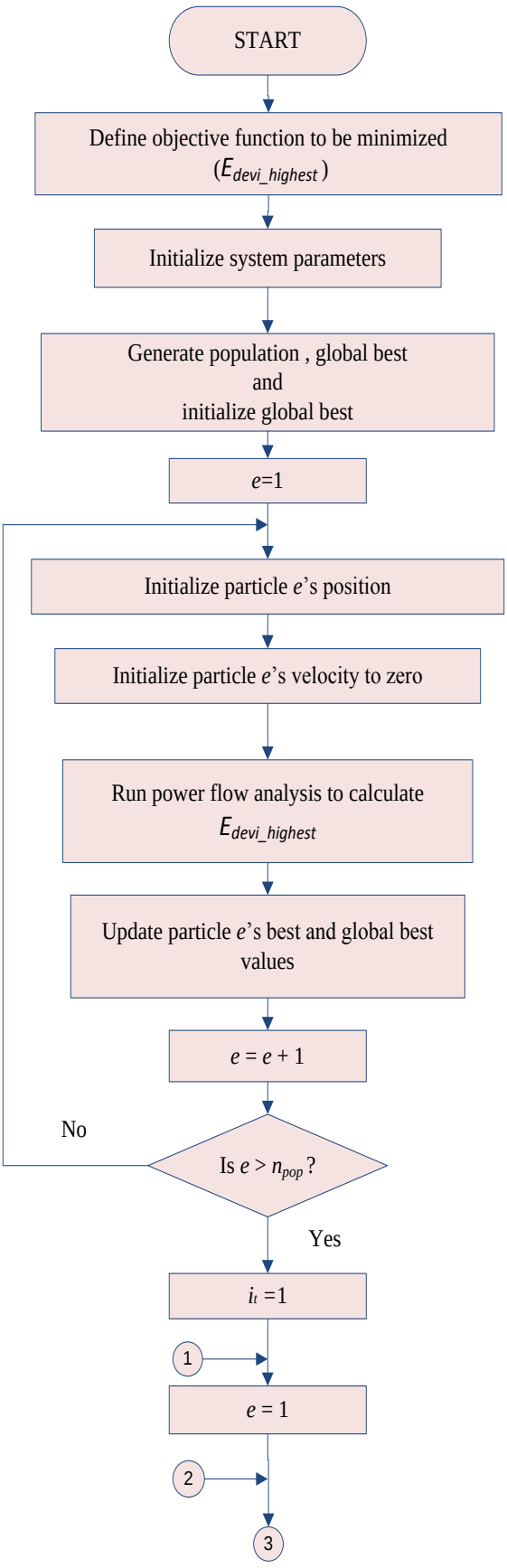
START
Define objective function to be minimized ($E_{devi\_highest}$)
Initialize system parameters
Generate population , global best and initialize global best
e=1
Initialize particle e's position
Initialize particle e's velocity to zero
Run power flow analysis to calculate $E_{devi\_highest}$
Update particle e's best and global best values
e = e + 1
No
Is $e > n_{pop}$?
Yes
i_t =1
1
e = 1
2
3

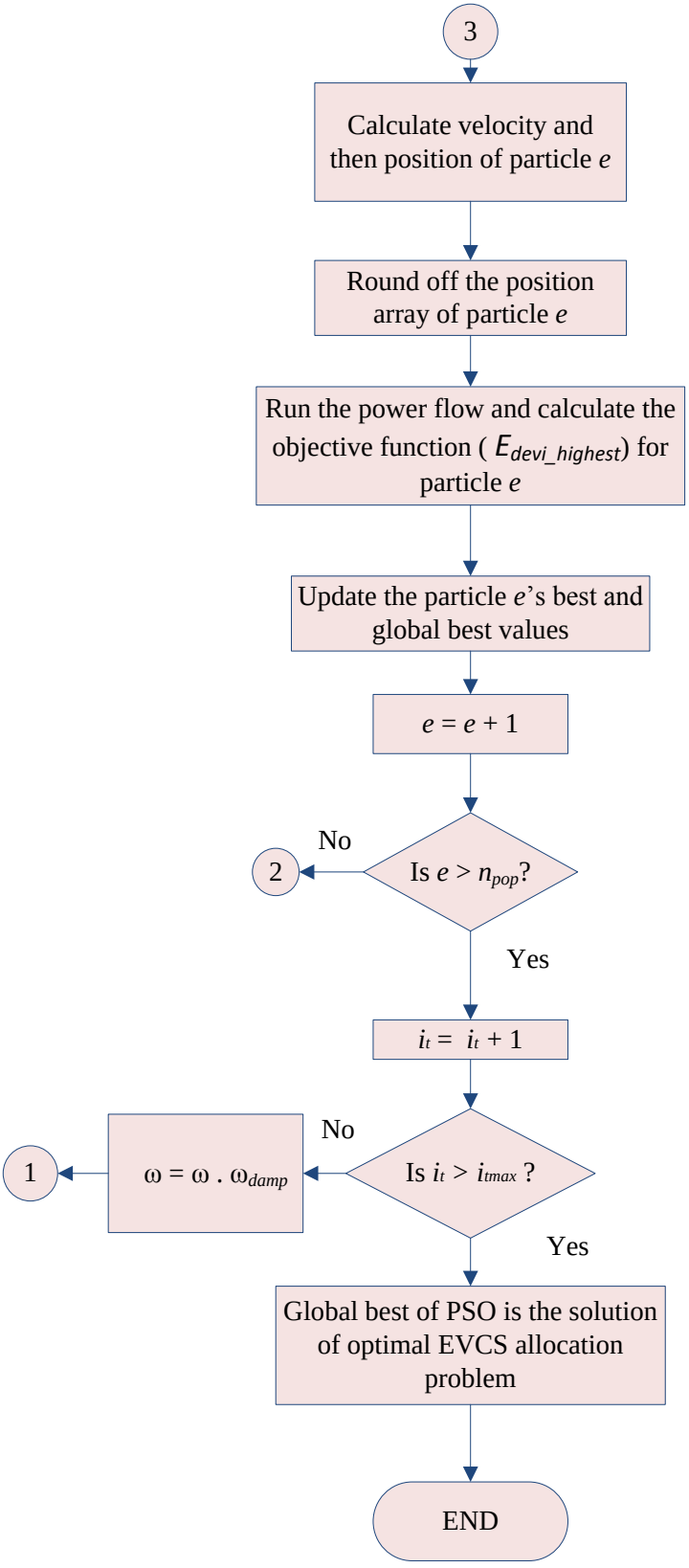

Figure 15. Flow chart of the proposed PSO technique

3.7 Powell's Particle Swarm Optimization (PPSO) Technique

PPSO is an enhanced version of conventional PSO algorithm through amalgamation of powell's technique [Yang et al., 2017; Narang et al., 2017]. It is preferred over conventional PSO for enhanced convergence along with accurate global optimum solution. The population (number of particles) generated is presented by *s*. The particle is denoted by the index g where,$1 \leq g \leq$ s The number of decision variables is p for each particle (p dimensional search space). The iteration number is set to 1 i.e., $t_{PPSO} = 1$. After population generation and parameter initialization, updating of the velocities and positions of all the particles is accomplished by the following equations:

$$V_g(t_{PPSO}) = \omega(t_{PPSO}).V_g(t_{PPSO}-1) + c_{1PPSO}.r_{1PPSO}.\Big(L_g(t_{PPSO}-1) - X_g(t_{PPSO}-1)\Big) + c_{2PPSO}.r_{2PPSO}.\Big(G(t_{PPSO}-1) - X_g(t_{PPSO}-1)\Big) \quad (48)$$

and

$$X_g(t_{PPSO}) = X_g(t_{PPSO}-1) + V_g(t_{PPSO}) \quad (49)$$

The current local best position of g^{th} particle $L_g(t_{PPSO})$ and the global best position of the entire swarm $G(t_{PPSO})$ are calculated by computing fitness function (which is a function of $X_g(it_{PPSO})$) for all particles and updating the particles' local best values as well as global best value of the entire swarm. At this juncture, it is worth mentioning that particles' local best positions and global best position of the entire swarm are *p* dimensional arrays (as search space is *p* dimensional). $\omega(t_{PPSO})$ is the inertia coefficient at running iteration. c_{1PPSO} and c_{2PPSO} are the cognitive and social parameters, respectively. r_{1PPSO} and r_{2PPSO} are the random numbers generated. After completion of PSO portion of PPSO algorithm, powell algorithm is initiated by setting $P_0 = G$. Linearly independent directions are taken as $[d_1, d_2, \dots, d_P]$ (=d_{pop}). Each of these directions is a p dimensional array. The next step is to generate the population by calculating λpop (a constant) in such a way that $f\big(P_{pop-1} + \lambda_{pop}.d_{pop}\big)$ is minimum and henceforth, setting is done as $P_{pop} = (P_{pop-1} +$

$\lambda_{pop}.d_{pop}$) for $pop = 1, 2, \dots, p$.

After setting up the powell's population, the integer a is calculated in such a way that $f(P_{a-1}) - f(P_a)$ is maximum, where $1 \leq a \leq p$.

The next step is to evaluate: $\Delta = f(P_{a-1}) - f(P_a), f_3 = f(2P_p - P_0), f_2 = f(P_p), f_1 = f(P_0)$

After calculating the values of Δ, f_1, f_2 and f_3; the next job is to check whether both equations (50) and (51) are satisfying simultaneously or not.

$$f_3 < f_1 \tag{50}$$

and

$$(f_1 - 2f_2 + f_3)\,(f_1 - f_2 - \Delta)^2 < 0.5\,\Delta((f_1 - f_3)^2 \tag{51}$$

If yes, then ζ is taken as $\zeta = (P_p - P_0)$ and λ is calculated such that, $f(P_p + \lambda\,\zeta)$ is minimum. Henceforth, the $d_a$value is set to $d_a = \zeta$ and $[d_1, d_2, \dots, d_a, \dots, d_p]$ are considered as new directions for the next iteration. $(P_p + \lambda\,\zeta)$ is taken as the starting point, i.e.,$P_0 = (P_p + \lambda\,\zeta)$ in $t_{PPSO} = (t_{PPSO} + 1)$ if next iteration is required. If equations (50) and (51) don't satisfy simultaneously, then old directions $[d_1, d_2, \dots, d_p]$ are considered as new directions along with $P_0 = P_p$ in next iteration, if required. After completion of the powell portion of PPSO algorithm, the updated P_0 value is used to find out $f(P_0)$. This value is then compared with $f(G)$ corresponding to previously obtained global best position (G). If f$(P_0) < f(G)$, then the newly revised global best position of the entire swarm for the current iteration is $G = P_0$ and the corresponding fitness function is $f(G) = f(P_0)$. Otherwise, the global best (G) value of the entire swarm for the current iteration will remain same as achieved previously. If the termination criterion is not satisfied, the iteration number t_{PPSO} is set to $t_{PPSO} = (t_{PPSO} + 1)$ and the next iteration is initiated by updating the velocities and positions of all the particles as before. Figure 16 illustrates the flow chart of the proposed PPSO algorithm.

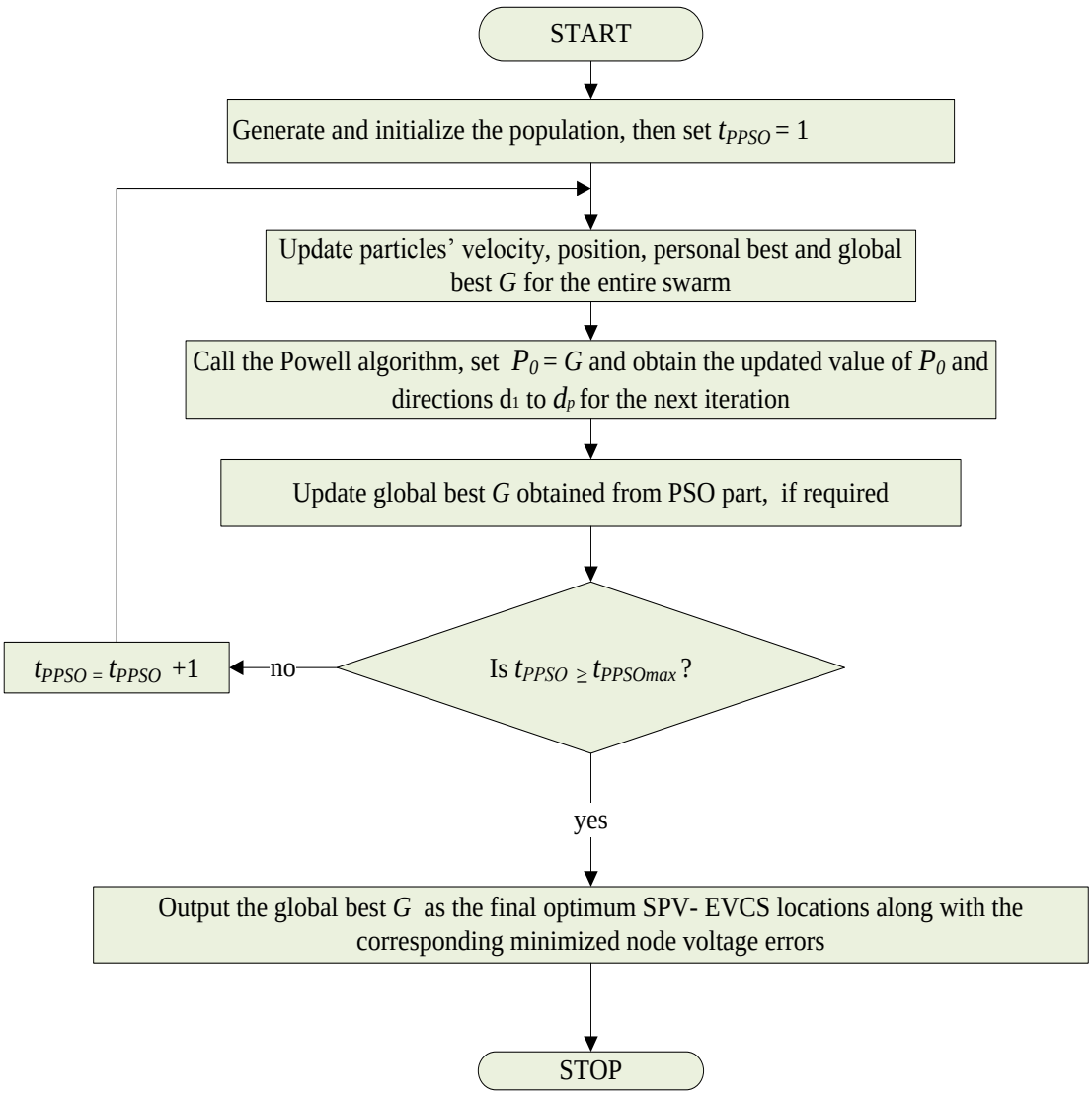

Figure 16. Flow chart of the proposed PPSO technique

3.8 Improved New Binary Particle Swarm Optimization (INBPSO) Technique

The conventional PSO optimization technique has several advantages and disadvantages. One of the major drawbacks of the technique is it is a population-driven evolutionary algorithm mainly used in continuous domain [Nezamabadi-pour et al., 2008]. This method is not suitable for discrete domain without any further modification, as constant updating of the particles' velocities and positions leads to the results falling in the category of rational numbers, which are continuous in

nature. For this reason, the global optima obtained in each iteration must be rounded off to the nearest natural number for optimum EVCS allocation purpose. The best suitable technique for solving problems related to discrete domain, where the decision variables only can take up some discrete values within a pre-defined set in the search space, is the BPSO technique. Unlike the conservative PSO, the BPSO technique generates and uses the strings of binary numbers [0, 1] for each decision variable [Nezamabadi-pour et al., 2008]. These strings of decision variables having a finite string length are placed side by side (row-wise) in a matrix to form the dimension of each particle of the population. As each binary string gives birth to a natural number by binary to decimal conversion, the results are discrete in nature. Thus, it's a very powerful tool to solve optimization problems related to discrete domain. The optimum EVCS allocation problem falls under the category of discrete domain as the system nodes are all-natural numbers, which are discrete in nature. Thus, the best fit for the solution of this problem is BPSO technique. But, due to some shortfalls encountered by the BPSO technique like a) very high probability (near to 1) due to high positive velocity b) very low probability (near to 0) due to high negative velocity c) probability of 0.5 instead of zero value at zero velocity d) the trapping of output in local optima instead of achieving the global optima due to the problem mentioned at point c e) opposition to convergence due to change in particle position bits without consideration of the previously stored bits; this technique is often avoided [Nezamabadi-pour et al., 2008]. To overcome the problems associated with BPSO, INBPSO method is introduced which is a modification over the conventional BPSO method to get the required benefits [Nezamabadi-pour et al., 2008].

Unlike the BPSO, the INBPSO technique uses modified equations for the probability and new position calculation. The ruling equations for this technique are:

$$v_{fd}(t_{INBPSO}) = \omega(t_{INBPSO}).v_{fd}(t_{INBPSO}-1) + c_{1INBPSO}.r_{1INBPSO}.\left(p_{bestfd}(t_{INBPSO}-1) - x_{fd}(t_{INBPSO}-1)\right) + c_{2INBPSO}.r_{2INBPSO}.\left(g_{bestd}(t_{INBPSO}-1)\right) \quad (52)$$

where, $v_{fd} \epsilon [+v_{max}, -v_{max}]$

$$\omega(t_{INBPSO}) = \omega_{max} + ((\omega_{min} - \omega_{max}).\frac{(t_{INBPSO}-1)}{(t_{INBPSOmax}-1)} \quad (53)$$

where, $\omega_{min} \leq \omega(t_{INBPSO}) \leq \omega_{max}$

$$S\left(v_{fd}(t_{INBPSO})\right) = Sigmoid\ \left(v_{fd}(t_{INBPSO})\right) = 1/(1 + e^{-\,v_{fd}(t_{INBPSO})}) \quad (54)$$

$$S'\left(v_{fd}(t_{INBPSO})\right) = 2.\left|Sigmoid\ \left(v_{fd}(t_{INBPSO})\right) - 0.5\right)| \quad (55)$$

$$S''\left(v_{fd}(t_{INBPSO})\right) = A + (1 - A).S'\left(v_{fd}(t_{INBPSO})\right) \quad (56)$$

$$A = h.(1 - e^{\frac{-F}{\tau}}) \quad (57)$$

The syntax used for updating the x_{fd} values is shown in Figure 17.

```
.
.
If        rand() < S''(v_fd(t_INBPSO))
then
x_fd(t_INBPSO) = exchange x_fd(t_INBPSO − 1)
else
x_fd(t_INBPSO) = x_fd(t_INBPSO − 1)
end
.
.
```

Figure 17. Syntax for updating the x_{fd} values

Here, v_{fd}, x_{fd}, p_{bestfd} and g_{bestd} are the d^{th} dimensional elements of the f^{th} particle's velocity, position, local best position, and global best position of the swarm, respectively. For holding the elements of all particles including the f^{th} particle, corresponding matrices are formed. The f^{th} row elements of these matrices are:

$V_f = [v_{f1}, \dots, v_{fd}, \dots, v_{iD}]$, $X_f = [x_{f1}, \dots, x_{fd}, \dots, x_{iD}]$, $P_{bestf} = [p_{bestf1}, \dots, p_{bestfd}, \dots, p_{bestfD}]$ and $G_{best} = [g_{best1}, \dots, g_{bestd}, \dots, g_{bestD}]$.

The d^{th} dimensional elements of particle f for all these aforesaid matrices except the velocity matrix are the binary bits, which are confined in binary domain only i.e., they can only take up the values [0,1]. The elements of velocity array are rational numbers. The maximum and minimum allowable range of these elements are $+v_{max}$ and $-v_{max}$ as mentioned in equation (52). Each decision variable has a string length L and the total number of such decision variables is n_{var}. The n_{var} is equal to p i.e., the total number of EVCSs to be allocated optimally mentioned earlier. Henceforth, the maximum dimension of each particle f denoted by D is evaluated by the equation:

$$D = L.n_{var} \tag{58}$$

d is the dimension index and $1 \leq d \leq D$. $\omega(t_{INBPSO})$, $c_{1INBPSO}$, $c_{2INBPSO}$, $r_{1INBPSO}$, $r_{2INBPSO}$ and $rand()$ are the inertia coefficient, cognitive parameter, social parameter, and three randomly generated numbers in between the interval [0, 1], respectively. $\omega(t_{INBPSO})$ is a variable coefficient whose value gradually decreases at successive iterations following equation (53). S, $S'$and S'' are the sigmoid, new, and improved new probability functions of v_{fd}, respectively. S' function is introduced to resist itself from taking the values near to 1 for highly positive v_{fd} and near to 0 for highly negative v_{fd} unlike the sigmoid probability function S. Moreover, when all particles are stirring towards the best position (p_{bestfd}), the velocities of the particles are zero. For $v_{fd} = 0$, S is 0.5, but S' is 0 for which, S'' becomes A. A is a tunable factor introduced for preventing the stagnation of the optimization algorithm. h is a constant. τ is the time constant defined based on the facet of the algorithm. F is called the failure contour. The occurrence of a failure means the particle's local best value or global best value of the entire swarm is not improving further. This condition denotes that the algorithm is trapped in local optima. Because of the failure, F is incremented. As a result, A becomes nonzero (increases) and following equation (56), mutation occurs in the probability function

to pull out the optimum value out of the local optima. If success is achieved, i.e., the optimum solution is not trapped in local optima, then $_F$ is 0 and in turn, A becomes 0. Henceforth, $S' = S''$ i.e., mutation is not required. Henceforth, the mutation of the probability function facilitates an opportunity to the INBPSO algorithm not to fence in the local optima and look for a new solution. t_{INBPSO} is the current iteration number and $(t_{INBPSO} - 1)$ signifies the previous iteration number of the INBPSO. $1 \leq t_{INBPSO} \leq t_{INBPSOmax}$. $t_{INBPSOmax}$ is the maximum iteration number of the proposed INBPSO technique. When t_{INBPSO} =1, then $v_{fd}(t_{INBPSO} - 1)$, $x_{fd}(t_{INBPSO} - 1)$, $p_{bestfd}(t_{INBPSO} - 1)$ and $g_{bestd}(t_{INBPSO} - 1)$ present $v_{fd}(0)$, $x_{fd}(0)$, $p_{bestfd}(0)$ and $g_{bestd}(0)$ values, respectively. These are the 0^{th} iteration (initial) values of the d^{th} dimensional elements of f^{th} particle's velocity, position, best position, and global best position of the entire swarm. Figure 18 represents the flow chart of the proposed INBPSO algorithm.

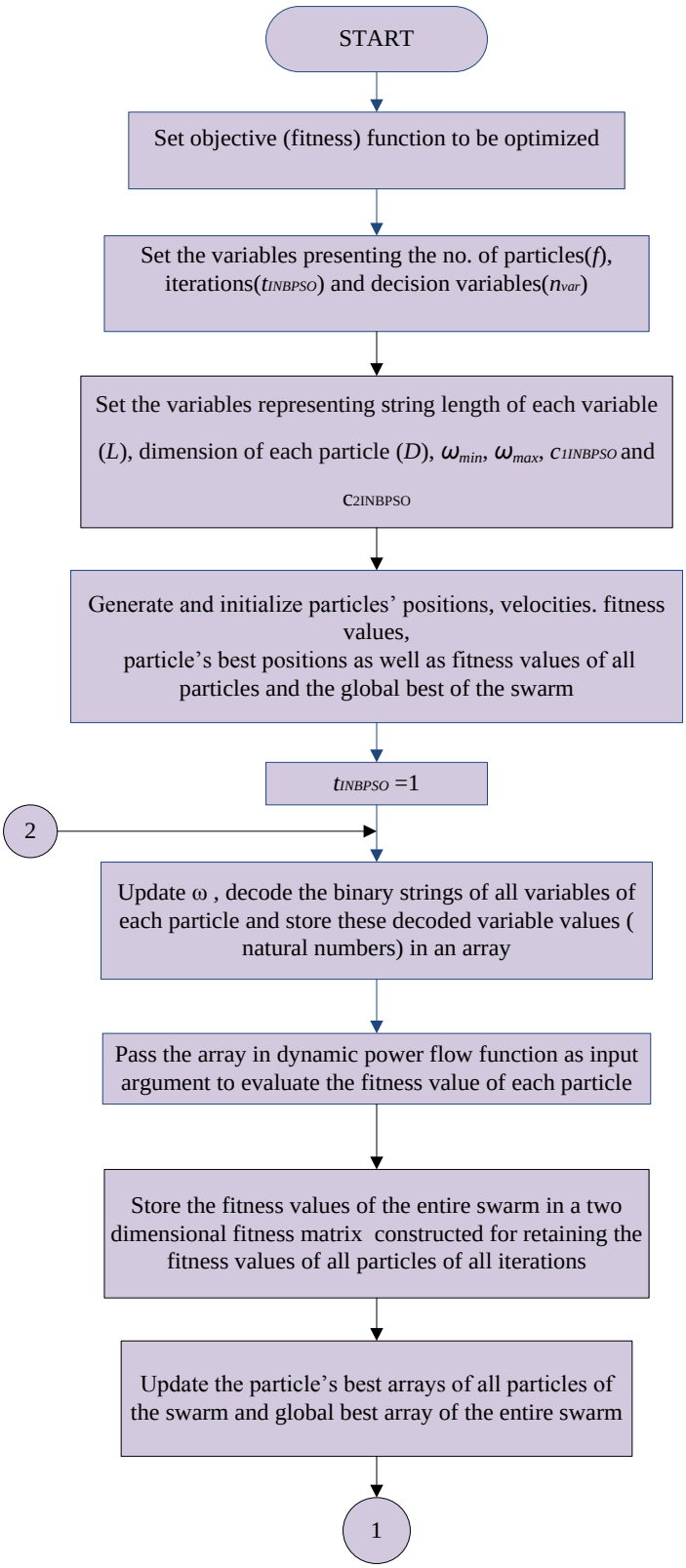
START
Set objective (fitness) function to be optimized
Set the variables presenting the no. of particles(f), iterations(t_{INBPSO}) and decision variables(n_{var})
Set the variables representing string length of each variable (L), dimension of each particle (D), ω_{min}, ω_{max}, $c_{1INBPSO}$ and $c_{2INBPSO}$
Generate and initialize particles' positions, velocities. fitness values,
particle's best positions as well as fitness values of all particles and the global best of the swarm
t_{INBPSO} =1
2
Update ω , decode the binary strings of all variables of each particle and store these decoded variable values (natural numbers) in an array
Pass the array in dynamic power flow function as input argument to evaluate the fitness value of each particle
Store the fitness values of the entire swarm in a two dimensional fitness matrix constructed for retaining the fitness values of all particles of all iterations
Update the particle's best arrays of all particles of the swarm and global best array of the entire swarm
1

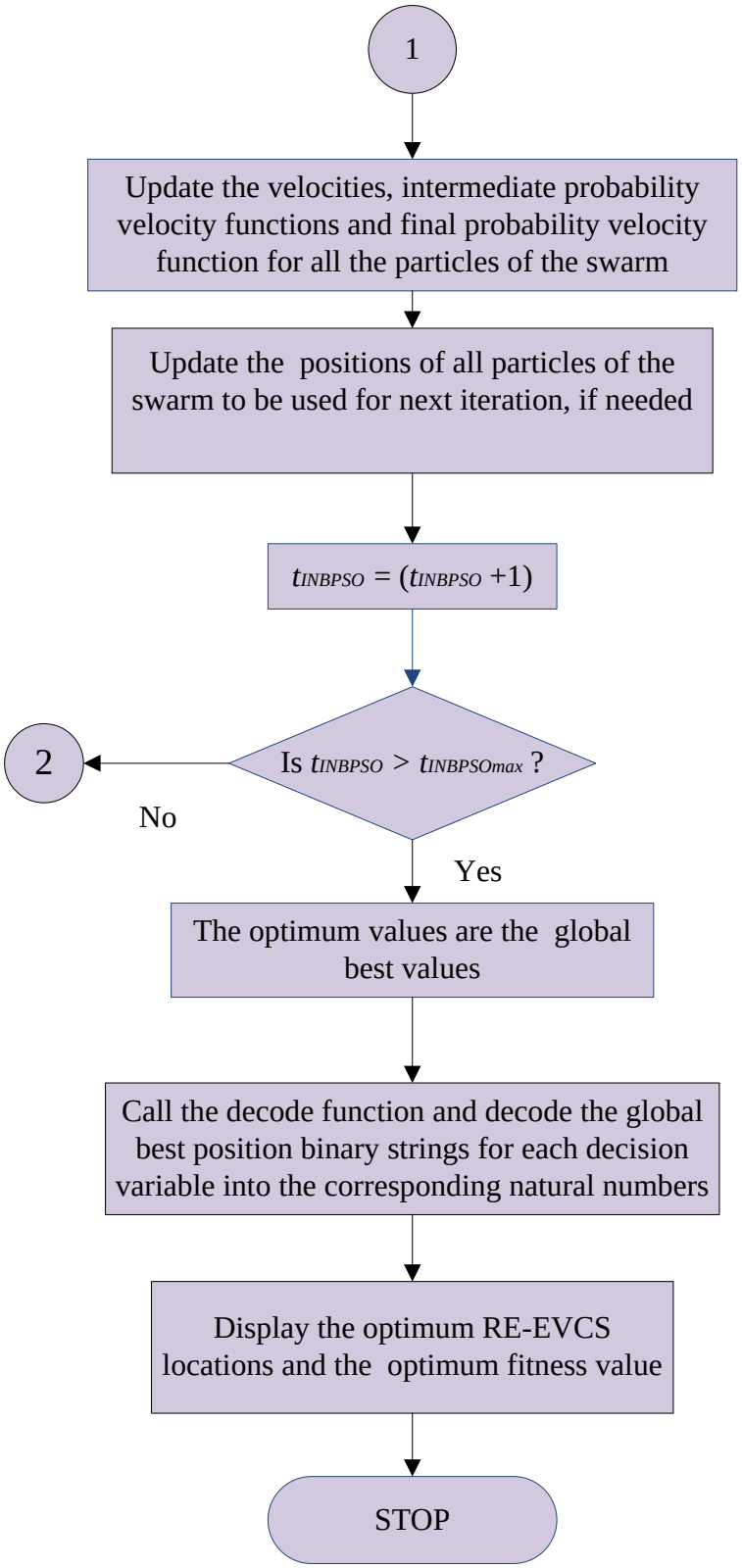

Figure18. Flow chart of the proposed INBPSO technique

3.9 Genetic Algorithm (GA)

GA is a very prevalent evolutionary optimization method invented by Holland in 1975 [Yang, 2020; Katoch et al., 2020]. It is a recurrently castoff method to discover the optimal as well as near-optimal solutions to tough problems which else would yield an era to solve. Most commonly, it is used to solve innumerable optimization difficulties related to engineering investigation and machine learning. Multi objective optimization can easily be tackled with this technique [McCall, 2005; Mirjalili, 2019]. Nature is always an inordinate basis of encouragement to manhood. GA is a search-oriented procedure founded on the ideas of natural choice and genetics. Nevertheless, GA is a subdivision of a considerably grander branch of computing acknowledged as evolutionary algorithm. This evolutionary technique has been established by John Holland along with his coworkers and students at the University of Michigan [Yang, 2020]. In GA, a population or pool of conceivable solutions (sets of chromosomes) to a given problem is prepared first. Each chromosome consists of genes. During successive iterations (like generations in biological genetics), these probable solutions undertake recombination in between the parent chromosomes and transformation in the same parent chromosome itself, thus replicating the behavior or process that occurs in case of natural genetics. The outcome of these aforesaid processes is the creation of new children. Each chromosome (or candidate solution) is allotted a fitness value. This fitness value is calculated by constructing a suitable objective function. The chromosomes having better fitness values are facilitated with a greater opportunity to mate and produce more fitter off-springs. In a nutshell, it can be commented that, the technique follows the Darwinian Theory, extensively used in genetics which establishes the popular concept 'Survival of the Fittest'. This is how, at successive iterations (generations), better individuals or solutions get evolved, till the stopping criterion is met. Though GA is adequately randomized by its natural attribute, but it has the capability to perform much better than the previously used random local search technique, where several trials of numerous random solutions are accomplished while keeping track of the best one ever achieved. Another notable difference in between the random local search technique and GA is unlike the random local search, GA doesn't require

storing of huge historical information from the very beginning. Only the information regarding the parents is sufficient to produce quality children from the previous generation. The process for producing quality or fitter off-springs is based on selection, mutation, and crossover techniques in between the parents. The lucrative and advantageous features facilitated by GA are [Katoch et al., 2020]:

• No previous system information is required for starting the optimization.
• It is faster and competent compared to the outdated methods.
• It has a highly efficient parallel processing proficiency.
• It is suitable for optimizing in both continuous and discrete domains equally.
• It is very much appropriate for multi-objective optimization.
• It provides multiple solutions, not just a single solution.
• Always an intermediate solution set is achieved at every generation and the solution set keeps on improving over the time.
• Beneficial for the very large search space, where a hefty number of constraints are involved.
• The offspring is generated from the best parents (elite chromosomes) to provide a faster convergence towards the global minima.

However, GA has some limitations like the other optimization methods. These are:

• It is not appropriate for all problems, especially simple problems where an ample amount of information is available.
• As fitness of each chromosome of the entire population is evaluated recurrently in each generation (iteration), this method is computationally laborious for some problems.
• Due to stochastic feature, sometimes optimum solution along with its' quality is not guaranteed.
• Skillset is required for implementing this technique accurately, otherwise GA will lack of convergence to the optimal result.

The general syntax of GA is shown in Figure 19.

.

.

$$[\,x, fval\,] = ga(\,@fitnessfunction, nvars, \tilde{A}, \tilde{b}\,, A_{eq}, b_{eq}, lb, ub, options)$$

$$options = optimoptions\,('ga', 'PlotFcn', \{@plotfun1, @plotfun2, \ldots\})$$

.

.

Figure 19. The general syntax of GA

x is the array for storing the optimum values of the decision variables. $fval$ array stores the optimum value of the fitness function. $nvars$ array holds the total number of decision variables to be fed into the fitness function. $\tilde{A}$ and $\tilde{b}$ are the matrix and array for holding the linear inequality constraints, whereas A_{eq} and b_{eq} are the corresponding matrix and array for storing the linear equality constraints. lb and ub arrays contain the lower and upper limits of the decision variables. $options$ array outputs different plots as per the user choice. $optimoptions$ and $PlotFcn$ are the in-built functions used to outline various plots as per the plot functions available in GA MATLAB environment. These several plot functions are denoted by $plotfun1$, $plotfun2$, etc.

The steps involved in GA are:

Initial population generation: Before starting the optimization, initial population is generated either by choosing random values amongst the higher and lesser bounds of the independent decision variables in the p dimensional search space or by providing the initial values of these variables.

Evaluation: Evaluation is the process by which the fitness function of a chromosome (objective function) is evaluated based on the values of the decision variables (genes) present inside it. Each member of the population (chromosome) is assigned a fitness value. This fitness value is the driving force of the entire evaluation process as it

regulates individual chromosome's environmental adaptation capability and survival probability in the succeeding generation.

Selection: Selection is the procedure of choosing parentages for mating and recombining in a view of fulfilling the objective of creating children for the next generation. In this context, the selection process is very vital for achieving a good convergence rate as only good parents can produce quality off-springs which can lead the problem to healthier solutions. Nevertheless, utmost care should be taken to stop one tremendously suitable solution from dominating the whole population within an insufficient number of generations. The reason behind this protective measure is to maintain diversity among the chromosomes of a population. Sustaining good amount of variety in the population is tremendously critical for the feat of the anticipated process. The domination of the whole populace by only one awfully acceptable solution is called early convergence which is an objectionable condition. There are different methods available for parent selection. In between them, one of the most prevalent method is fitness proportionate selection technique. In this method, every chromosome gets a chance to turn out to be a parent with a likelihood proportionate to its fitness value. Consequently, healthier chromosomes own a higher prospect of pairing and spreading their attributes to the subsequent generation. Nevertheless, this strategy imposes a selection compression to the more suitable chromosomes within the population, sprouting better chromosomes over the period. There are two varieties of fitness proportionate selection named roulette wheel selection (RWS) and stochastic universal sampling (SUS). But the major shortfall of this method is its incapability for solving the problem where the fitness value may become negative. To overcome this difficulty, other selection functions have been developed. Amongst them, the K-Way tournament selection function is an extremely popular one, which randomly picks K number of chromosomes from the population and selects the best of them as a parent in first trial. The same procedure is repeated at successive trials for deciding on the next parents. Rank selection (RS) method is another popular method which can also deal with negative fitness values and is best suited for the entities having very close fitness values. Therefore, each chromosome has roughly the similar likelihood of getting nominated as a parent irrespective of

their relative fitness values if fitness is the key factor for selection. Henceforth, the selection pressure upon the healthier chromosomes reduces considerably thus leading GA to select poor parents. To overcome this difficulty, the concept of fitness is replaced by the rank. Every chromosome is graded conferring to the fitness value attained by it. The parent selection is dependent upon the rank of each chromosome and not their fitness values. The higher ranked chromosomes have higher chances to get selected. Random selection is another type of selection process where the parents are randomly selected from the population. There is no such organized set of rules like the other previously mentioned selection techniques. There is no selection pressure upon the healthier chromosomes. Hence, this approach is usually not followed.

Crossover: After completion of selection process, the main process of generating off-spring gets started. The crossover is comparable to the biological crossover i.e., reproduction. During this process, multiple groups of parents (chromosome pairs) are nominated, thus giving birth to one/more children with the gene (genetic substance) belonging to the parents. It is usually applied with a high probability. There are several methods of crossover like scattered, constraint dependent, two-point, single-point, heuristic, intermediate and arithmetic. One-point crossover is a prevalent one, where a crossover point is randomly chosen. Afterwards, the ends of the two selected parents are exchanged to generate new off-springs. Multi point crossover is another widespread crossover method where, more than one crossover points are chosen simultaneously. Alternating segments of two parents undergoing crossover are exchanged to generate new off-springs.

Mutation: Mutation is another prime process of offspring production, where a small random twist is introduced in the chromosome, for getting a fresh solution. It is cast-off for sustaining diversity by incorporating some variations in the population. It usually has a low probability. Mutation arbitrarily picks up few chromosomes from the population and makes few amendments in their characteristics. The in-built mutation functions are constraint dependent, gaussian, uniform and adaptive feasible.

3.10 MATLAB/Simulink Model for Multiple SPV-EVCS Integrated Distribution Network:

3.10.1 Model description

For power management study, three identical SPV-EVCSs are designed with an ESU installed inside each EVCS for storing the excess energy from the associated PV array. The optimum node numbers obtained from a case study regarding the optimum allocation of EVCSs are chosen for power injection into the distribution system.

Each EVCS is primarily getting power from the integrated PV panel. The PV panels are connected to the DC link buses inside each EVCS. For one EVCS under consideration, the DC link bus is connected to the input of the three-phase inverter. The inverter converts the DC power to three-phase AC power. The three-phase AC output of the inverter is passing through the L-C filter (three-phase) and a three-phase transformer before feeding to the distribution network. The power factor and the magnitude of the current supplied to the distribution network is controlled by the inverter triggering voltage controller based on *d-q* theory. Active and reactive power control is achieved as per the requirement.

On the other side, the DC link bus relates to two cascaded buck converters, which are controlled by PID controllers for the desired output voltages. At the output of the first buck converter, the ESU is connected. The ESU is charged at 400 V. The PID controller is designed to maintain its output voltage at 400 V. The voltage requirement of EV charging is considered as 48 V. Hence, a second stage buck converter is designed to reduce the DC voltage level to 48 V. Figure 20 presents the MATLAB/Simulink model of the proposed multiple SPV-EVCS integrated distribution network. Figure 21 shows internal architecture of the developed model. Figures 22(a) and 22(b) present the *d-q* component segregation using phase locked loop (PLL) and *d-q* power control circuit developed for active and reactive power regulation.

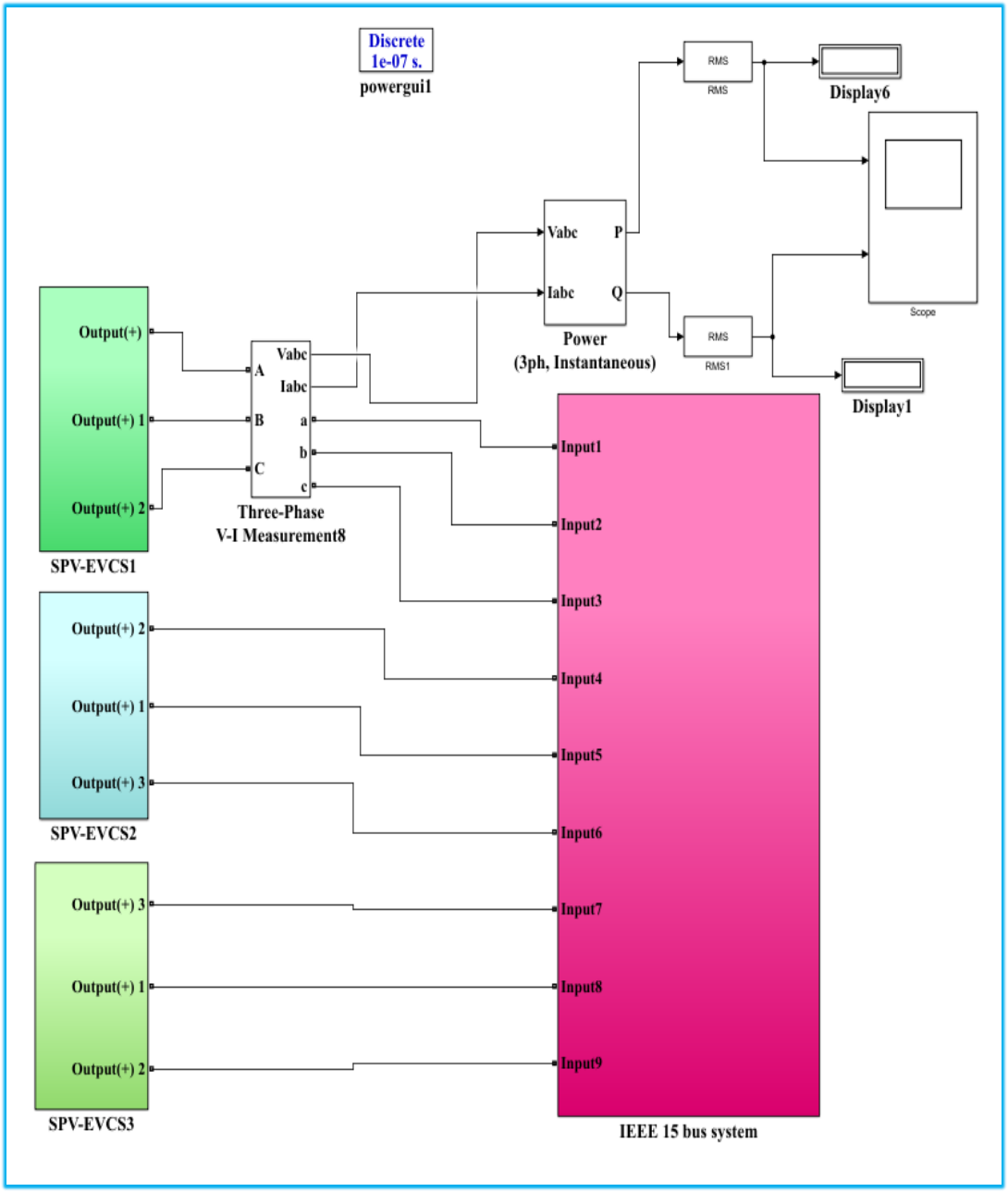

Figure 20. Simulink model of the proposed multi SPV-EVCSs integrated distribution network (main model)

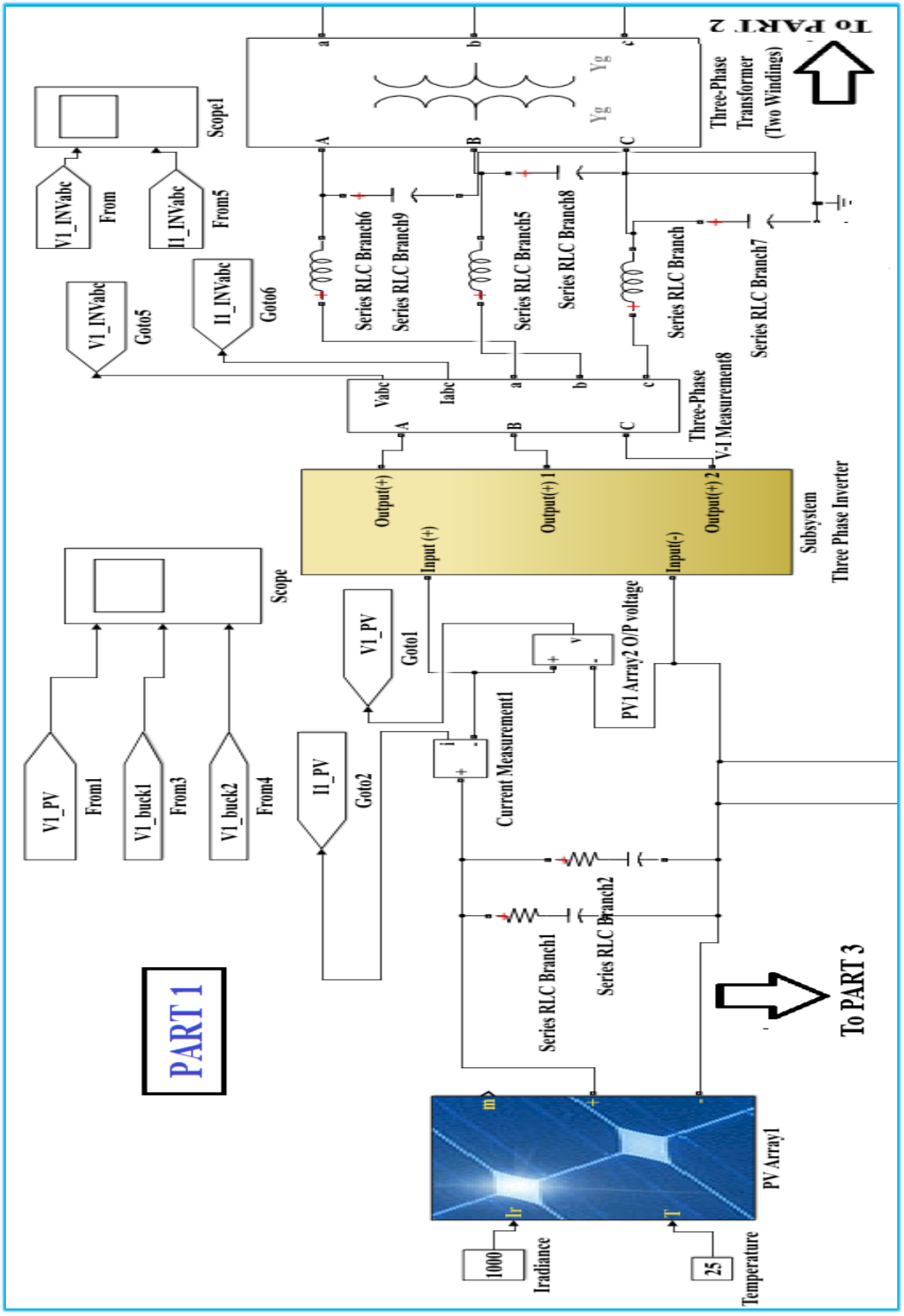

Figure 21. Internal architecture of the developed model (part 1)

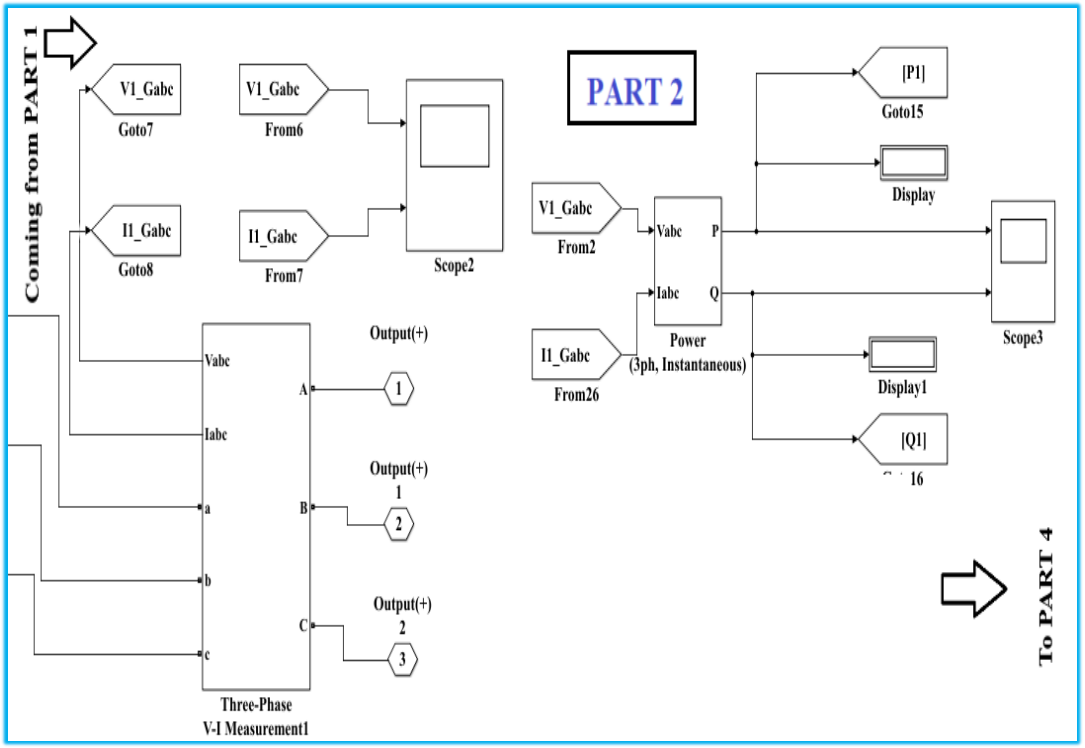

Figure 21. Internal architecture of the developed model (part 2)

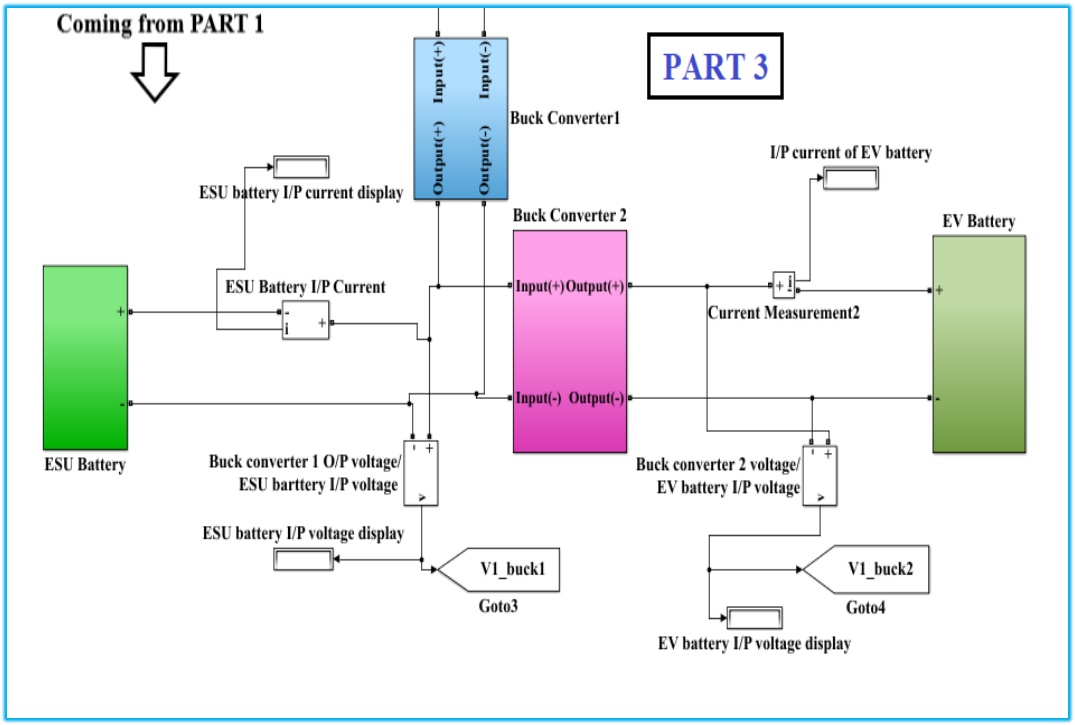

Figure 21. Internal architecture of the developed model (part 3)

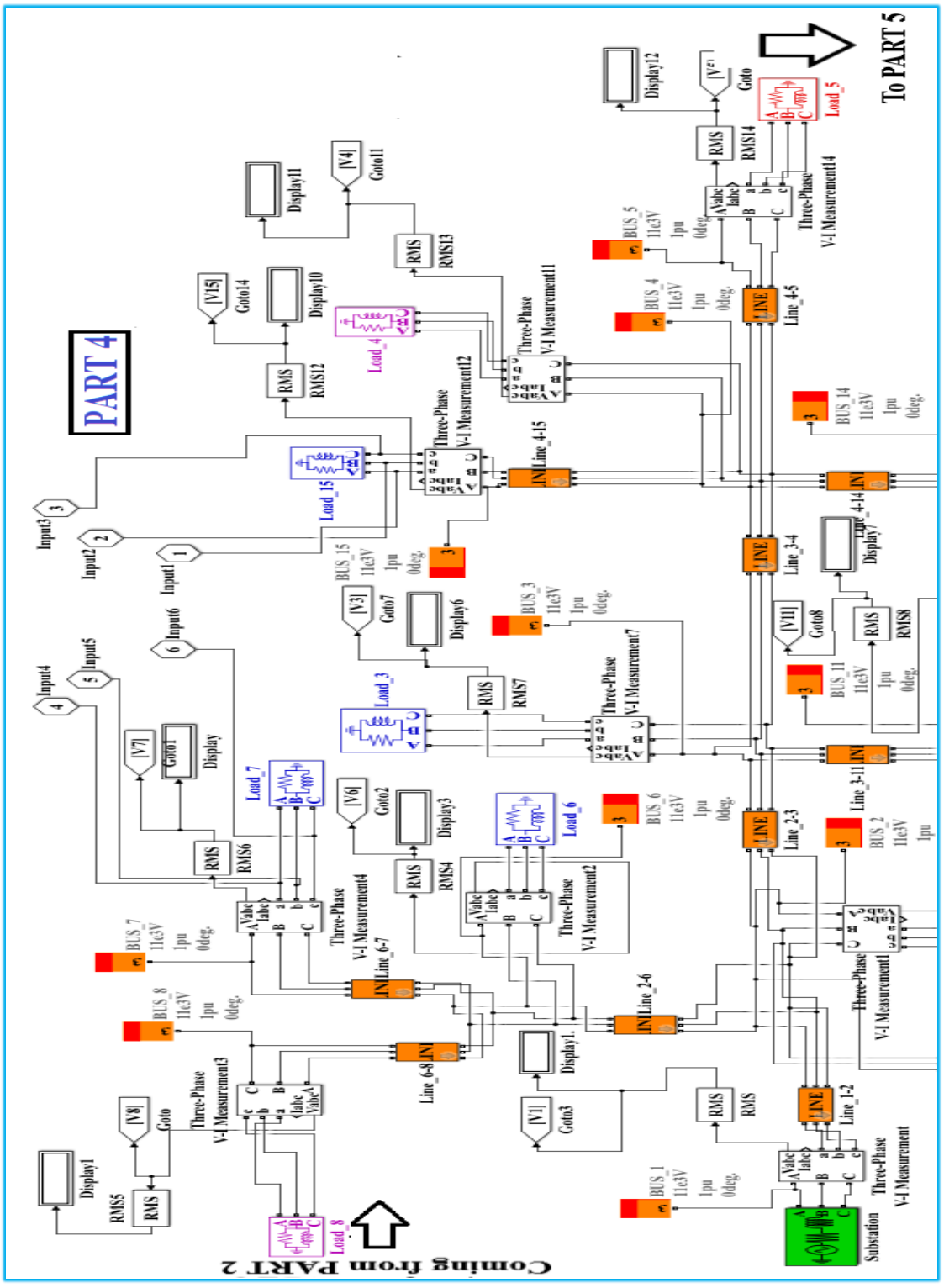

Figure 21. Internal architecture of the developed model (part 4)

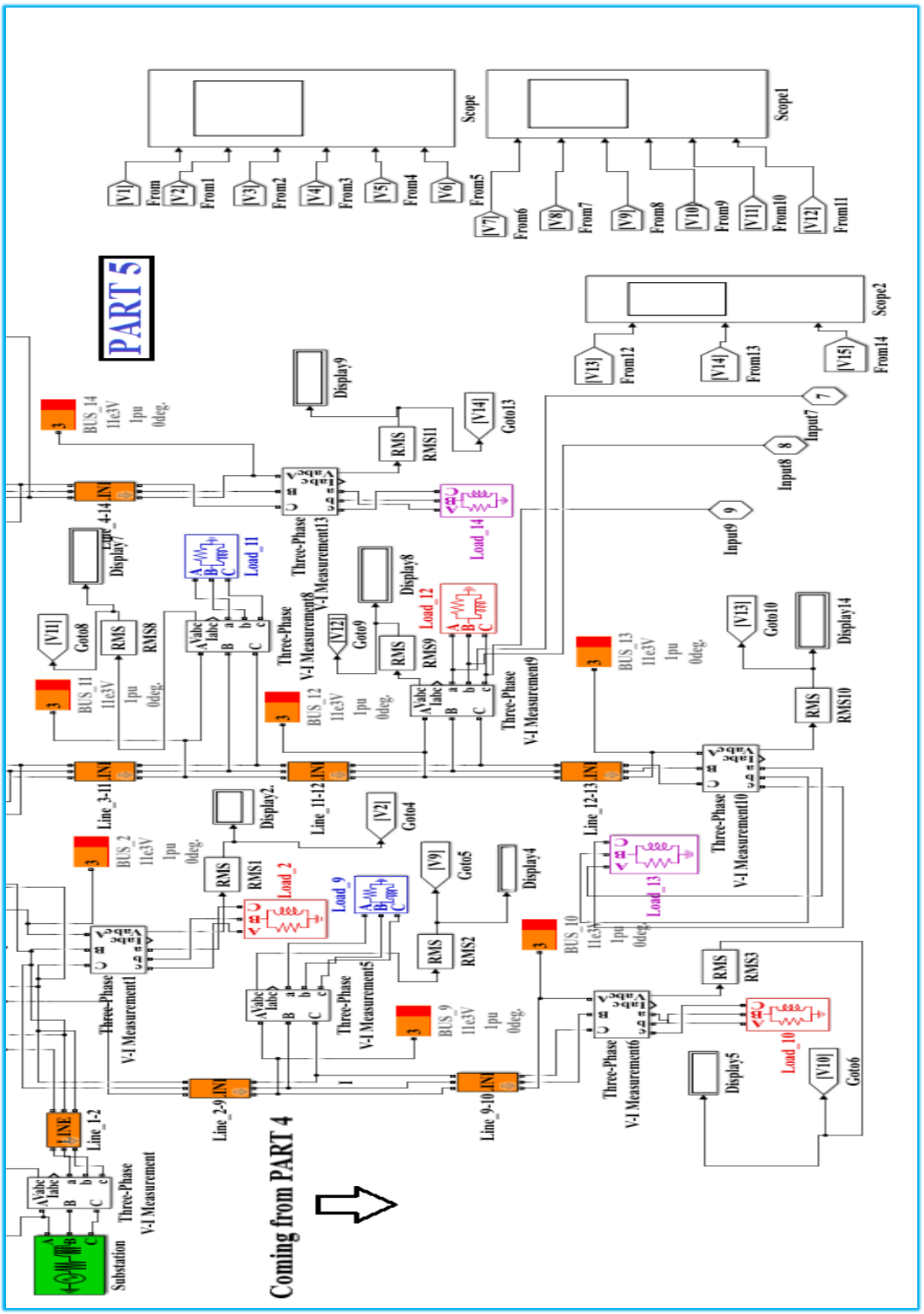

Figure 21. Internal architecture of the developed model (part 5)

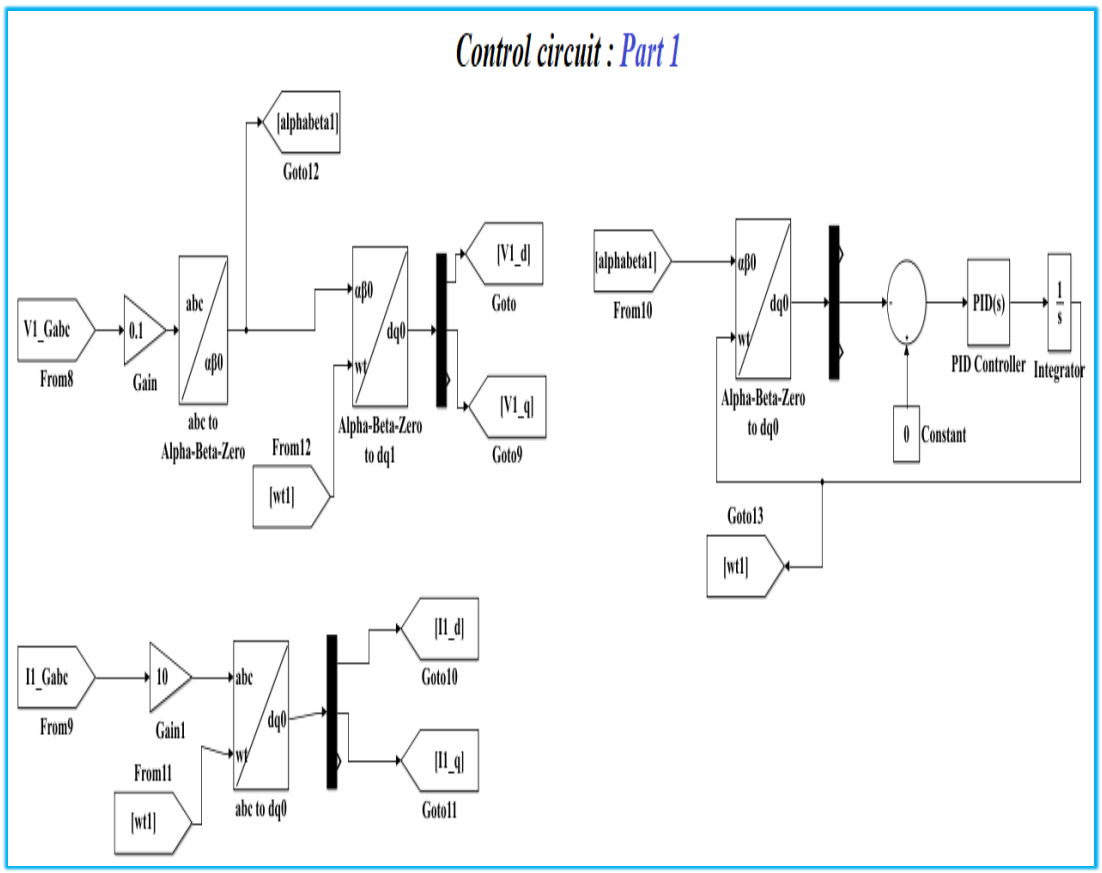

Figure 22(a). *d-q* components segregation by using PLL

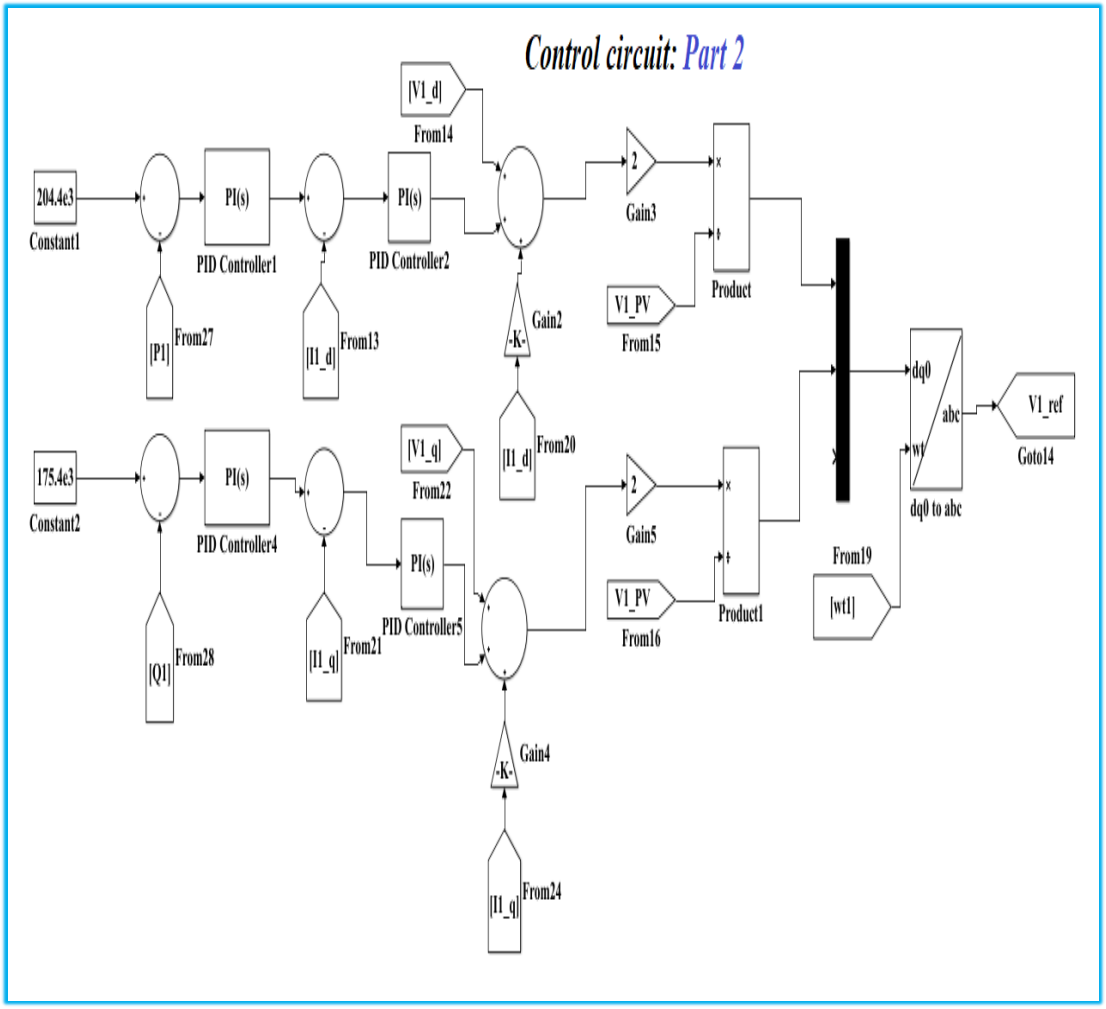

Figure 22(b). *d-q* axis power control circuit

3.10.2 PV array

The equivalent circuit for solar PV cell is shown in Figure 23(a). It essentially consists of a current source in parallel with a diode. The resistances R_S and R_{SH} are the equivalent series and shunt resistances. For an ideal cell, R_{SH} is infinite and as a result, it would not facilitate a substitute route for current movement. The ideal R_S value would be zero. Practically, the PV cells are clustered in series/parallel to form a larger unit named PV module. Again, a group of such modules are assembled in series/parallel to construct a PV panel or PV array to generate output power. The equivalent circuit for PV module is shown in Fig. 23(b).

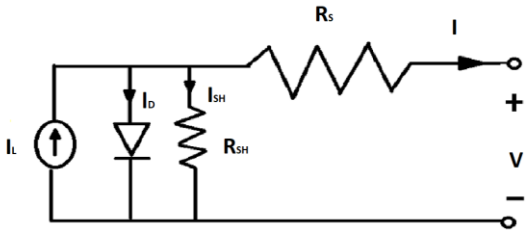

Figure 23(a) Equivalent circuit of a PV cell

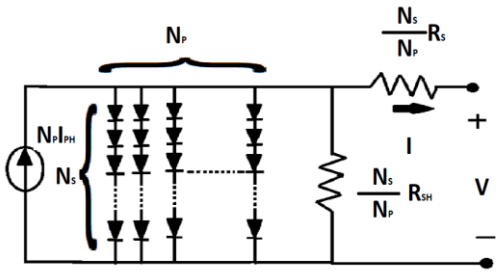

Figure 23(b) Equivalent circuit of a PV module

The voltage-current (*V-I*) characteristic equation of PV solar module is given by [Datta et al., 2014]:

$$I = N_p I_{PH} - N_p I_o \left[exp\left(\frac{\left(V + I(\frac{N_S}{N_p})R_s\right)}{N_S.\alpha.V_T} \right) - 1 \right] - \frac{(V + I(\frac{N_S}{N_p})R_S}{(\frac{N_S}{N_p})R_{SH}} \quad (59)$$

where, I_{PH} is the photo current generated by sunlight. I_o is the diode reverse saturation current. α denotes the diode ideality factor. V and I are the PV module output voltage and current, respectively. N_P is the number of parallel paths created by the clusters of PV cells. N_S denotes the number of PV cells linked in series to create each parallel path.V_T is the PV cell thermal voltage.

$$V_T = \frac{K.T}{q} \tag{60}$$

where, K is the Boltzmann constant having the value of 1.3805×10^{-23} J/K; T is the operating temperature in Kelvin; q is the electron charge having a value of 1.60×10^{-19} C.

Photo current of a PV cell is given by [Datta et al., 2016]:

$$I_{PH} = \left(I_{PH-STC} + K_i(T - T_{STC})\right)\frac{G_{ir}}{G_{ir\,STC}} \tag{61}$$

where, I_{PH-STC} is the short circuit photo current produced at standard test conditions (STC); T_{STC} and $G_{ir\,STC}$ imply the temperature and irradiance at STC; K_i is the cell's-short circuit current coefficient; T denotes the operating temperature in Kelvin; G_{ir} is the irradiance (in W/m^2). The short circuit current coefficient K_i is usually provided by the manufacturer.

The cell's saturation current varies with cell temperature, which is presented by:

$$I_o = \frac{\left(I_{PH-STC}+K_i(T-T_{STC})\right)}{\left[exp\left(\frac{\left(V_{OC-STC}+K_V(T-T_{STC})\right)}{.\alpha.V_T}\right)-1\right]} \tag{62}$$

where, V_{OC-STC} is the open circuit voltage of PV cell at STC; K_V is the open circuit voltage coefficient.

The *I-V* and *P-V* characteristics (shown in Figure 24) of the 1Soltech 1STH-215-P PV module [S1PVD, 2021] at STC are observed as per the parameters mentioned in Table 1.

Table 1 Electrical characteristics data of PV module 1Soltech 1STH-215-P [S1PVD, 2021]

Electrical characteristics	Values
Open-circuit voltage (V_{OC})	36.3 V
Short-circuit current (I_{SC})	7.84 A
Voltage at maximum power point (V_{mp})	29 V
Current at maximum power point (I_{mp})	7.35 A
Maximum power at STC (P_{max})	213.15 W
Temperature coefficient of I_{SC}	0.102%/^{0}C
Temperature coefficient of V_{OC}	- 0.36099%/^{0}C
Shunt Resistance (R_{SH})	313.3991 Ω
Series Resistance (R_S)	0.39383 Ω
Light generated current (I_{PH})	7.8649 A
Diode saturation current (I_o)	2.9259 ×10 $^{-10}$ A

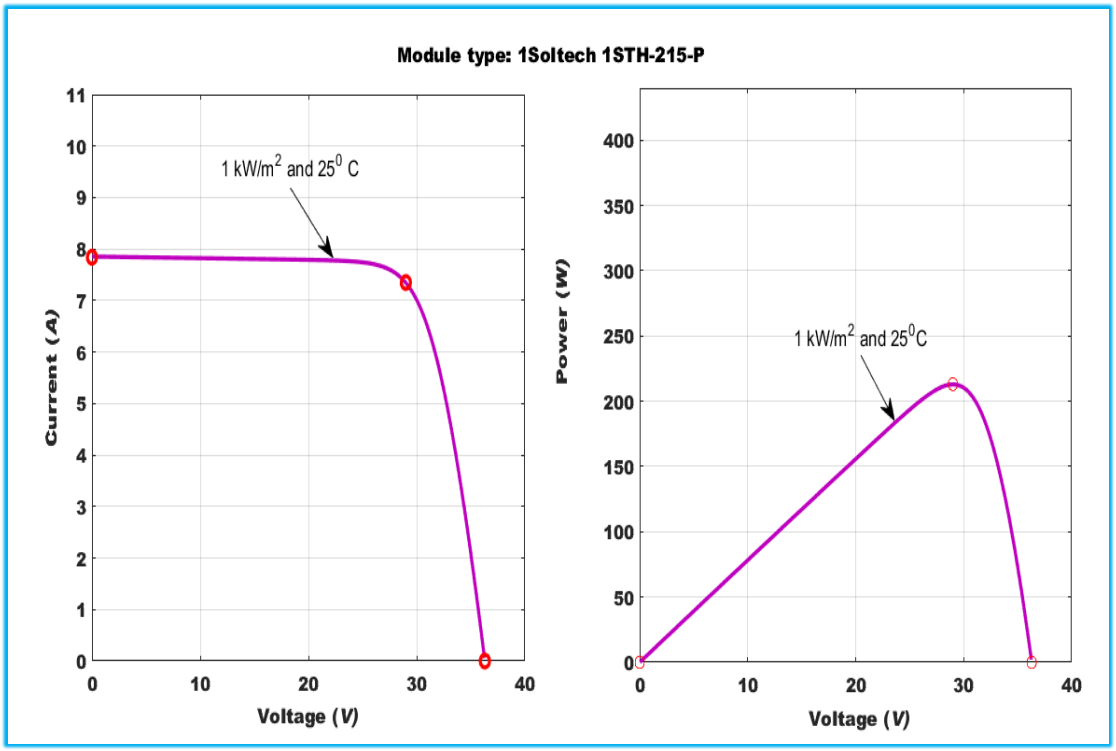

Figure 24. *I-V* and *P-V* characteristics of the PV module at STC

From the *P-V* characteristics, it is observed that, the voltage (V_{mp}) and current (I_{mp}) corresponding to the maximum power point (MPP) is unique. PV array output power depend on the solar irradiance and ambient temperature. With disparities in irradiance and/or temperature, the MPP changes. A PV array, comprising of 34 parallel strings and each string with 38 series modules, are simulated. The *I-V*, *P-V* characteristics of the PV array at different irradiances at constant temperature [i.e., T_{STC} (25^0 C)] and at different temperatures at constant irradiance [i.e., $G_{ir_{STC}}$ (1000 W/m^2)] are presented in Figures 25(a) and 25(b), respectively.

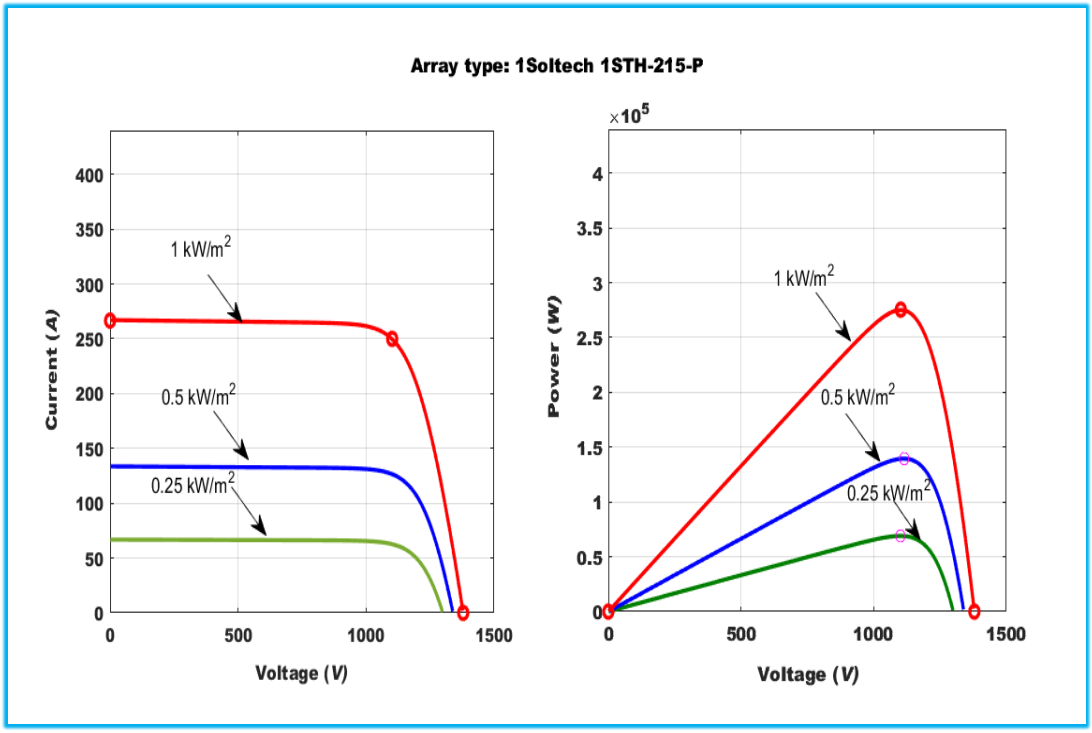

Figure 25(a) *I–V* and *P–V* characteristics of the PV array for different irradiances at T_{STC} (25^0 C)

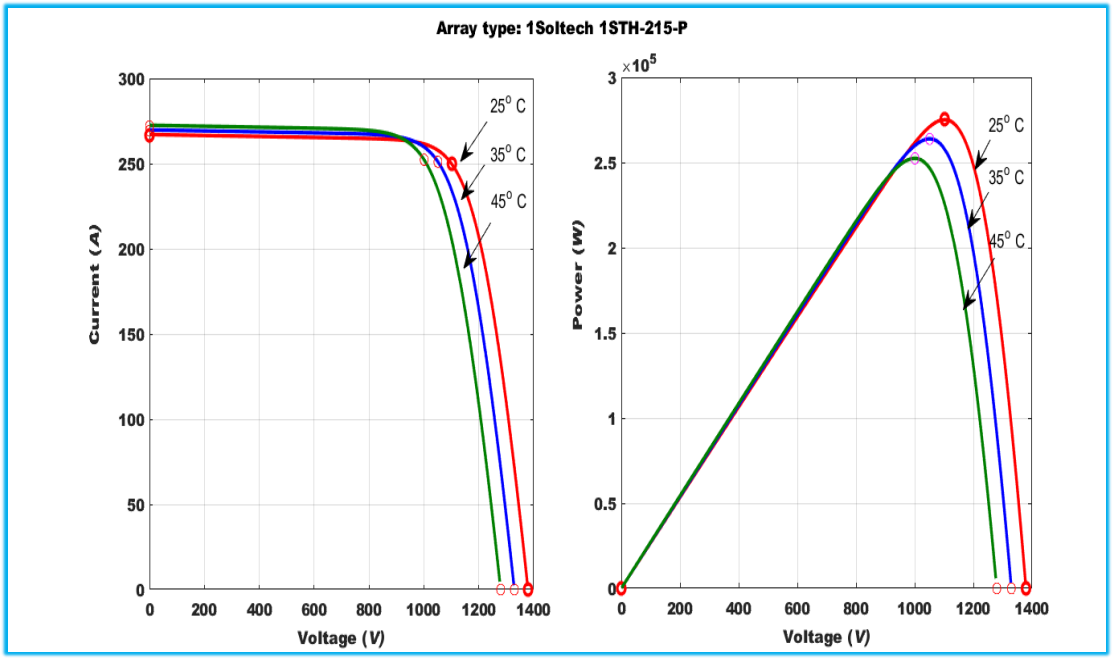

Figure 25(b) *I–V* and *P–V* characteristics of the PV array for different temperatures at $G_{ir\,\mathrm{STC}}$ (1000 W/m^2)

3.10.3 Three phase inverter

An inverter is designed with power semiconductor devices which converts the power from DC to AC at the required frequency and output voltage. Inverters are classified as: voltage source inverter and current source inverter. In the voltage source inverter, the DC input voltage is kept constant, whereas in current source inverter the DC input current is held constant. The three-phase power output from the inverter is delivered into the distribution network through the three different phases which are 120^0 out of phase with each other.

Figure 26 shows a three-phase inverter circuit for injecting SPV-EVCS power into the distribution network. Six insulated gate bipolar transistors (IGBTs) with flyback diodes are used in this configuration. For proper switching control, the six IGBT switching operations have to be synchronized so that each single switch operates for 60^0 span stepwise. This waveform consists of a zero voltage period among the positive and negative of the square-wave produced. Space vector pulse width modulation (SVPWM) technique is applied by generating high frequency

carrier wave. The three-phase sine waves generated by the power controllers (*d-q* based) are compared with the carrier wave and then passed through the NOT gates to produce the gate triggering pulses. The pulses are generated in such a way that the three-phase output quantities are exactly delayed by 120^0 to generate a 3 phase AC supply. There are two conduction modes of the three-phase inverters namely 180^0 and 120^0 conduction modes. In the proposed work, 180° conduction mode is adopted. In this type of conduction approach, each IGBT conducts for 180° period before turning off for the next entire 180° period, though each switch is activated/deactivated at intervals of 60°. The (S1, S4); (S3, S6) and (S5, S2) couples are complementary to each other. Each IGBT of the couples conducts for 180^0 and during that period, the other complementary couple members remain turned off and vice versa. The upper row IGBTs, i.e., S1, S3 and S5 conducts with a phase delay of 120^0 with each other. At $\omega t = 0$, if the IGBT S1 starts conducting, then exactly after 120^0 phase delay, S3 will be turned on and after 240^0, S5 will be turned on. The same relationship is applicable for the lower row IGBTs, i.e., S4, S6 and S2. The output terminals of the three-phase inverter are connected with the three-phase transformer (via L-C filters) for amplification of the AC voltage required for injecting power into the distribution network. There should be a phase angle between the phase voltage and current for a stipilated active and reactive power injection.

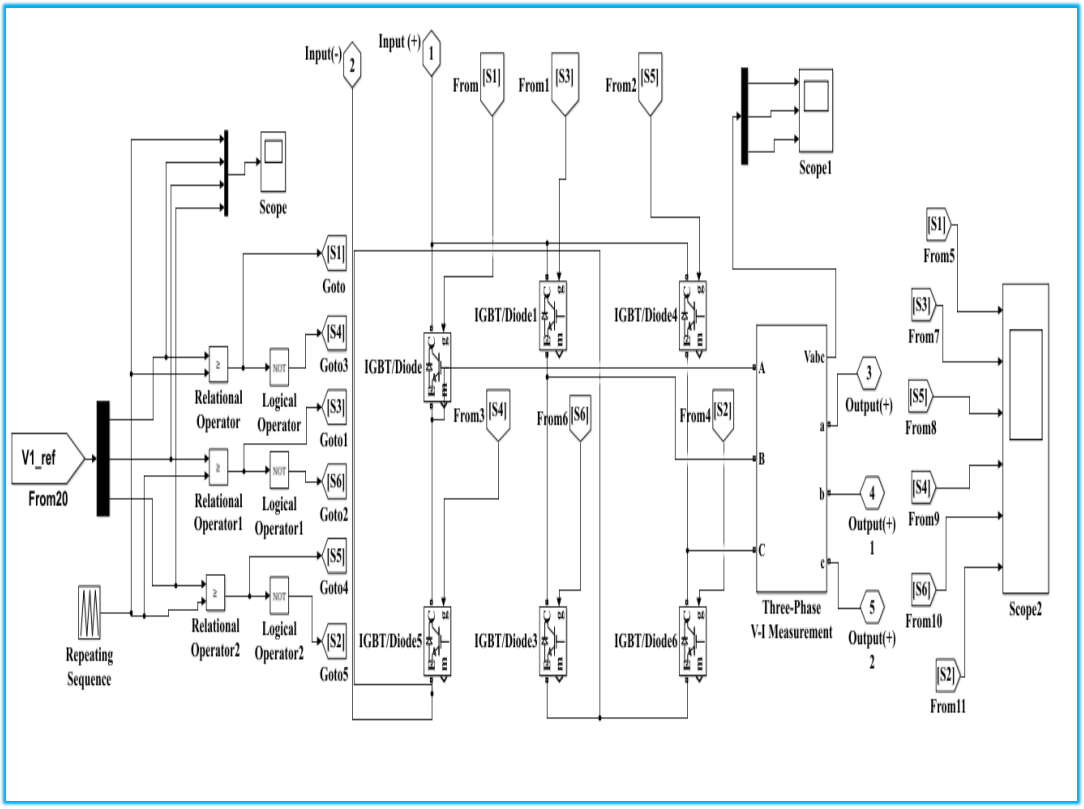

Figure 26. Three phase inverter circuit

3.10.4 The control circuit

The control circuit of the multi SPV-EVCS integrated model is designed to control the *d* and *q* axes (active and reactive) powers. Firstly, a PLL is designed to find out the phase (ωt) in between the α-β frame and *d*-*q* frame, where *d* component of volatge V_d is alligned with the distribution network voltage. After exploration of ωt, the *d* and *q* components of network volatges (L-G) and the currents are segrigated using the Clarke transformation (*abc* to $\alpha\beta 0$) and Park transformation ($\alpha\beta 0$ to *dq0*) blocks. The V_d, V_q, I_d and I_q components are calculated. These values are utilized in *d* and *q* axis power controllers to control the active and reactive powers to be injected into the distribution network. Figure 22(a) presents the internal design of the PLL and *d*-*q* components division of network voltages (L-G) and currents. Figure 22(b) presents the *d*-*q* axis power controller circuits. The outputs of these power

controllers (active and reactive) are normalized for getting the required instantaneous duty cycle components. Hence, these components (*d-q* axis) are combined and re-transformed by '*dq0* to *abc*' transformation block to obtain the reference three-phase voltages for the SVPWM generator.

3.10.5 Three phase transformer

The function of a three-phase transformer is to either step up or down the AC volatge level at the output. The three-phase transformer involves six windings: three primaries and three secondaries. The windings on each side (primary and secondary) can be connected with each other either in delta or star arrangements. Step up power transformers are required at the junction point of generation and transmission to step up the transmission volatge level to several kilovolts. Contrarily, the distribution transformers are installed at the distribution substations and at various points of the distribution network for stepping down the volatge levels to the lower values required for consumer use. In the proposed model, the output terminals of the three-phase inverter have been connected with a three-phase step up transformer (via L-C filters) for stepping up the AC voltage upto the compatible distribution network voltage level.

3.10.6 IEEE 15-bus system

The IEEE 15-bus system is chosen for the power flow management related study as a test bed. It's a radial distribution system, consisting of 15 buses. Bus no 1 is the substation bus. There are 5 laterals and 2 sublaterals in total. The active and reactive power demands are 1126.5 kW and 1251.182 kVAR, respectively. The suitable nodes identified for multi SPV-EVCS integration has been utilized for injecting power into the distribution system. The outputs of the three-phase tranformers inside each SPV-EVCS are connected with the optimum nodes/buses of the distribution network for the reqiured active and reactive power injection. Figure 21 (parts 4 to 5) presents the developed Simulink model of the IEEE 15-bus system.

3.10.7 Buck converters

The buck converter is a step-down DC to DC power converter which steps down the voltage level from its input to the output. To reduce voltage ripples, capacitive filters, occasionally in conjunction with inductors are used at the input and output sides of the converter. For the proposed power management study, two buck converters are used in cascade to step down the DC link bus voltage to 400 V and 48 V sucessively for each of the three identical SPV-EVCSs. The reason behind using these two buck converters lie in the fact that, for charging the ESU, 400 V power supply is needed; and for EV charging purpose, 48 V is needed. PID controllers are designed for each converter to retain the desired voltage levels. Figures 27 and 28 represent the Simulink models of the first and second stage buck converters, respectively.

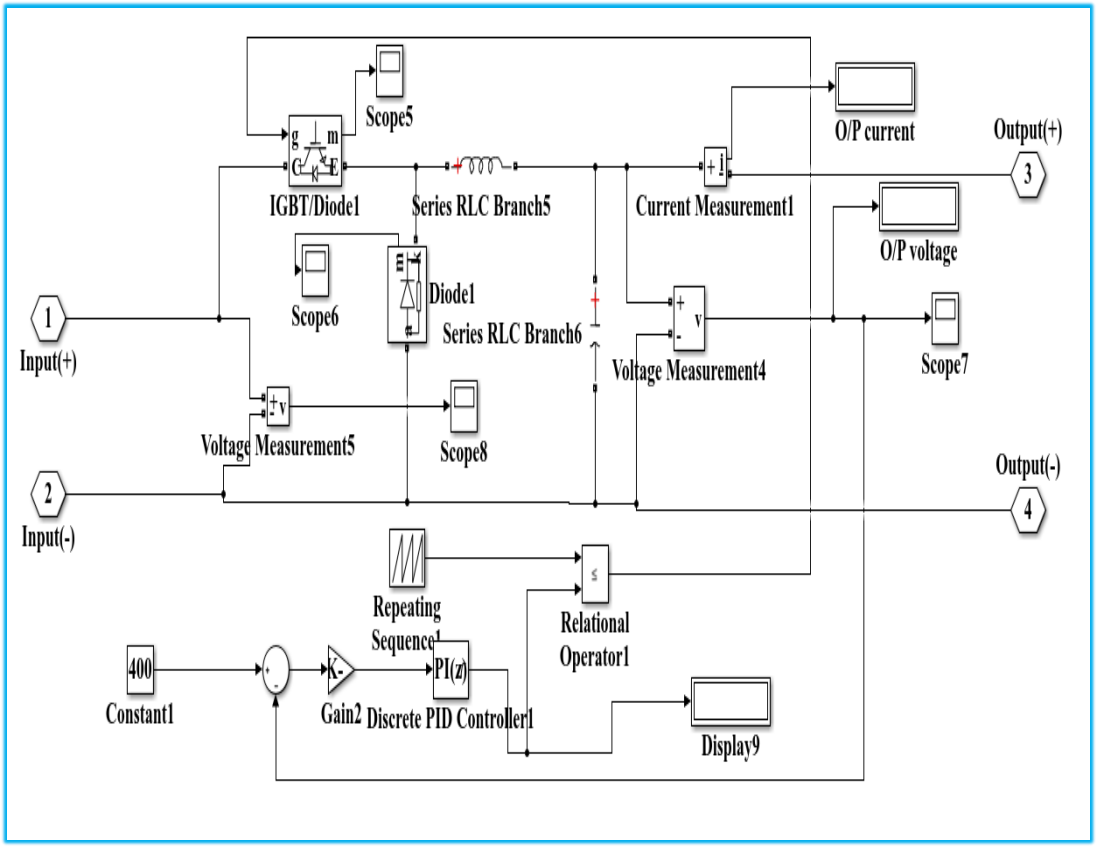

Figure 27. Simulink model of the first stage buck converter

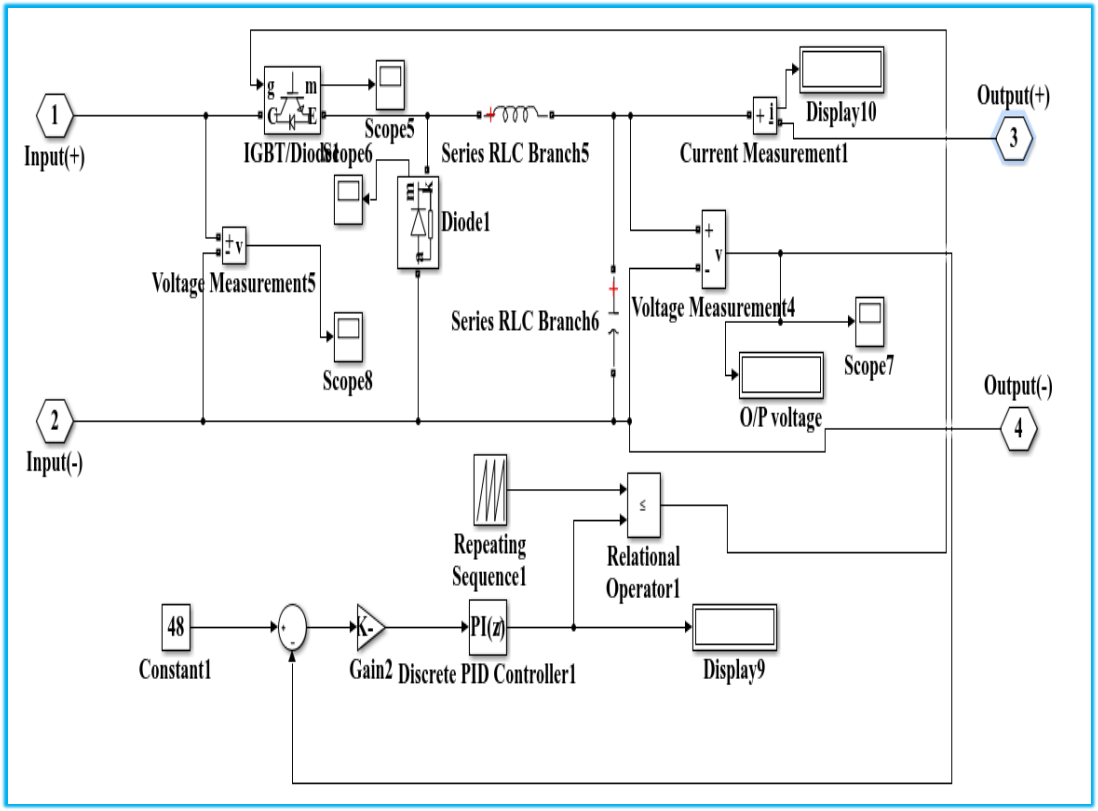

Figure 28. Simulink model of the second stage buck converter

3.10.8 ESU and EV batteries

Batteries are the energy storage elements which store electrical energy to be used later. The chief characteristics of a battery are discussed below.

A) Battery capacity: During the discharging cycle, the battery can deliver a constant current for certain hours holding a demarcated cutoff voltage. This is due to the total charge stored inside the battery. The total charge stored is called the battery capacity. It is denoted by the ampere-hour (Ah) unit. 1 Ah is equal to 3600 C. Battery capacity depends on the temperature, the battery aging, battery type and the rate of discharge. If the discharge rate is high, then the battery capacity is low.

B) Energy density: The quantity of energy that can be stored per cubic meter of battery volume is called the energy density. It is articulated in watt-hour/cubic meter (Wh/m^3). This is a significant parameter at the time of selecting a specific battery technology for conveyance applications, where compact design is essential because of the space crunch.

C) Specific power: Specific power is the power capacity of a battery per kilogram of its weight and is denoted by watt/kg . Some battery technologies propose high energy density with a low specific power.These type of batteries can store a large volume of energy, but can stream an insignificant volume of power immediately. In transport standings, this implies that a vehicle is capable of running a long distance, at a low speed. Defiantly, batteries having high specific power generally posess low energy density, as high discharge currents frequently reduce the existing energy hastily.

D) Cell voltage: The balanced thermodynamic reactions occuring inside the cell is responsible for the generation of cell voltage. The cell volatge is often tough to quantify. Hence, the open circuit voltage (V_{OC}) present in between the anode and cathode terminals is used for all practical purposes. For few battery technologies like lead-acid, the V_{OC} can be castoff as a basic state of charge (SOC) approximation. Another parameter often utilized is the closed circuit voltage (V_{CC}), which is dependent on the SOC, load current and cell's usage records. Battery manufacturers deliver the cell nominal voltage from its characteristics and that is usually used by the users for all practical application purposes.

E) Charging and discharging currents: Charging and discharging currents are the currents, that flow through the battery during the charging and discharging processes. Throughout the discharging process, electrons drift from the anode to the cathode, passes through the load and the electrolyte to complete the circuit and discharging current flows through the circuit. During the charging process, an exterior source is connected to feed energy into the battery. The charging current starts flowing through the circuit followed by oxidation at the positive electrode with a reduction at the negative electrode. For applied domains, the C-rate is utilized to present the charging / discharging currents comparative to the rated capacity. For specimen, a discharge rate of 1C signifies that within 1 hour time period, the battery will be fully discharged.

F) State of charge: The state of charge (SOC) is the ratio of the existing capacity and the nominal capacity which is the maximum conceivable charge capacity of the battery. The methods employed to estimate its value depends on the battery

technology used. A fully charged battery possesses a SOC of 1 or 100% , whereas a fully discharged battery contains a SOC of 0 or 0%. The rated capacity which is termed as the beginning of life (BOL) capacity, is frequently utilized as the reference value. SOC is the vital area to look at while controlling a battery powered system for securing the power retorts due to variations in operating conditions. The SOC significantly depends on the C-rate and the temperature. It is reliant on the principles of electrochemistry, thermodynamics and material constraints of the adopted battery technology.

G) Depth of discharge: Depth of discharge (DOD) is another important battery parameter which is expressed by the ratio of discharge capacity relative to its maximum capacity. The maximum suggested DOD level is dependent on the battery technology used. DOD is useful for enhancing the overall cycle life.

H) Cycle life: Another important battery parameter is the cycle life which governs the total number of charging/discharging cycles experienced by the battery before reaching a fixed point of energy capacity or other performance standards. The charging/discharging current rates, environmental circumstances like temperature, humidity, etc. and the DOD influence the cycle life. The cycle life provided by the manufacturer generally differs slightly from the real time scenerio as the industrial experiments are conducted under specific charging/discharging environments. Figures 29 and 30 present the Simulink models of the ESU and EV batteries respectively, used in the power management related study.

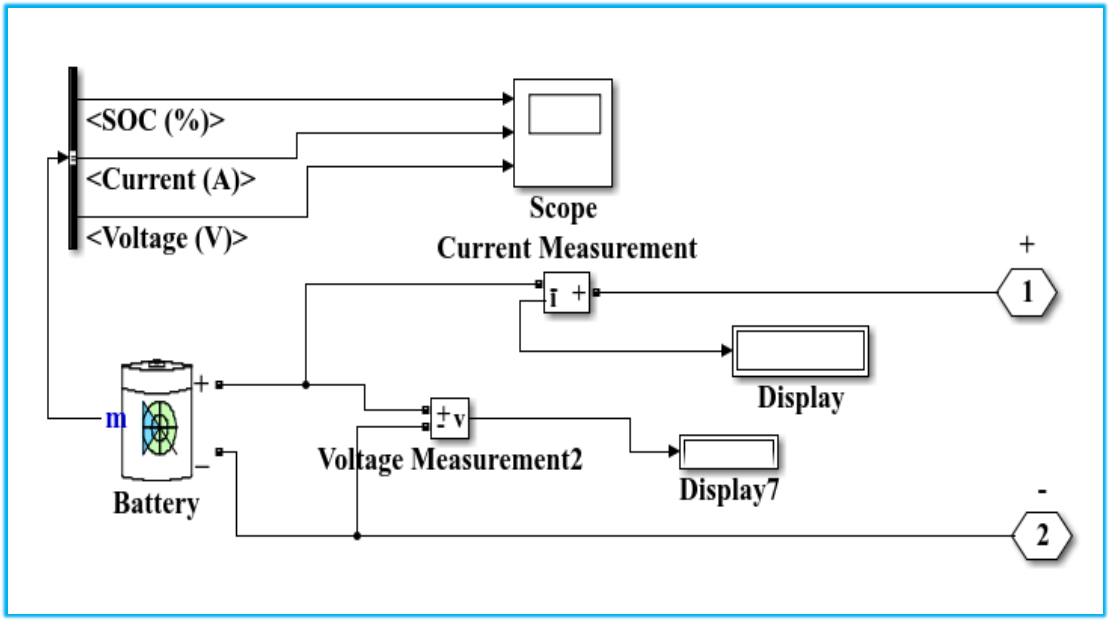

Figure 29. Simulink model of the ESU battery

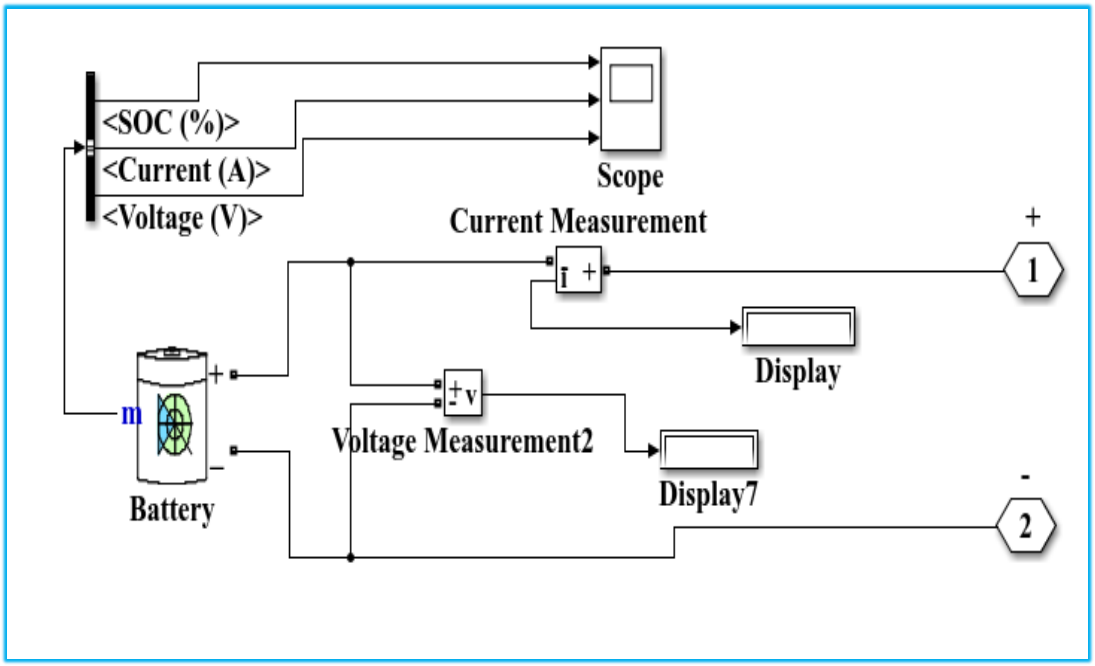

Figure 30. Simulink model of the EV battery

3.11 Conclusion

This chapter complies a detailed presentation on the different models and methods required for studying the optimum allotment of EVCSs. Different optimization techniques colloborated with power flow analysis are required to carry out the optimization study. Power flow analysis methods named BFSM and another efficent one are reported. Subsequently, the optimization techniques utilized viz. PSO, PPSO, INBPSO and GA are discussed. Voltage and loss sensitivity analyses to be applied for scrutinizing the feasibilty of the optimum network nodes are presnted. Finally, the Simulink model for distribution network integrated multiple SPV-EVCSs along with all the associated functionalities is explored for conducting the power management related study.

CHAPTER -4

SYSTEM VALIDATION AND RESULTS

4. SYSTEM VALIDATION AND RESULTS

4.1 Introduction

The problem formulation of the optimum EVCS allocation study is presented in **Chapter 2**. And, **Chapter 3** has presented elaborately on the developed models and methods for perusing the optimum allocation of EVCSs and power management study. In connection, this chapter presents the various case studies of the optimum EVCS allocation and power management along with the validated results.

Four case studies to contemplate the optimum allocation of EVCSs are carried out considering different mode of power flow between EVCSs and power distribution network. It is the first phase of the research work. *Case Study 1* focuses on optimum allocation of EVCSs in IEEE 15-bus system considering unidirectional power flow in load mode (distribution network to EVCSs). PSO technique collaborated with an efficient power flow analysis is applied. In *Case Study 2*, the competent PPSO technique collaborated with BFSM is utilized for effective allocation of SPV-EVCSs in IEEE 69-bus radial distribution system considering bi-directional power flow (in between distribution network and EVCSs). In *Case Study 3*, the INBPSO technique (discrete domain) in collaboration with an efficient power flow analysis is applied for optimum allocation of EVCSs in IEEE 15-bus system considering bi-directional power flow. Whereas, in *Case Study 4*, GA amalgamated with BFSM is adopted for optimum allocation of RE-EVCSs in power injection mode (power flow from EVCSs to distribution network), where IEEE 33-bus system is taken as a test bed system. The voltage sensitivity analysis and loss sensitivity analysis are also performed in different case studies.

The multiple SPV-EVCS integrated network model (Simulink model, presented in **Chapter 3**) is utilized for power management study as the second phase of the research work. The model is investigated under two conditions: a) SPV-EVCSs delivering power only to the distributed network (under no EV and ESU charging condition), and b) SPV-EVCSs delivering power simultaneously to ESUs, EVs and distribution network (under condition of excess SPV generation).

All investigated results in connection with the optimum allocation of EVCSs and power flow management are presented.

4.2 First Phase of the Research Work

During the first phase of the proposed work, effective allocation of EVCSs is accomplished considering different modes of operation, distribution network configurations and optimization techniques. Renewable energy specifically solar PV based EVCSs have been taken into consideration during most of the case studies involving power injection into the distribution network. Integration of these solar PV powered EVCSs at strategic positions of the distribution system is done considering them as energy suppliers (as distributed generators) to the distribution system during peak loading hours (at daytime). It is assumed that the tariff rate is low during nighttime due to the absence of heavy industrial loads, and the EVs are being charged inside their respective charging cum parking lots in residential areas. Thus, their charging requirement is comparatively low at daytime, during industry working hours. The EVCSs are situated nearby the industrial belt and EVs are kept at offices/industries. Due to the less charging demand of EVs in industrial peak loading hours, the EVCS can deliver the surplus power into the distribution network. Conversely, the EVCS can draw bare minimum power from the healthy network for EV charging in adverse weather conditions when the PV power is not available and ESU is out of charge. Four case studies are conducted. In *Case Studies* 1 and 2, the objective function 1 is utilized for minimization of node voltage errors. In the *Case Studies* 3 and 4, objective function 2 is used for minimizing the node voltage errors and total active line loss of the network.

4.2.1 Case Study 1: A study on voltage profile of the EVCS integrated IEEE 15-bus system under load point mode of operation

Case Study 1 is carried out on the IEEE 15-bus radial distribution system shown in Figure 31. The active and reactive power demands of the chosen network are 1126.5 kW and 1251.182 kVAR, respectively. The base values are selected as 100 MVA, 11 kV. The normalized voltage sensitivity indices of all nodes are premeditated by finding out the deviations in all the node voltages due to their own reactive power variations, excluding the main feeder node or the first node. The reason behind excluding the feeder node lies in the fact that, no load point relates to the feeder node and there is no possibility of load point integration at this node. For evaluating the voltage sensitivities of all other nodes, an incremental change in reactive power of the n^{th} node is introduced and the conforming incremental change in node voltage is found by power flow analysis. Figure 32 presents the normalized voltage sensitivity indices of the test network.

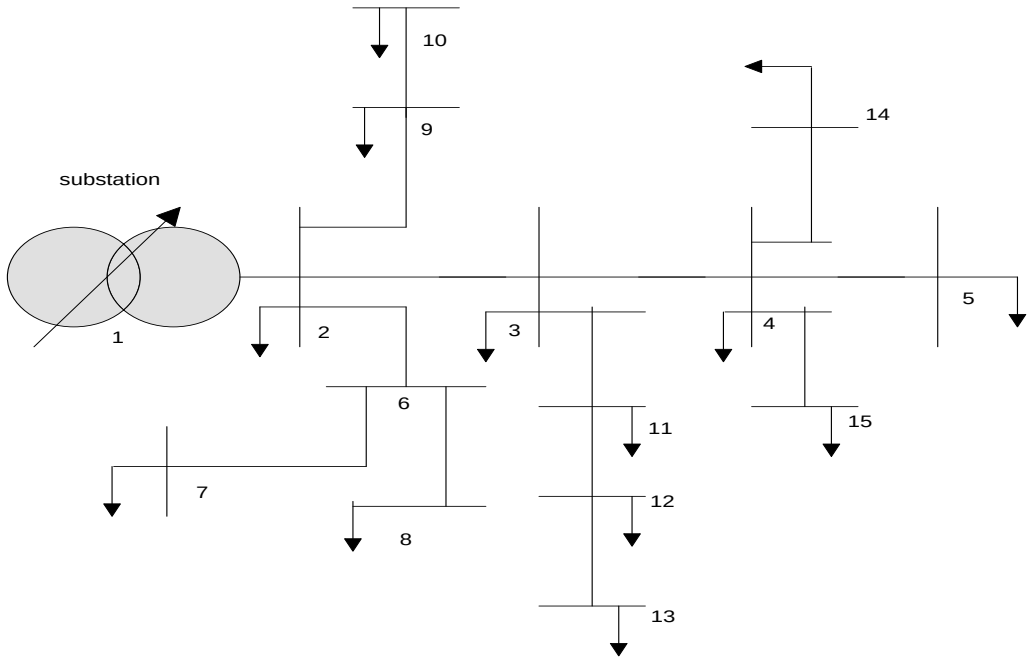

Figure 31. Single-line diagram of IEEE 15-bus system

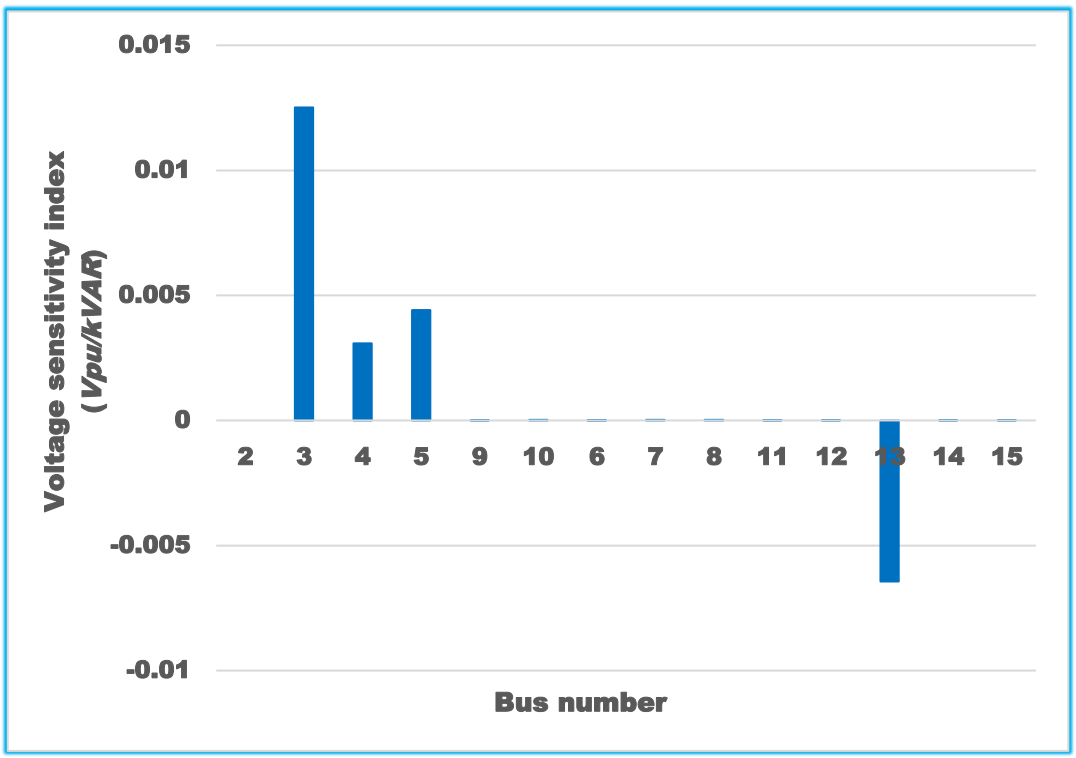

Figure 32. Normalized voltage sensitivity indices of IEEE 15-bus system

From the voltage sensitivity analysis results, it is detected that node number 13 is unsuitable for power injection/extraction to/from the system because of negative VSI at the node. The other nodes are having positive VSIs to sustain system stability. But amongst them, node numbers 3, 4 and 5 achieve high positive VSIs. Consequently, these are the relatively weaker nodes for power extraction. Amid these three nodes, node 3 is unsuitable for power extraction for high positive VSI at this node. The other two nodes, i.e., nodes 4 and 5, can be taken for EVCS integration under load point mode. After completion of sensitivity analysis, progressively increased numbers of equal capacity EVCSs are integrated with the grid to examine the consequence of newly integrated EVCSs upon the system voltage profile. The objective is to find out the maximum number of EVCSs supported by the network without negotiating the voltage profile. A fast and efficient power flow analysis technique collaborated with PSO optimization is applied. For the implementation of the PSO algorithm, the value of ω_{damp} is taken as 0.99. Both $c_1$and c_2 are set to 0.5. r_1 and r_2 are taken from the uniform distribution interval [0 1]. For determining the power capacity of each

EVCS, maximum 2 EV charging facility per EVCS is assumed. The 8 kW DC chargers are taken for the EV charging purpose. Hence, the total power used up by 2 EVs are 16($2 \times 8 = 16$) kW DC. Rectifier efficiency is taken as 90%. Hence, the rectifier input power available is 17.78 ($16 \times 100/90$) kVA. Considering distribution network power factor as 0.7, the active and reactive powers drawn from the network are 12.444 (17.78×0.7) kW and 12.7 (17.78×0.7141) kVAR congruently by each EVCS. The per unit values of these powers are 0.00012444 pu and 0.000127 pu. Three trials are conducted taking 2, 3 and 4 EVCS allocation. The global best values, i.e., optimum values of highest over and under voltage deviations ($|e_{overvol-h}|$ and $|e_{undervol-h}|$) along with the optimum EVCS locations are apprehended in each trial. The results are illustrated in Table 2.

Table 2 Optimum feasible EVCS locations for progressively augmented EVCS numbers along with the optimum over and undervoltage errors in load point mode

No. of EVCSs ↓	**Optimum feasible locations (buses)** →	**EVCS**			$\|e_{overvol-h}\|$ (pu)	$\|e_{undervol-h}\|$ (pu)
2	2	9	-	-	0	0.057
3	8	9	10	-	0	0.058
4	8	9	9	10	0	0.0593

From the results presented in Table 2, it is perceived that maximum 3 numbers of EVCSs of specified capacity are viable to be connected at optimum locations (buses) 8, 9 and 10. Increasing the EVCS number to 4, two recurring optimum locations at node number 9 are found, which is unbefitting practically. The optimum nodes 8, 9 and 10 attained from the case study are substantiated with the results obtained from sensitivity analysis and found to be acceptable. The highest over and under voltage errors (0 pu and 0.058 pu) are noticeably lesser compared to the restricted voltage error limits (± 0.1 pu) [Faddel et al., 2018]. That's why, these locations are taken as the optimum EVCS locations suitable for the EVCS integration.

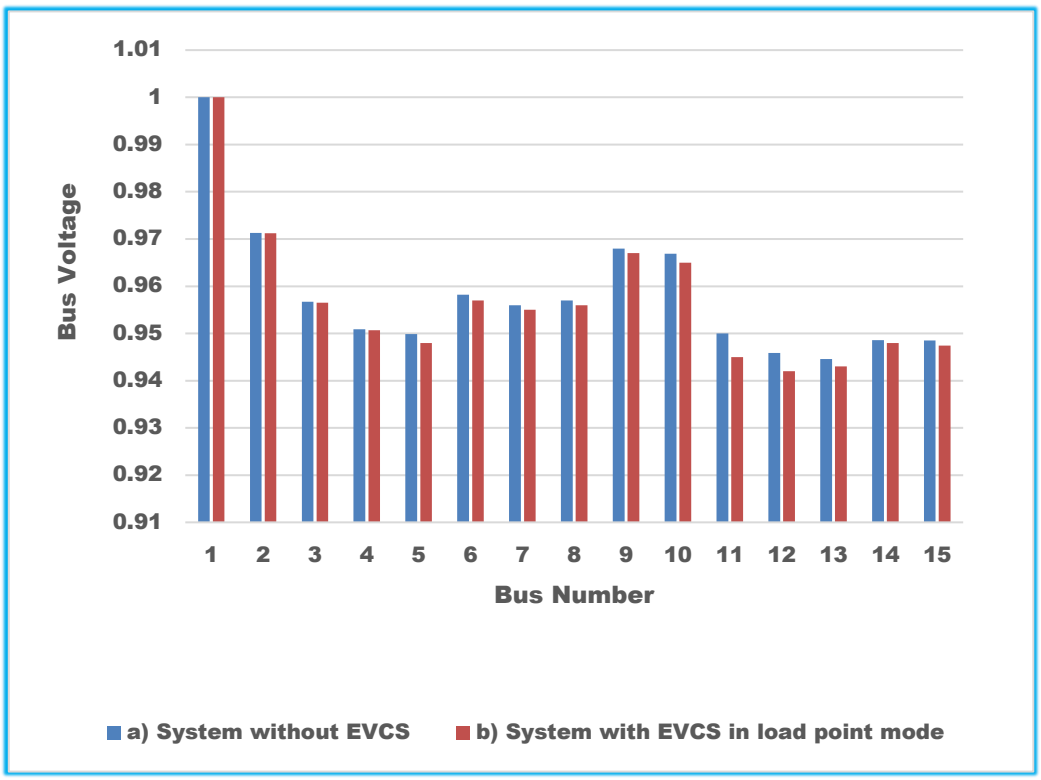

Figure 33. Comparison of node voltage profiles of a) system without EVCS and b) system with EVCS in load point mode in IEEE 15-bus system

Figure 33 presents a comparison among the voltage profiles of the a) network without EVCSs and b) network with EVCSs operating in load point mode. For the system without EVCS, the highest over and under voltage errors are 0 pu and 0.0554 pu, respectively. From the analysis, it is inferred that voltage profile of the system with EVCS under load point mode is a little bit degraded compared to the voltage profile without EVCS, but still, it is under the prescribed limit.

4.2.2 Case Study 2: Bi-directional SPV-EVCS integration with IEEE 69-bus system for voltage profile upgradation at power injection mode

During this case study, effective positioning of SPV-EVCSs in the IEEE 69-bus power distribution network is carried out with the help of BFSM amalgamated PPSO technique. The BFSM algorithm is employed for evaluation of the fitness function. The aim behind using this upgraded version of PSO is to get precise results within a moderate number of iterations, thus eliminating the insecurity coming from

premature convergence. The decision variables are the *p* numbers of SPV-EVCS locations (*p* dimensional search space).

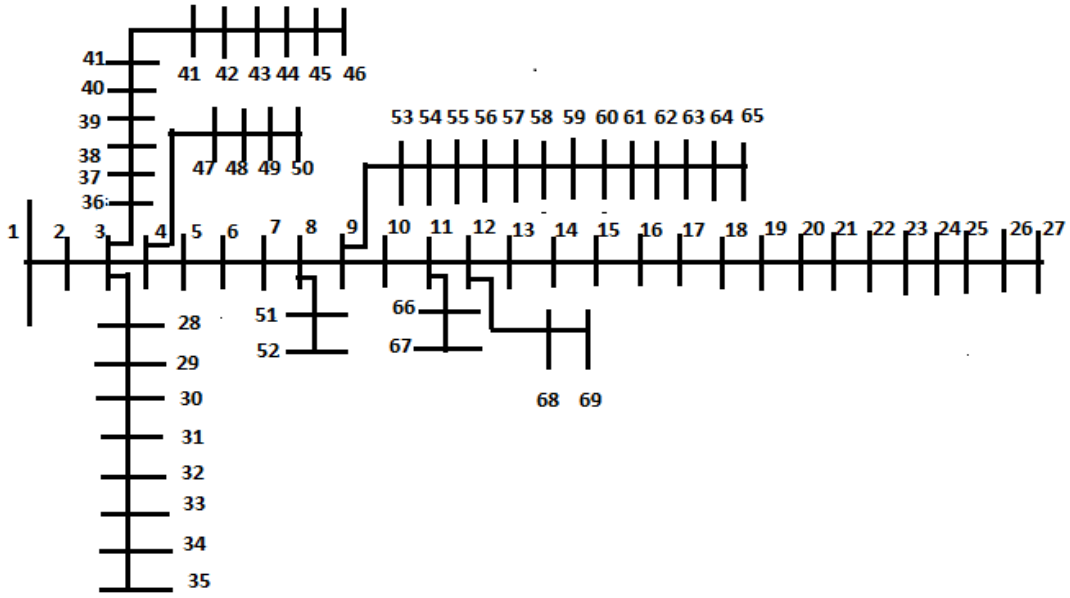

Figure 34. Single-line diagram of IEEE 69-bus system

The IEEE 69-bus radial distribution system is shown in Figure 34 with a total load of 3802.2 kW and 2694.6 kVAR. The base values are selected as 100 MVA, 12.66 kV. The permissible maximum voltage error range is ± 0.1 pu. [Faddel et al., 2018].

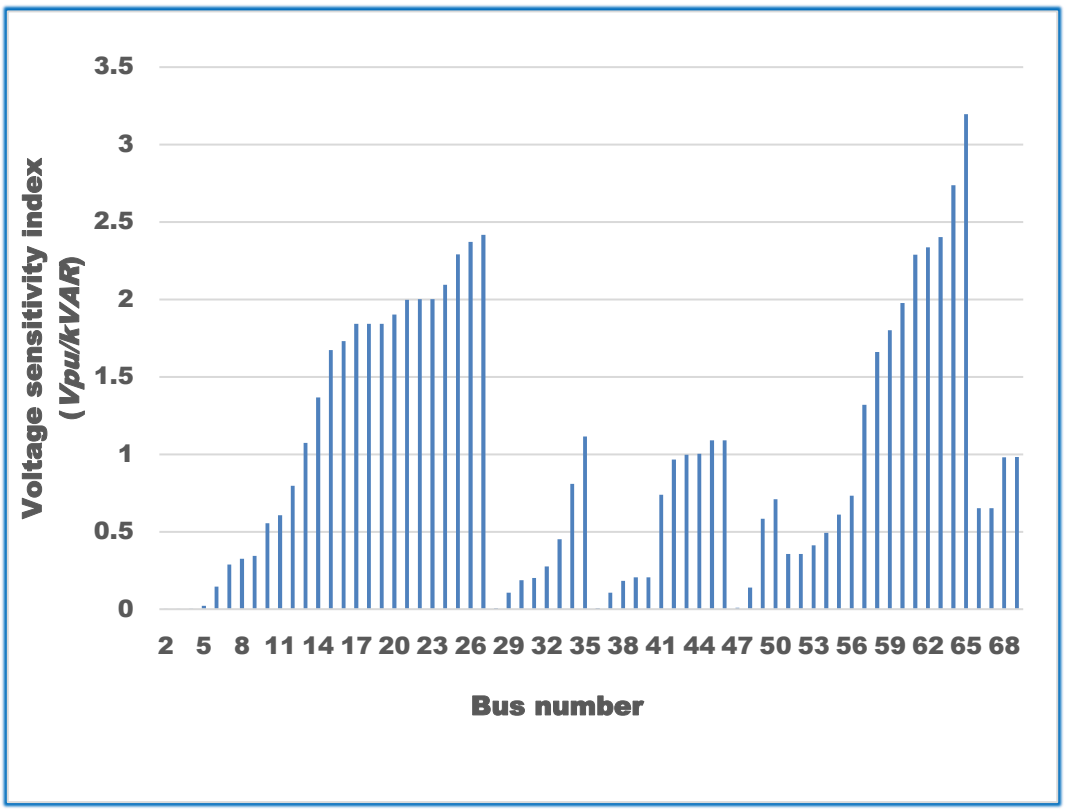

Figure 35. Normalized voltage sensitivity indices of the IEEE 69-bus system

Figure 35 presents the voltage sensitivity indices of all network nodes under consideration. There is no bus having negative VSI. As VSI of all nodes are positive, power injection (restricted amount) in any node may not cause for instability. The buses having low VSI are considered as strong buses from power extraction point of view. On contrary, for the power injection, the nodes having comparatively higher positive VSI values are the best suited nodes. After voltage sensitivity analysis, the optimum allocation of SPV-EVCSs is obtained in power injection mode. The maximum active and reactive power injecting capacities of all SPV-EVCSs are taken identical keeping a provision of charging 100 EVs simultaneously in each SPV-EVCS. The 8 kW DC chargers are considered to charge 100 EVs simultaneously from the integrated PV generation unit, thus creating a requirement of 800 (100 × 8) kW DC power charging in total. Considering inverter efficiency as 90%, the apparent power delivered to the distribution network under no EV charging requirement condition is 720 (800 × 0.9) kVA. If power factor of the distribution network

connected system is 0.7, the injected active ($P_{injected}$) and reactive ($Q_{injected}$) powers are 504 kW (0.00504 pu) and 514.182 kVAR (0.005142 pu approx.), respectively. In PPSO execution, several trials have been taken. It is detected that, with the increased number of SPV-EVCSs beyond 8, the system performance deteriorates in view of the highest over and under voltage errors. That's why, maximum 8 numbers of SPV-EVCSs can be connected at the optimum locations. Table 3 represents the augmented number of SPV-EVCSs allocation (from 1 to 8) including their effects on highest voltage errors.

Table 3 Optimum feasible SPV-EVCS locations in each trial along with the highest under and over voltage errors in power injection mode

No of SPV-EVCS ↓	**Optimum feasible SPV-EVCS locations (buses) →**								$\|e_{overvol-h}\|$ (pu)	$\|e_{undervol-h}\|$ (pu)
2	65	64							0.0068	0.0320
3	58	63	57						0.0068	0.0242
4	21	62	60	65					0.0067	0.0138
5	61	21	64	63	62				0.0067	0.0058
6	63	60	62	25	49	60	-	-	0.0002	0.00575
7	65	60	49	29	65	46	27	-	0	0.01316
8	**40**	**60**	**45**	**58**	**49**	**20**	**64**	**65**	**0.0001**	**0.0058**

As shown in Table 3, the maximum 8 SPV-EVCSs integration is possible where the optimum bus locations (buses) are (40, 60, 45, 58, 49, 20, 64, 65). The results are substantiated with the voltage sensitivity investigation to ensure stability of the integrated system.

Table 4 Feasible SPV- EVCS locations as load points

Optimum SPV-EVCS locations (buses) →								$\|e_{overvol-h}\|$ (pu)	$\|e_{undervol-h}\|$ (pu)
40	60	45	58	49	20	64	65	0	0.0375

Afterwards, the 8 SPV-EVCS integrated system is examined in load point mode (shown in Table 4). Maximum 2 EVs charging simultaneously per SPV-EVCS is considered. From Table 4, it is seen that the highest over and under voltage errors are under postulated limits.

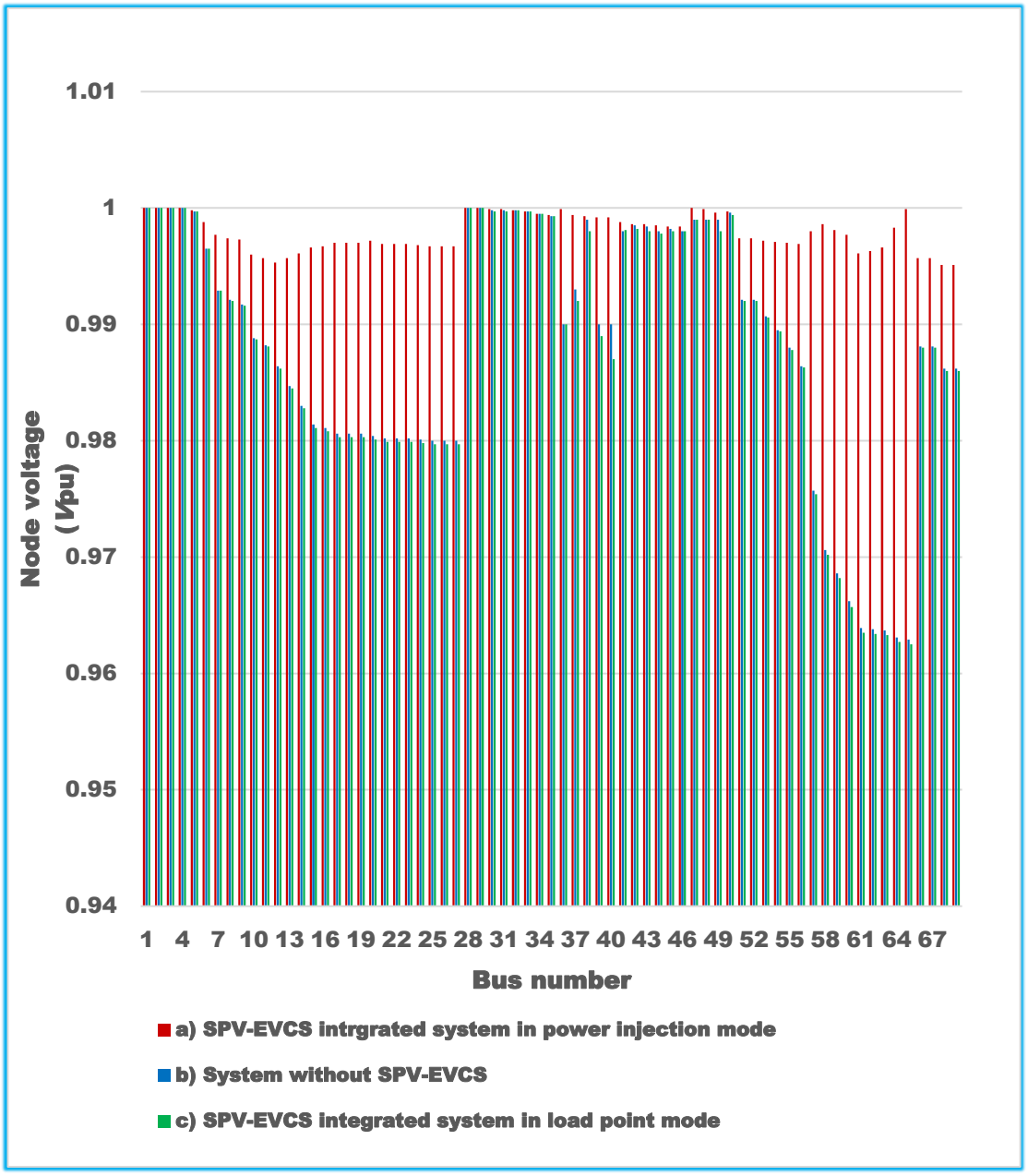

Figure 36. Comparative analysis of node voltage profiles of a) SPV-EVCS integrated system in power injection mode, b) system without SPV-EVCS and c) SPV-EVCS integrated system in load point mode in IEEE 69-bus system

From the comparative analysis presented in Figure 36, it is evident that the network voltage profile is far better with the SPV-EVCS integration while functioning in power injection mode. There is a small voltage profile degradation under load point mode compared to the SPV-EVCS unintegrated condition. However, it is in acceptable limit. The highest under voltage deviations in all modes are under stipulated limit. Thus, it can be concluded that, the proposed methodology provides an effective solution in enhancement of voltage profile in a EVCS integrated power distribution network.

4.2.3 Case Study 3: Bi-directional RE-EVCS integration with IEEE 15-bus system for voltage profile upliftment and minimization of line losses in power injection mode

In this case study, IEEE 15-bus radial distribution system is considered for the optimum RE-EVCS allocation. The base power and voltage are chosen as 100 MVA and 11 kV as in *Case Study* 1. As per the usual convention [Faddel et al., 2018], the maximum tolerable voltage error limits are ± 0.1 pu. The proposed BFSM amalgamated INBPSO technique is applied for optimal RE-EVCS allocation.

At first, both the voltage and loss sensitivity analyses are performed on the network nodes to investigate the fitness of each node for RE-EVCS integration. Subsequently, the total optimal power capacity of the RE-EVCSs in power injection mode is estimated by using the optimum RE-EVCS diffusion level μ_{max}. Once, the total optimum power capacity is calculated, the probable sets of optimum number and sizes of all EVCSs are formed as per the requirement of the society considering numerous aspects. Optimum allotment of the progressively augmented number of EVCSs of optimum sizes is done by the proposed INBPSO technique. The total active power line loss and network voltage profile are substantiated to guarantee the power quality. The optimum sites attained under power injection mode of operation are further validated with the voltage and loss sensitivity analysis to ensure the stability of the integrated system. After this, the effects of EVCS integration are studied by taking load point mode of operation.

The voltage sensitivity indices of the network nodes are already presented in Figure 23. From the voltage sensitivity analysis results, it can be clearly said that node number 13 is inappropriate for power injection into the system due to its negative VSI. Apart from the node 13, all the other nodes are possessing positive VSIs. Among them, node numbers 3, 4 and 5 are holding high positive VSIs. Hence, these are the comparatively weaker nodes of the system, thus less suitable for power extraction. But they may be suitable for power injection. As VSI of node 3 is comparatively high, the node is highly suitable power injection. Nodes 4 and 5 can be utilized for RE-EVCS integration. The rest of the nodes (except 1, 13) may support a limited power injection. Additionally, loss sensitivity analysis is carried out to examine the effect of load active power variation on total active power loss of the integrated system. Figure 37 presents the loss sensitivity indices of the network nodes.

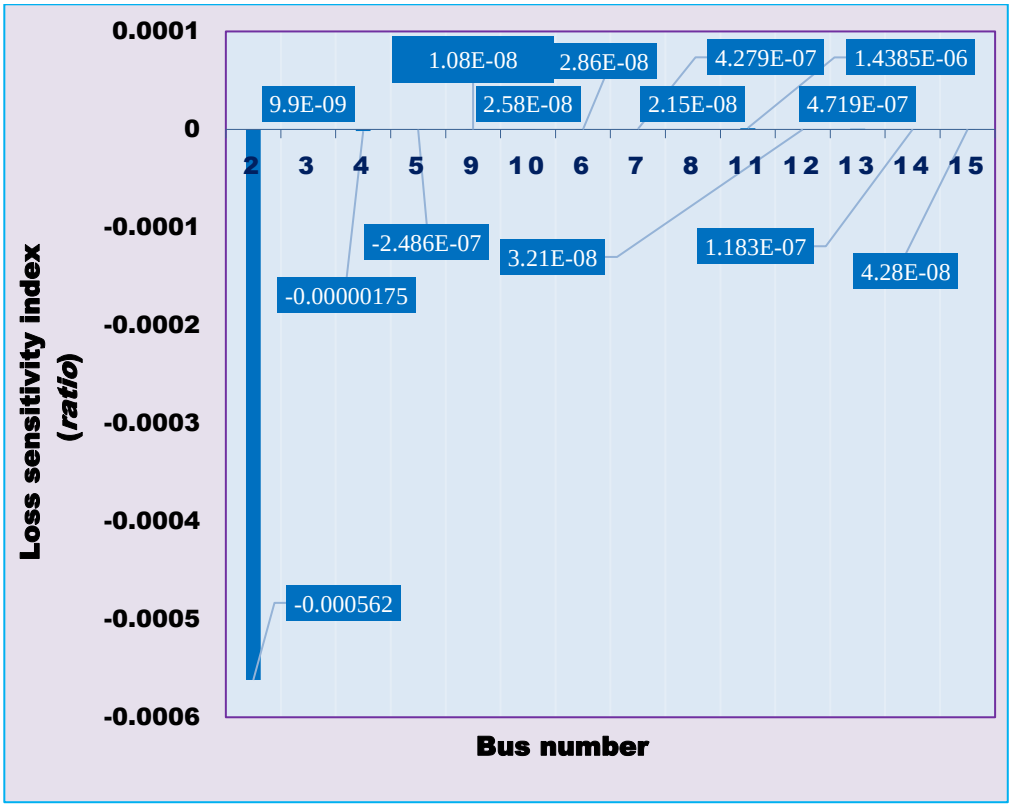

Figure 37. Loss sensitivity indices of IEEE 15-bus system

From the loss sensitivity analysis, nodes 2, 4 and 5 are possessing negative LSIs. These are the unbefitting nodes for power injection as well as extraction. The other nodes are holding positive LSIs. Among the other nodes, the nodes situated near the ends of main feeder, laterals and sub-laterals are the appropriate nodes for power injection because of high positive LSIs. The ranks of the nodes with respect to LSI values in decreasing order are (11,13,7,14,15,12,6,10,8,9,3). Nodes 11,13,7,14,15 and 12 may be considered as the most suitable for RE-EVCS integration in power injection mode. After the voltage and loss sensitivity analyses, the evaluation of optimum number as well as size identification of RE-EVCSs is done. The maximum RE-EVCS diffusion level (μ_{max}) is taken as 54.43%. For the IEEE 15-bus test bed, 0.011264 pu is the total active load power demand. Considering 54.43% RE-EVCS diffusion level, the optimum (maximum) active power injection capacity of EVCSs in power injection mode in total is 0.006132 pu. Taking 3 EVCSs simultaneously, the maximum active power injection capacity of each EVCS is 0.002044 pu. After calculating the optimum active power injection capacity of EVCSs including their optimum number, the evaluation of their reactive power injection capacity is accomplished. The distribution system power factor is considered as 0.759. Thus, the maximum reactive power injection capacity of EVCSs is computed as $(0.002044.\tan(cos^{-1}\,0.759))$ pu i.e., 0.001754 pu. In general, after assessing the total maximum active (P_{Tot}) and reactive power (Q_{Tot}) injection capacities of the network, the maximum permissible individual capacities of p numbers of identical RE-EVCSs are taken as P_{Tot}/p and Q_{Tot}/p. For three SPV-EVCS, $p = 3$. The INBPSO technique is employed to optimally allocate the EVCSs in the power distribution network (IEEE 15-bus) considering operation in power injection mode.

After that, two additional trials are carried out by altering the number of identical EVCSs with decreased power capacity. New EVCS capacities are taken as P_{Tot}/p, Q_{Tot}/p, $p = 4, 5$). However, the total maximum active and reactive power injection capacities are same as previous. Table 5 illustrates the results of these three successive trials.

Table 5 Optimum allocation of optimum number of RE-EVCSs having optimum capacities in power injection mode

Total No of RE-EVCSs	**Active power capacity / RE-EVCS**	**Reactive power capacity / RE-EVCS**	**Fitness function value**	**Optimum RE-EVCS locations (buses) →**					**CVD** (**pu**)	**Total active power loss of the network** (**pu**)
3	**0.002044**	**0.001754**	**0.4316**	**7**	**12**	**15**	**-**	**-**	**0.3017**	**0.00015476**
4	0.001533	0.000741	0.5608	4	4	7	12	-	0.3714	0.0002234
5	0.0012264	0.000594	0.5519	5	7	12	13	15	0.3617	0.000224

From Table 5, it is observed that for 3 RE-EVCSs of identical sizes, the cumulative voltage deviation (CVD) and the total active power loss (P_{LOSS}) of the network are 0.3017 pu and 0.000155 pu, respectively. With an increase in the number of EVCSs (with decreased power capacities of individual as total power capacities P_{Tot}/p, and Q_{Tot}/p are fixed), the CVD and power loss (P_{LOSS}) are increased. In case of 4 EVCSs ($p = 4$), there are two repeated EVCS locations at bus number 4, which is inappropriate practically. Moreover, node 4 is having negative LSI. For 5 EVCS ($p = 5$), the node numbers 5 and 13 are unbefitting for EVCS allocation due to the negative LSIin node 5 and negative VSI in node 13. Therefore, a maximum 3 EVCSs of optimum capacities (0.002044 pu active and 0.001754 pu reactive) can be allotted at optimum buses (i.e., 7, 12 and 15) to attain the minimum CVD and line active power loss P_{LOSS}.

The compliance of these optimally assigned RE-EVCSs as load points are investigated to confirm their operation in bi-directional approach. For the study, maximum 10 EV charging capacity per RE-EVCS has been assumed. The 8 kW chargers are assumed for the EV charging. Henceforth, the total power consumed by each RE-EVCS is 80 kW DC. The grid side rectifier efficacy is 90%, and subsequently, the input power of the rectifier unit is 88.89 ($80 \times 100/90$) kVA. Taking the distribution network power factor of 0.9, the active and reactive power

capacities of each EVCS are 80 (88.89 × 0.9) kW, i.e., 0.0008 pu, and 38.76 (88.89 × 0.436) kVAR, i.e., 0.0003876 pu, correspondingly. Table 6 presents the performance of these optimally allotted RE-EVCSs in load point mode.

Table 6 Performance study of the optimally allocated RE-EVCSs in load point mode

Total No of RE-EVCSs	**Active power capacity / RE-EVCS**	**Reactive power capacity / RE-EVCS**	**Fitness function value**	**Optimum RE-EVCS locations (Buses)→**					**CVD** (**pu**)	**Total active power loss of the network** (**pu**)
3	0.0008	0.0003876	0.845	7	12	15	-	-	0.6957	0.00076222

The CVD and P_{LOSS} of the system without EVCS integration are 0.5145 pu and 0.0005145 pu, respectively. From Table 6 results, on contrary to the system without EVCS, both the CVD and P_{LOSS} have been increased to some extent in load point mode of EVCSs. But the results are acceptable.

Figure 38 shows an evaluation of load voltage profiles of a) RE-EVCS unintegrated system, b) RE-EVCS integrated system in power injection mode, and c) RE-EVCS integrated system in load point mode. Form this study, it is apparent that, in RE-EVCSs integrated system in power injection mode, all node voltages have increased with slight overshoots (greater than 1 pu) in few nodes. But the overall CVD and P_{LOSS} have declined by the RE-EVCSs integrated system in power injection mode.

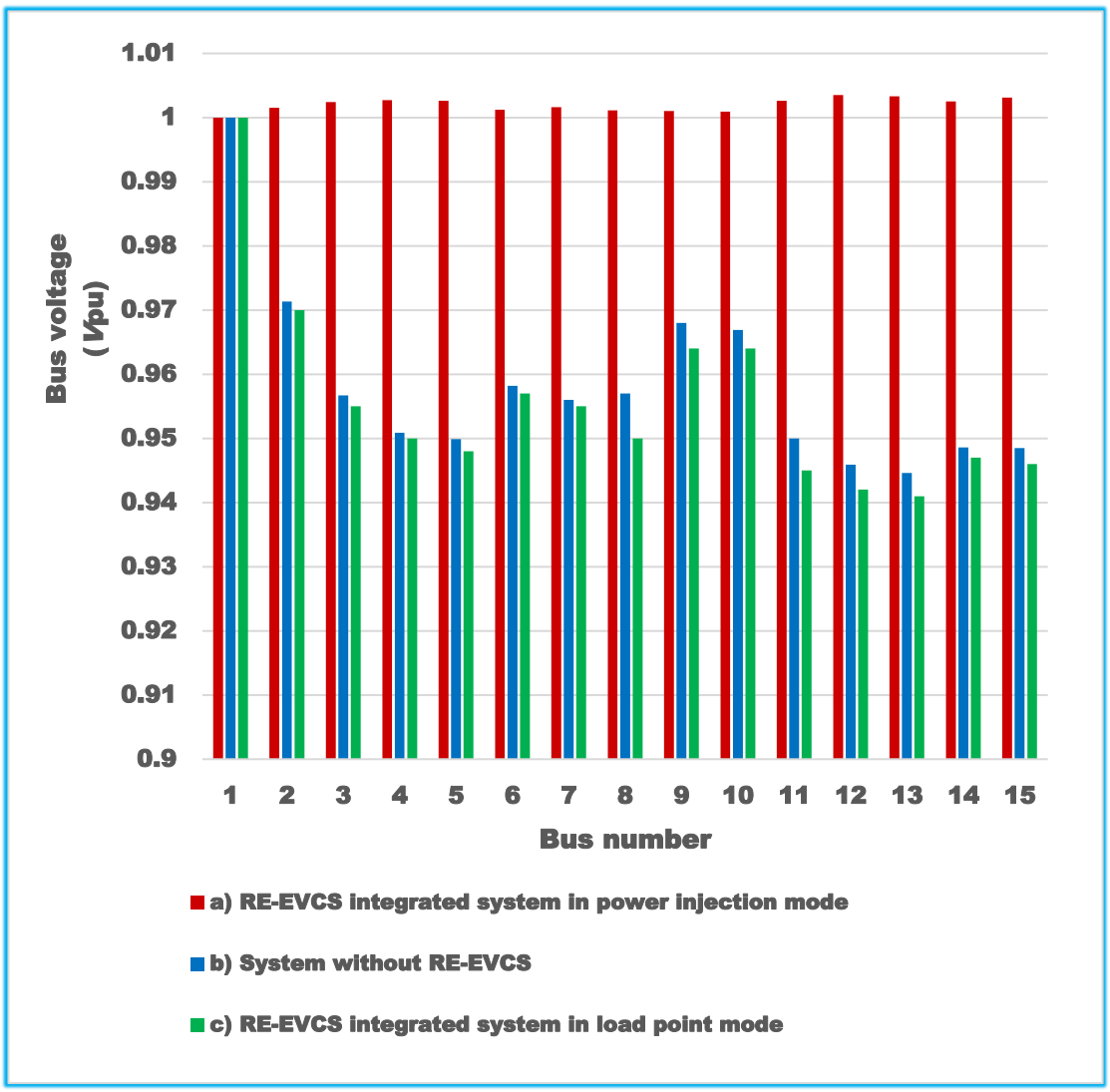

Figure 38. Comparison of voltage profiles of a) RE-EVCS unintegrated system, b) RE-EVCSs integrated system in power injection mode, and c) RE-EVCSs integrated system in load point mode in IEEE 15-bus system

In RE-EVCSs integrated system in load point mode, the voltage profile is slightly degraded, but it is within the restricted limits. The lower most voltage is 0.941 pu at node 13. The case study reveals that the optimally allocated RE-EVCS integrated system is appropriate in terms of system performance.

4.2.4 Case Study 4: RE-EVCS integration with IEEE 33-bus system for voltage profile improvement and line loss minimization in power injection mode

For optimal integration of RE-EVCS into the distribution network in power injection mode, a bi-objective GA is cast-off for lessening the total line loss and total voltage error. The IEEE 33-bus system is considered for simulation purpose. The total active and reactive power capacities of the IEEE 33-bus system are 3.715 MW and 2.3 MVAR, respectively. The network single-line diagram is presented in Figure 39. GA collaborated with the BFSM is exploited for location selection of six RE-EVCSs of stipulated sizes within the distribution network.

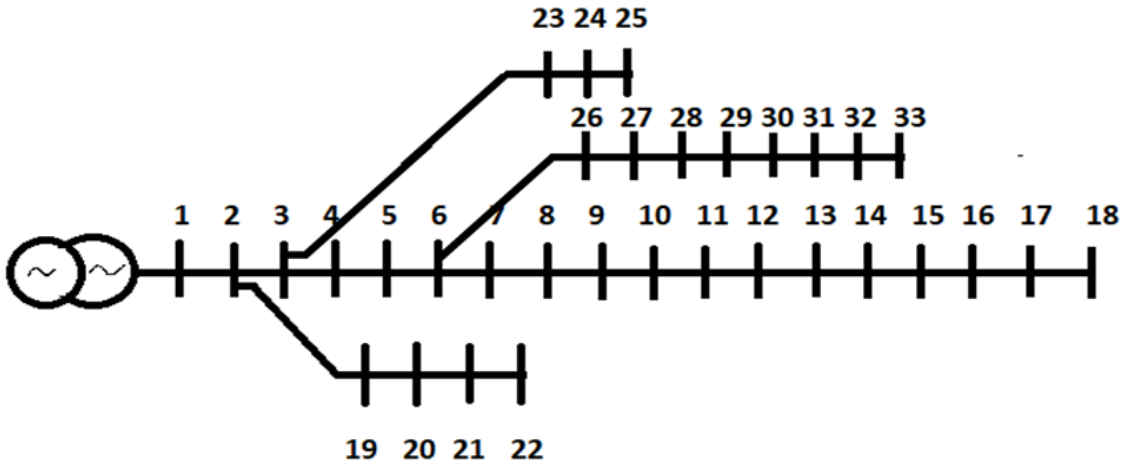

Figure 39. Single-line diagram of IEEE 33-Bus System

For starting the GA optimization, at first 20 individuals (chromosomes) are taken to form the population. 200 generations are selected. Tournament (having size 4) is chosen as selection function. Elite count is recognized as 0.05 multiple of population size. Intermediate crossover function is nominated with a crossover ratio of 1. Adaptive feasible mutation is performed with a crossover fraction of 0.8. Forward migration with a fraction of 0.2 is reserved. Six numbers of independent variables are taken for storing the initial as well as the updated RE-EVCS locations using the GA toolbox. The lower and upper bounds (2 and 33) of each variable are mentioned within the GA optimizer. The parameter settings for the GA optimizer are presented in Table 7.

Table 7 GA stricture setting

Parameters	Values
Size of population	20
Selection strategy	Tournament
Size of tournament	4
Count of elite parents	0.05*population size
Fraction of crossover	0.8
Mutation strategy	Adaptive feasible
Crossover strategy	Intermediate
Crossover ratio	1
Migration	Forward
Migration fraction	0.2
Number of generations	200
Stopping criteria:	Time bound: inf Fitness bound: - inf Stalling generation: 50 Stall time boundary: + inf Stall assessment: average change Function acceptance: e^{-3}
Plot functions:	• Selection • Expectation • Scores • Score diversity • Genealogy • Best fitness • Best individual

BFSM is incorporated for power drift scrutiny of the distribution system under both RE-EVCS integrated and unintegrated conditions. It is the key algorithm used to manipulate the fitness value of every member (chromosome) within the postulated population. All the independent variables are passed as arguments within the BFSM function. The objective (fitness) function is deployed after calculation of all line currents and node voltages. This fitness value is then returned into the GA optimizer for further processing.

The simulation results of the proposed bi-objective GA technique are presented in Figures 40-46. Active and reactive power of the six RE-EVCSs considering 50% penetration level [El-Fergany, 2015] are calculated as follows:

$$\boldsymbol{\mu = \frac{\sum_{k=1}^{p} P_{RE-EVCS}(k)}{\sum_{c=1}^{N_L} P_D(c)} = 50\%}$$

The base MVA and base kV are taken as 100 MVA and 12.66 kV. The total active and reactive powers drawn by the loads are 0.03655 pu ($\sum_{c=1}^{N_L} \boldsymbol{P_D(c)}$) and 0.0226 pu ($\sum_{c=1}^{N_L} \boldsymbol{Q_D(c)}$), respectively. Thus,

$$\boldsymbol{\sum_{k=1}^{p} P_{RE-EVCS}(k) = 50\% \times \sum_{c=1}^{N_L} P_D(c) = 50\,\% \times 0.03655 = 0.018275}\ \text{pu.}$$

As six identical RE-EVCSs are to be incorporated within the test network, the active power of each RE-EVCS is (0.018275/6) i.e.,($\boldsymbol{3.046 \times 10^{-3}}$) pu. The power factor of the injected power is taken as 0.876. Thus, the reactive power injected by each RE-EVCS is ($\boldsymbol{3.046 \times 10^{-3}}$) $\boldsymbol{\times \tan(cos^{-1} 0.876)}$ pu, i.e.,$\boldsymbol{1.677 \times 10^{-3}}$ pu.

Consequently, the active and reactive power arrays presenting the powers injected by the RE-EVCSs into the distribution network are:

$$\mathbf{P_{RE-EVCS}} = [\,\mathbf{3.046 \quad 3.046 \quad 3.046 \quad 3.046 \quad 3.046 \quad 3.046}\,] \times \mathbf{10^{-3}}$$

and

$$\mathrm{Q_{RE-EVCS}} = [1.677 \quad 1.677 \quad 1.677 \quad 1.677 \quad 1.677 \quad 1.677] \times 10^{-3}$$

These arrays are embedded within the BFSM function for updating the system active and reactive power according to the RE-EVCS locations (chromosomes) generated by the GA optimizer. The fitness function is evaluated.

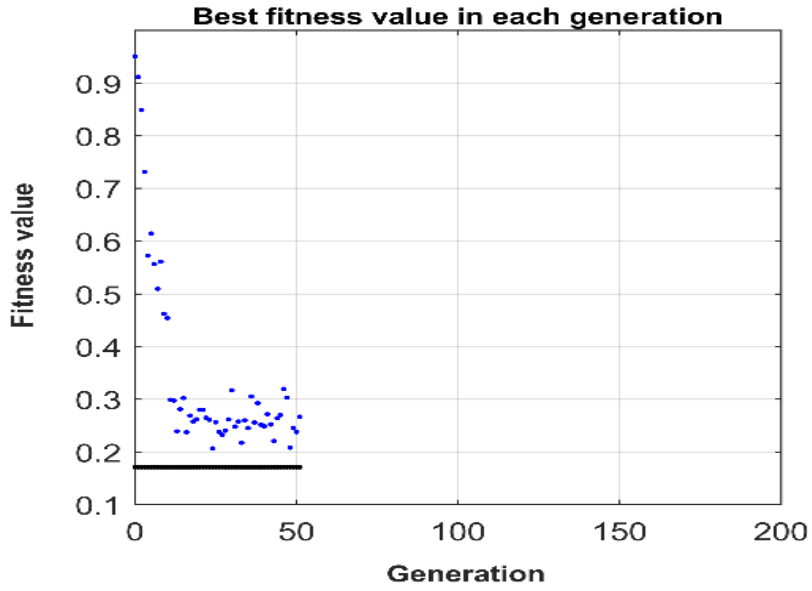

Figure 40. Best fitness value of each generation

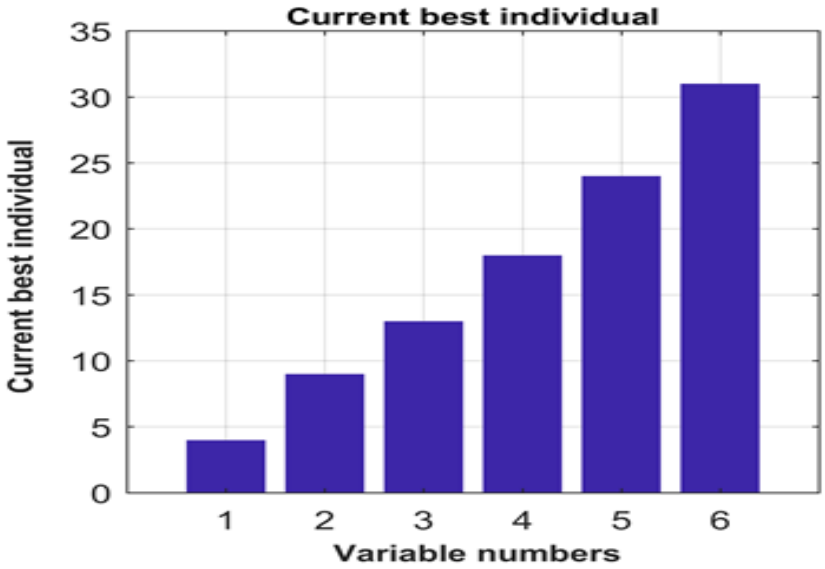

Figure 41. Best individual of each variable (gene)

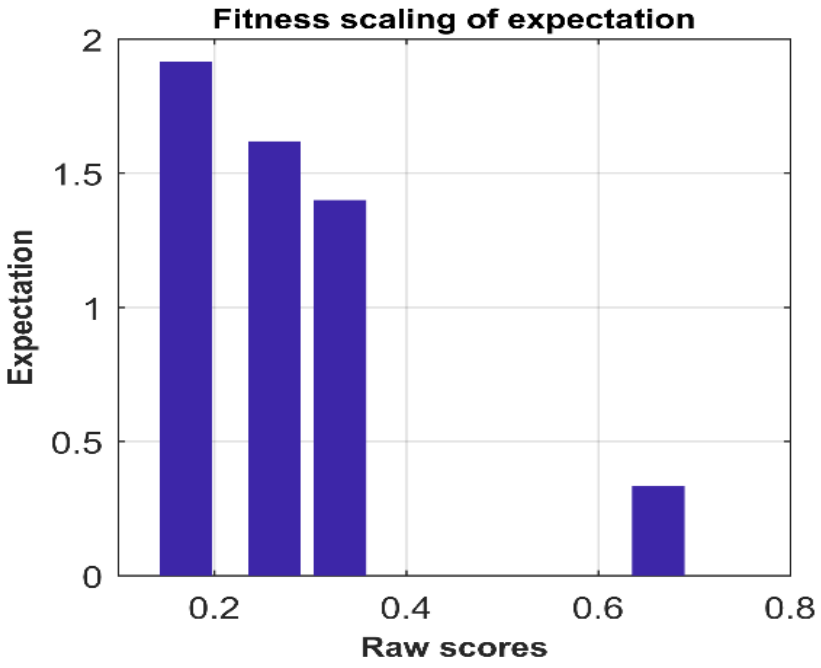

Figure 42. Score expectation

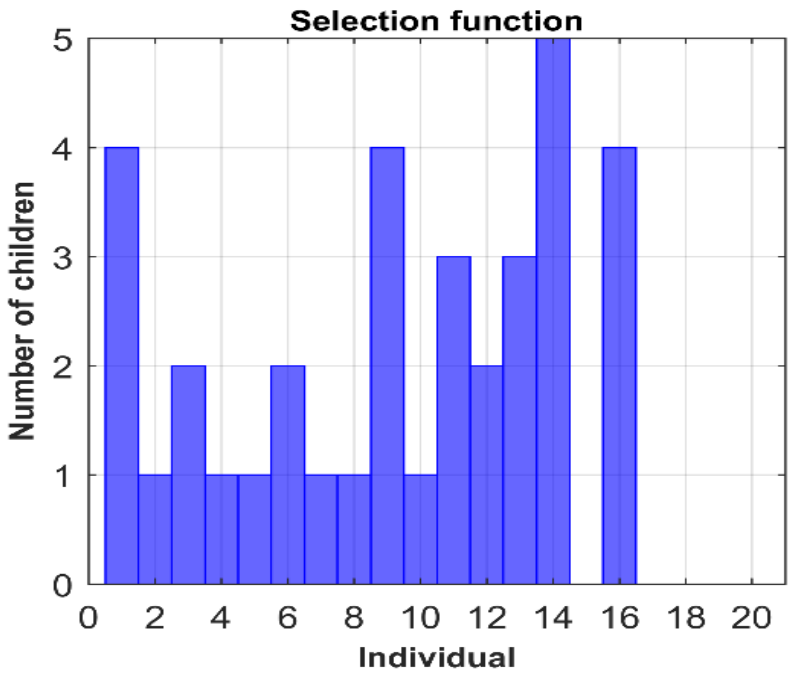

Figure 43. Selection of each chromosome

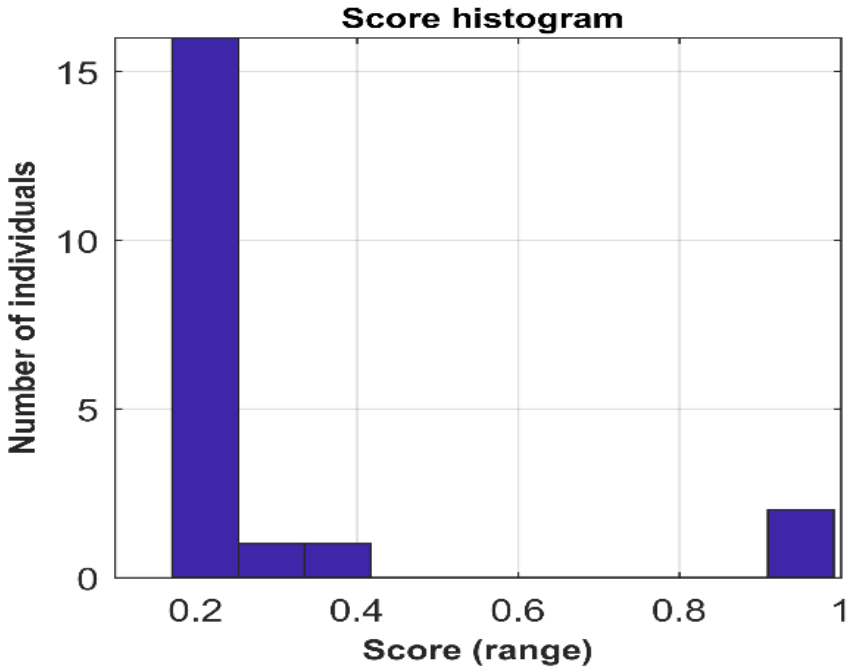

Figure 44. Score histogram

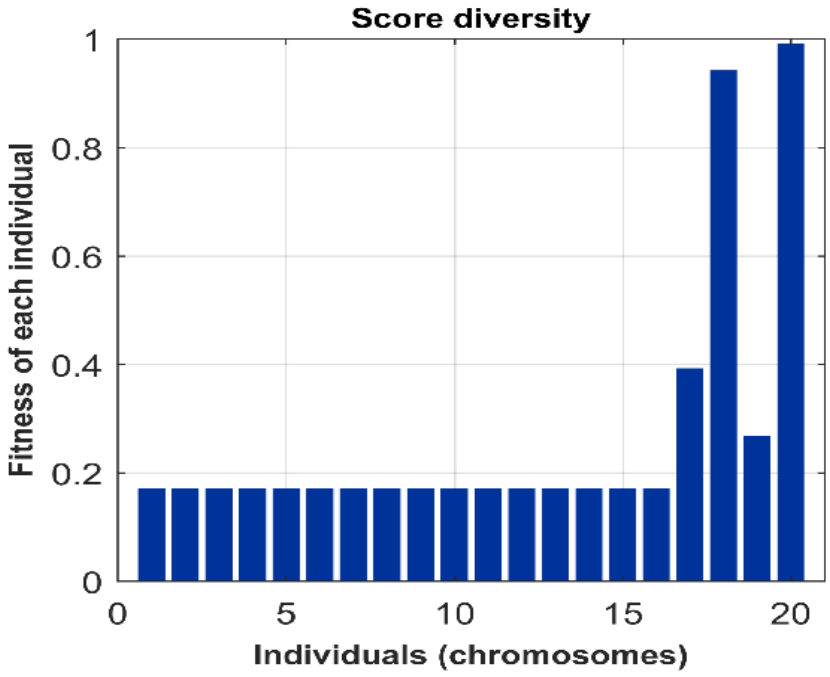

Figure 45. Score diversity (of chromosomes)

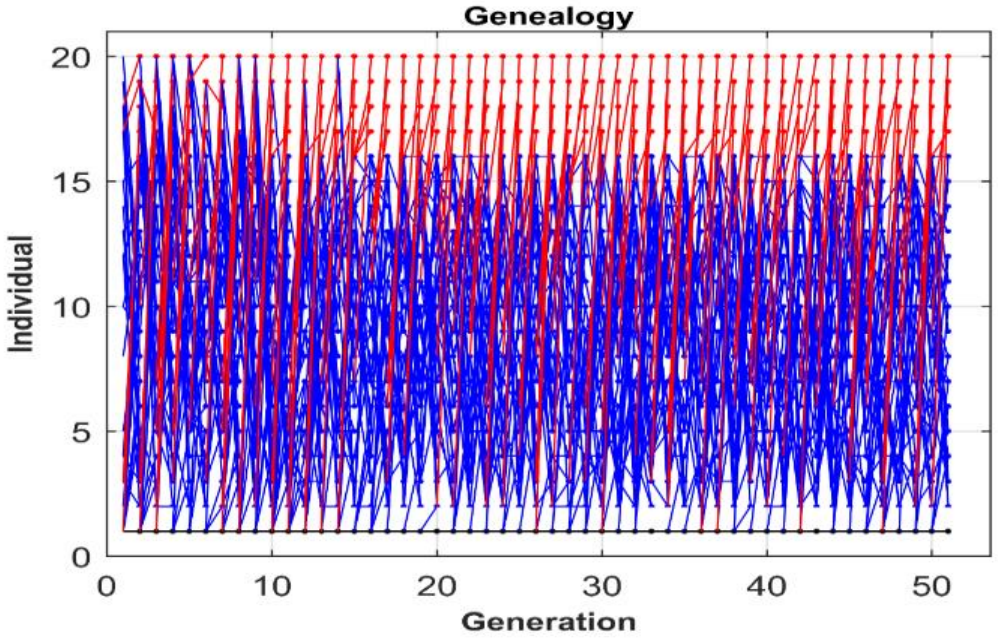

Figure 46. Genealogy

Figure 40 presents the best fitness function of each generation. Figure 41 shows the number of best individuals in each variable. Figures 42 - 46 present score expectation, selection of each chromosome, score histogram, score diversity (of individuals or chromosomes) and genealogy, respectively. According to the obtained results, the best optimum locations for integrating the RE-EVCSs with the distribution network are (4,9,13,18,24 and 31). The highest over and under voltage errors are found to be 0 and 0.0537 pu, respectively. The tolerance band for voltage deviation is ± 0.1 pu. Therefore, the results are highly satisfactory in terms of voltage deviation. The $\boldsymbol{CVD}$ and $\boldsymbol{P_{LOSS}}$ values are 0 pu (approximately) and 0.00063 pu (63 kW) considering 50% penetration level. The $\boldsymbol{CVD}$ and $\boldsymbol{P_{LOSS}}$ of the system without RE-EVCS integration are 1.7895 pu and 0.0025pu. All constraints and their ranges are verified and it is observed to stay within the allowable limits. Both the $\boldsymbol{CVD}$ and $\boldsymbol{P_{LOSS}}$ have reduced with the integration of RE-EVCSs. Moreover, the proposed methodology is providing superior results compared to results in El-Fergany, 2015, wherein the $\boldsymbol{CVD}$ and $\boldsymbol{P_{LOSS}}$ values are 0 pu and 82.78 kW with the same specifications. Further, the test results are compared with the results presented in

Kaushal and Tomar, 2017; where the active power loss is 190.6362 kW. Here, the active power loss is reduced to 63 kW. From the analysis of the results, it can be concluded that, the proposed methodology is giving superior results in terms of both voltage deviations and power loss minimization.

4.3 Second Phase of the Proposed Work

The second phase of the proposed work is carried out in two fragments for power flow management.

First fragment of second phase work:

During the first fragment of the work, a MATLAB/Simulink model for a the multiple (three) SPV-EVCS integrated distribution network along with their ESUs and EV batteries has been developed. The SPV-EVCSs are injecting the PV array power into the distribution network. It is assumed that there is no EV and ESU charging requirements. The total active and reactive power generated from the SPV-EVCS is fed through the node numbers 7, 12 and 15 of the system as per the results obtained from *Case Study* 3 of the first phase of the proposed work [refer sub-section 4.2.3]. The PV array generates DC power, which is fed to the three-phase inverter to convert DC power to AC. The three-phase AC output of the inverter is fed into the distribution network through a three-phase transformer. From the *Case Study* 3 of the first phase of work [refer sub-section 4.2.3], the optimum RE-EVCS locations are found to be node numbers 7, 12 and 15 in the IEEE 15-bus test bed. The active and reactive powers to be injected into the distribution network through each of these three optimum locations are 0.002044 pu (i.e., 0.002044×10^5 kW $=$ 204.4 kW) and 0.00175 pu (i.e., 0.001754×10^5 kVAR $=$ 175.4 kVAR), respectively. Therefore, the apparent power from each SPV-EVCS to the distribution network is $\sqrt{P_{injected}^2 + Q_{injected}^2} = \sqrt{(204.4 \times 10^3)^2 + (175.4 \times 10^3)^2} = 269.34$ kVA.

Three identical PV arrays with 34 parallel strings are configured. Each string consists of 38 series connected PV modules. Voltage and current of each module at maximum power point at STC are $V_{mp} = 29$ V and $I_{mp} = 7.35$A (refer Table 1 in Chapter 3). Hence, the total capacity of the PV array is 275.39 (29 × 7.35 × 38 ×

34) kVA. The PV generated power is taken higher than the required injected power considering system and component level losses. The 1Soltech 1STH-215-P PV module [S1PVD, 2021] is considered. The different parameter settings of the Simulink model are presented in Table 8.

Table 8 The parameters and their values used in the simulation-based study

Parameters	Values
PV array series connected modules per string	38
PV array parallel strings	34
DC link bus parallel RC branch capacitance	1000 μF
DC link bus parallel RC branch resistance	0.5 mΩ
Three phase inverter's repeating sequence frequency	10 kHz
L-C filter inductance value (per phase)	500 μH
L-C filter capacitance value (per phase)	100 μF
Three phase transformer connections (primary-secondary)	YG-YG
Transformer nominal power	550 MVA
Transformer frequency	60 Hz
Primary winding voltage (L-L) rating	1560 V
Secondary winding voltage (L-L) rating	15600 V
Transformer turns ratio	1:10
Primary winding resistance	$1\times 10^5\ \Omega$
Primary winding inductance	200 μH
Secondary winding resistance	$1\times 10^5\ \Omega$
Secondary winding inductance	3000 μH
Transformer magnetization resistance	1212.1 Ω
Transformer magnetization inductance	3.2152 H
Active power injection reference value	204.4kW
Reactive power injection reference value	175.4 kVAR

Buck converter 1: inductance	1.66×10^{-5} H
Buck converter 1: capacitance	5.76×10^{-5} F
Buck converter 1: PI controller's repeating sequence frequency	25 kHz
Buck converter 1: PI controller's reference voltage	400 V
Buck converter 1: PI controller' gain	1/400
Buck converter 1: PI controller' proportional gain	0.7
Buck converter 1: PI controller' integral gain	100
Buck converter 2: inductance	1.66×10^{-5} H
Buck converter 2: capacitance	5.76×10^{-5} F
Buck converter 2: PI controller's repeating sequence frequency	125 KHz
Buck converter 2: PI controller's reference voltage	48 V
Buck converter 2: PI controller' gain	1/48
Buck converter 2: PI controller' proportional gain	0.7
Buck converter 2: PI controller' integral gain	100
PLL: PI controller's proportional gain	10
PLL: PI controller's integral gain	50000
d axis power controller 1: proportional gain	0.25
d axis power controller 1: integral gain	0.001
d axis power controller 2: proportional gain	3.33
d axis power controller 2: integral gain	5000
q axis power controller 1: proportional gain	0.25
q axis power controller 1: integral gain	0.001
q axis power controller 2: proportional gain	3.33
q-axis power controller 2: integral gain	5000
ESU nominal voltage	400 V
ESU rated capacity	2800 Ah
ESU state of charge	20%
EV nominal voltage	48 V
EV rated capacity	280 Ah
EV state of charge	20%

Figure 47 presents the PV array output voltage waveform. From the waveform, the DC link bus voltage has attained 1250 V under steady state condition. Figure 48 presents the three-phase inverter output voltage (L-G) and current waveforms. The peak output voltage of inverter is 1250 V, and the RMS value is 883.9 V. The peak value of the current is 140 A (approx.) and the RMS value is 98.99 A. Figure 49 presents the three-phase control voltages and the repeating sequence in SVPWM generation. The step-by-step procedure of generating the three-phase control voltages are a) The three-phase control pulses are generated by the *d* and *q* axis power controllers b) The control pulses are normalized by multiplying each of them by the factor $(^{2}/_{V_{PV}})$ to generate the required *d-q* axis components of modulation index. c) These components are sent inside *d-q* to *abc* transformation (*dq0* to *abc*) block to generate the three-phase control voltages. Figure 50 shows the inverter gate triggering pulses generated. Figure 51 presents the three-phase transformer output voltage (L-G) and current waveforms. The transformer output voltage (L-G) is 11 kV (peak) and RMS value is 7778 V. The theoretical value of the transformer output voltage should be 10 times the inverter output voltage i.e. 8839 V. However, the simulated value is slightly less than the theoretical value. The output current has reached to 14 A (peak), which is $(^{1}/_{10})^{th}$ times the inverter output current. Figure 52 presents the RMS values of the active and reactive powers injected into the distribution system. From the results, it is observed that the active and reactive powers are 175 kW and 150 kVAR at steady state. These values are less than the expected values (204.4 kW and 175.4 kVAR). This is due the power loss in different components like PV panel, inverter, transformer, etc. The apparent power obtained at the transformer output is $\sqrt{P_{injected}^2 + Q_{injected}^2} = \sqrt{(175 \times 10^3)^2 + (150 \times 10^3)^2} = 230.49$ kVA, which is 38.85 kVA less than the theoretical value (i.e. 269.34 kVA).

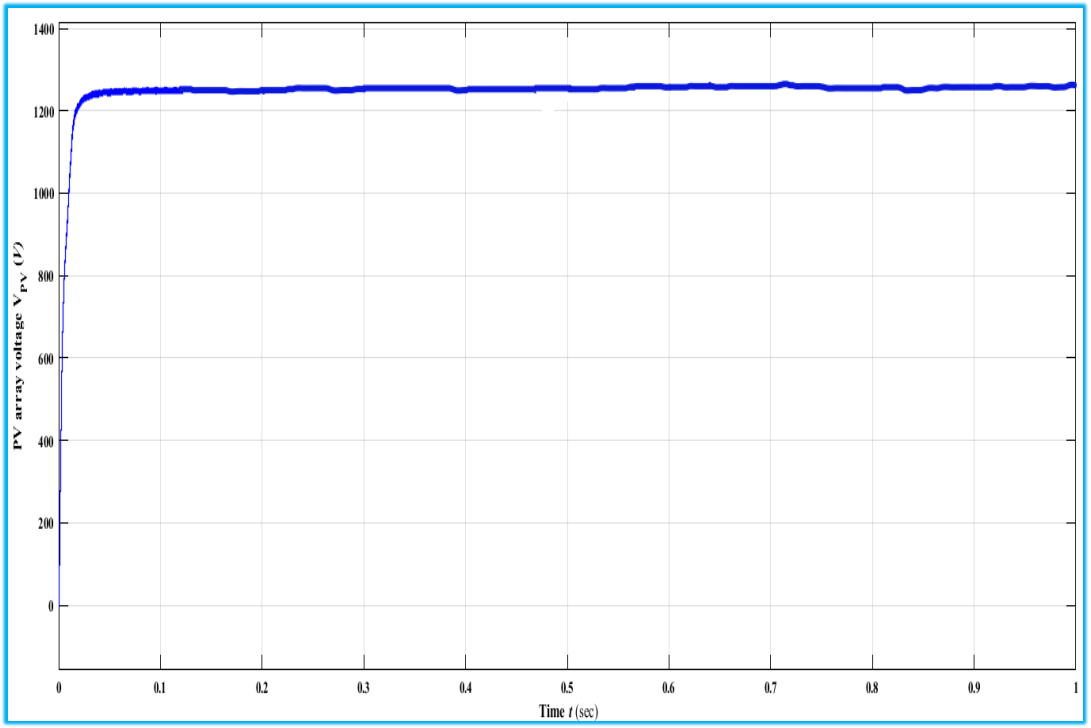

Figure 47. The PV array output voltage waveform

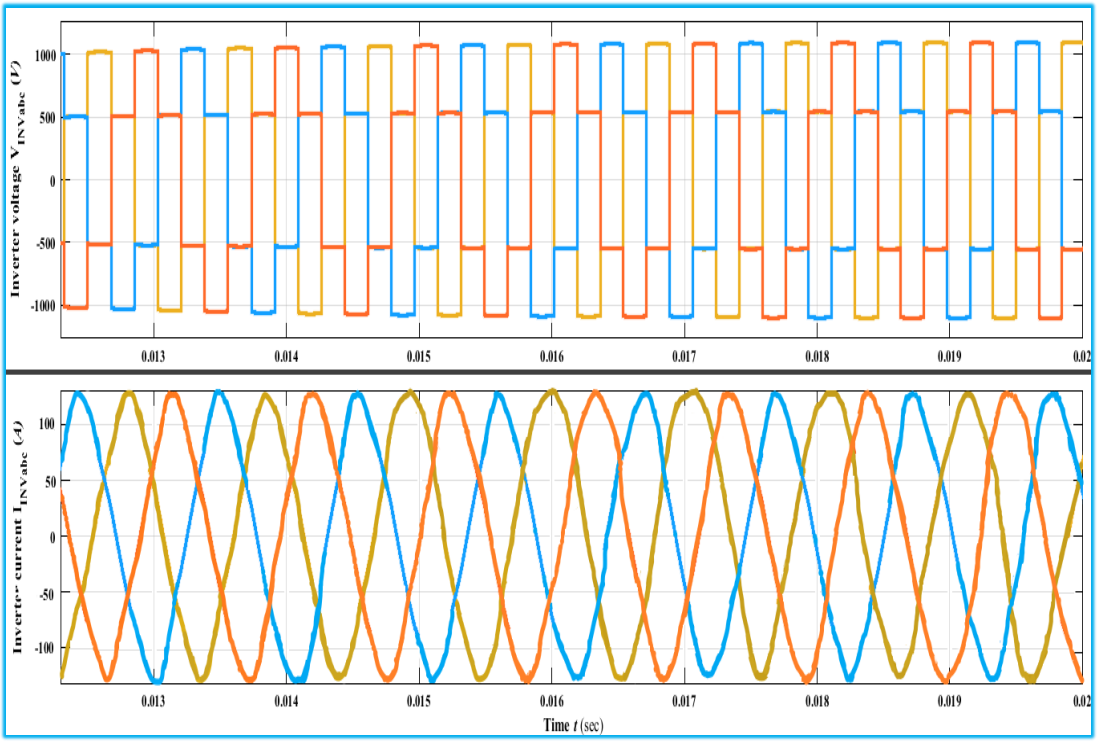

Figure 48. Three phase inverter output voltage (L-G) and current waveforms

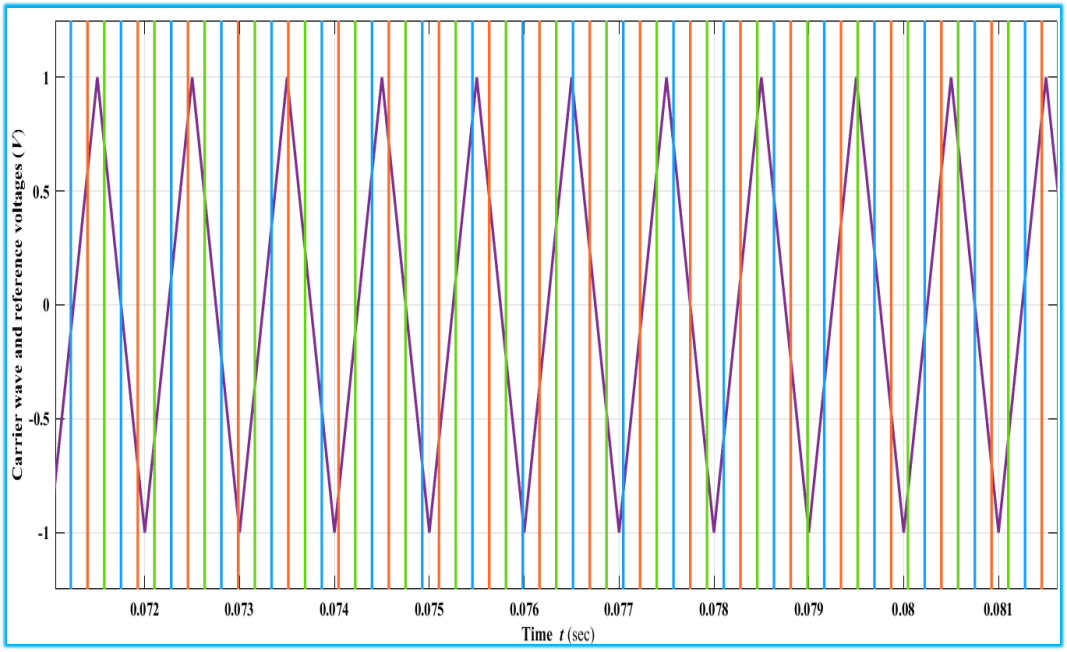

Figure 49. Three phase control voltages and the repeating sequence to produce inverter gate triggering pulses

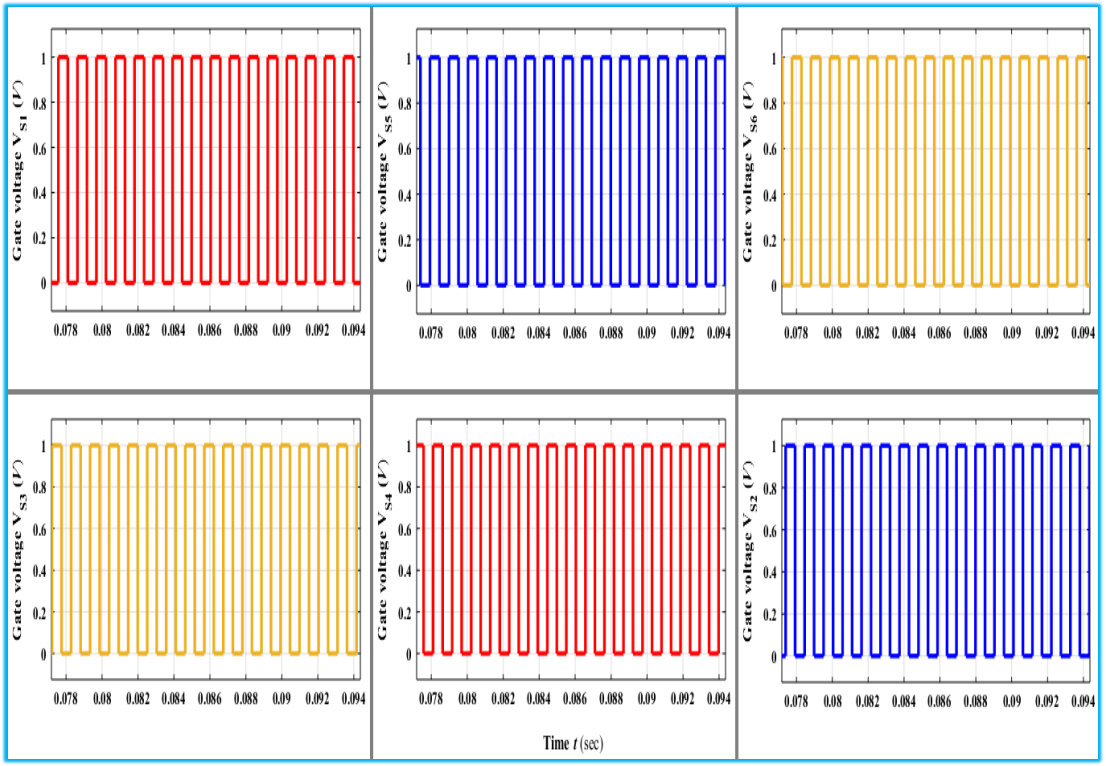

Figure 50. The gate triggering pulses generated for the inverter gate triggering

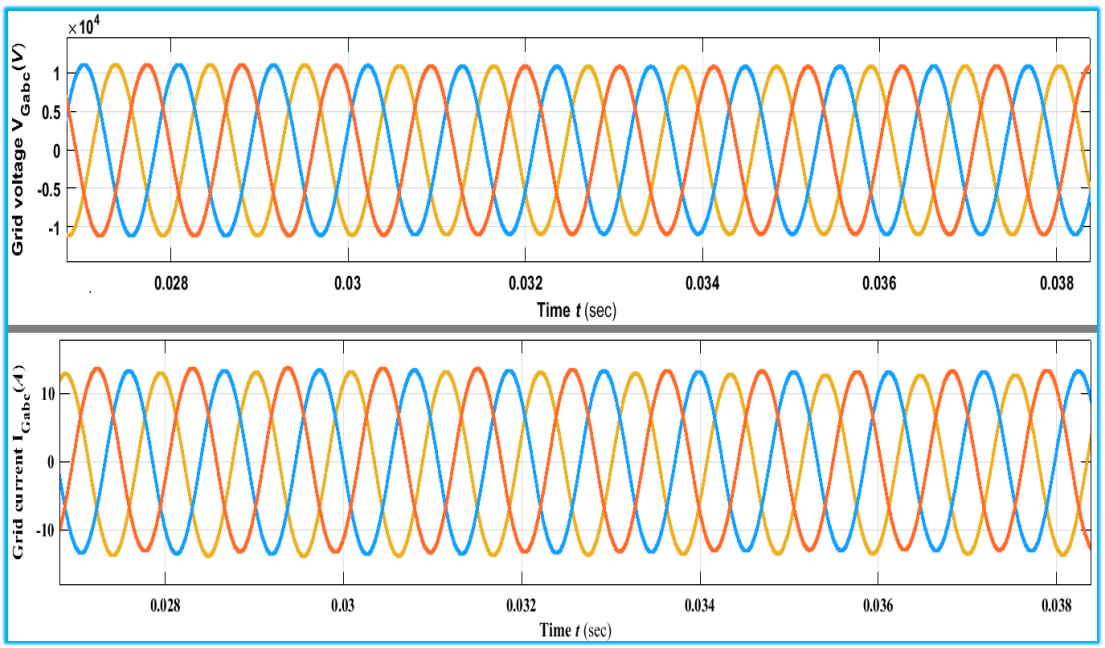

Figure 51. Three phase transformer output voltage (L-G) and current waveforms

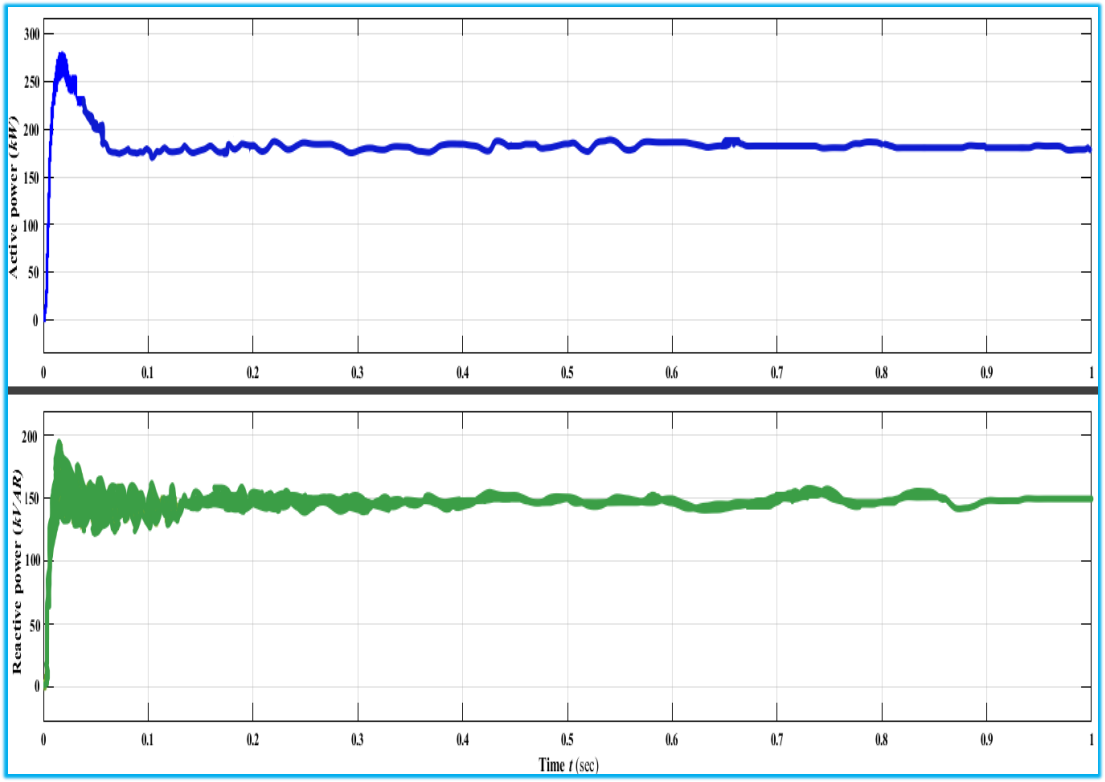

Figure 52. The active and reactive power (RMS) waveforms

The comparison of the voltage profiles of SPV-EVCS integrated and unintegrated system under the condition, where the SPV-EVCSs are injecting the total PV array power into the distribution network and there is no EV and ESU charging requirements; is accomplished. Figure 53 presents the comparison between the voltage profiles of SPV-EVCS integrated and unintegrated systems.

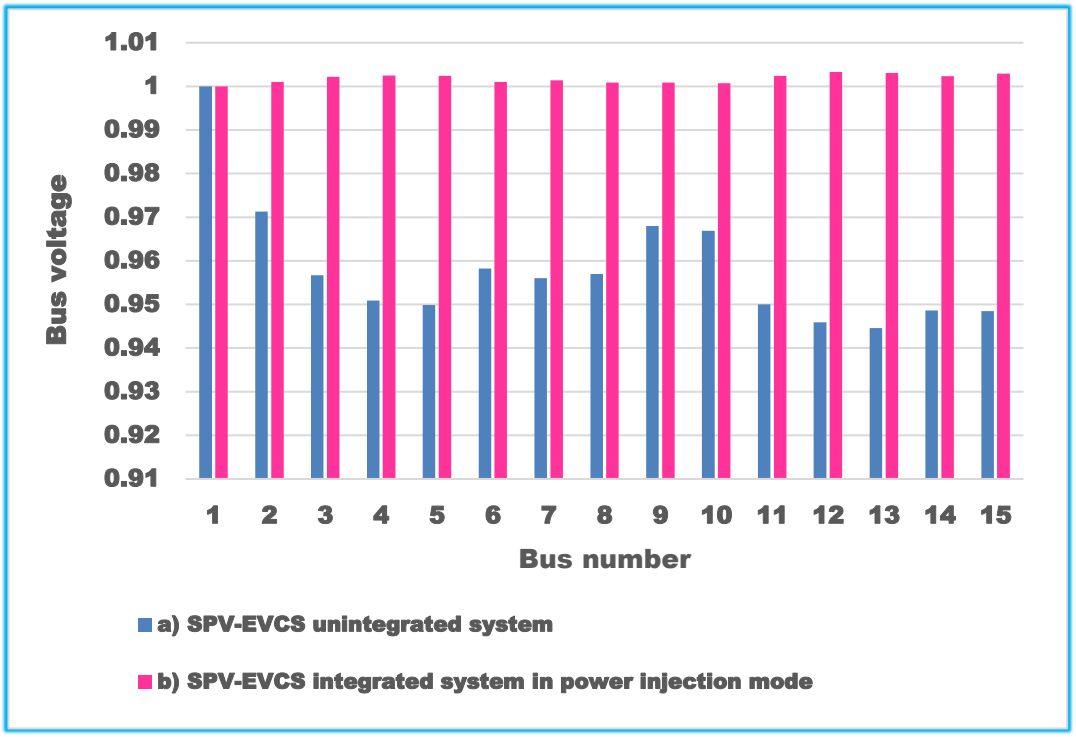

Figure 53. Comparison between the voltage profiles of a) SPV-EVCS unintegrated system and b) SPV-EVCS integrated system in power injection mode

From Figure 53, it is observed that the voltage profile of the IEEE 15-bus system is better under EVCS integrated condition than the unintegrated network. The result of the comparative study proves the efficacy of the integrated system.

Second fragment of second phase work:

During the second fragment of work, the ESU and EV are considered in power flow study of the integrated system. Two lithium ion batteries are taken: one for ESU and the other one for EV. The specifications of the batteries are given in

Table 8. The SOC of both the batteries is set to 20%. As a result, both of them are simultaneously charged by the the PV array power. The excess power from the PV array is injected into the distribution network. The DC link bus voltage is higher than the ESU rated voltage and buck converter 1 is employed with PID controller to step down the voltage level to 400 V. This voltage is reduced to approximately 48 V by using the second stage buck converter (buck converter 2). Figure 54 presents the PV array, ESU and EV voltages.

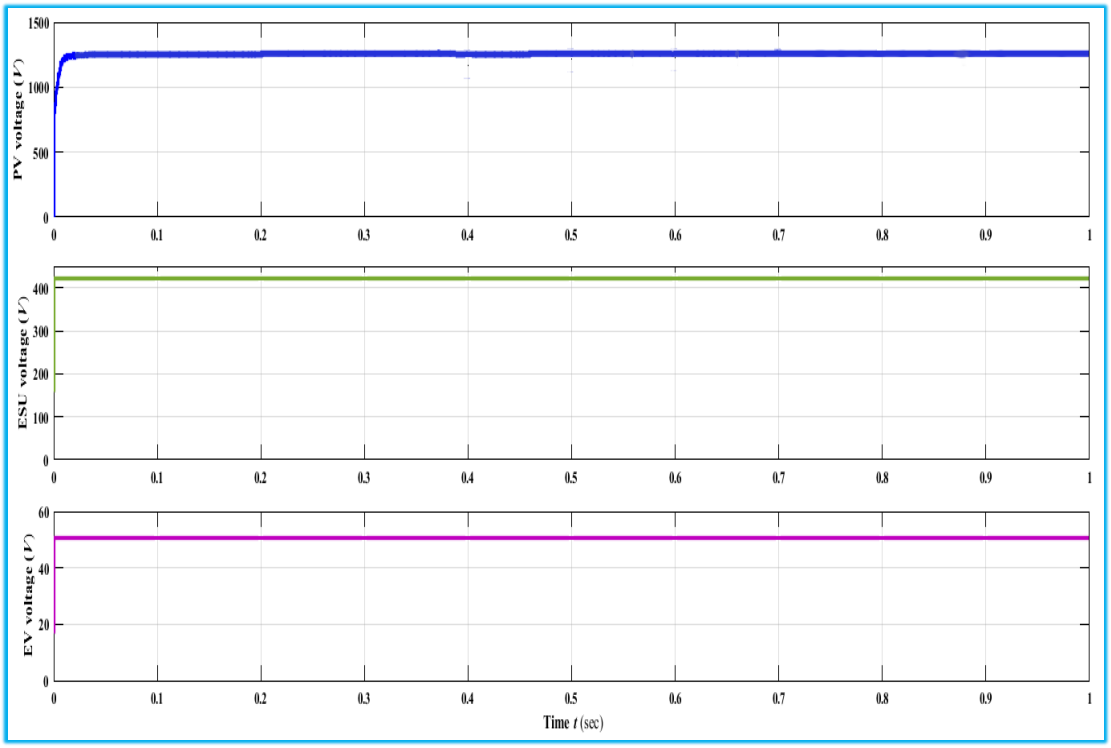

Figure 54. The PV array, ESU and EV voltages

From the simulation results, it is observed that, the output DC voltage of the buck converter 1 is 425 V and the output DC voltage of the second buck converter is 51 V, which are near to the desired values (400 and 48 V) respectively. The voltages and currents at different points of the integrated network is examined and found to be satisfactory to permit power flow between EVCSs and power distributed network.

4.4 Conclusion

Research work on multi EVCS integrated distributed network is considered in two phases. In the first phase, four case studies are conducted for optimal allocation of EVCSs in distribution networks, considering two different mode of power flow, namely, load point mode and power injection mode. Different optimization techniques collaborated with power flow algorithm such as BFSM are applied in an efficient manner for optimum allocation of EVCSs and results of all case studies are presented. The results reflect that, the EVCSs operating in load point mode in an integrated system, may degrade the voltage profile. Thus, to maintain the voltage profile and power loss within the allowable limits; both the EVCS capacity and location selection are important. The addition of RER integrated EVCSs with the distribution network at power injection mode can upgrade the voltage profile and minimize the system loss. The second phase of the work can be considered in two fragments. In first fragment, a simulation model of the multiple SPV-EVCS integrated distribution network is developed and power flow management study is conducted disregarding the ESU and EV changing. In the second fragment, the power flow management study is comprehended incorporating ESU and EV charging. The voltages, currents, and powers at different points of the integrated network are examined, which are found to be satisfactory to permit power flow between EVCSs and power distributed network.

CHAPTER 5

CONCLUSION

AND

FUTURE SCOPE

5. CONCLUSION AND FUTURE SCOPE

5.1 Conclusion

Effective allocation of EVCSs in a power distribution network is of great importance for preserving voltage profile and minimizing the system loss. The effective allocation of EVCSs in a power distribution network is considered as an optimization problem. Objective functions are formed with different associated parameters and system constraints. A detailed discussion on the objective functions, the related parameters, and constraints along with their boundaries are given. Useful mathematical models for the optimum allotment of EVCSs in power distribution networks are developed. Two popular power flow analysis methods, BFSM and an efficient one developed especially for the distribution network are presented elaborately. Several useful optimization techniques namely PSO, PPSO, INBPSO and GA are explored. Optimization techniques collaborating with power flow analysis are applied in solving optimum EVCS allocation problems. After these, a simulation model for multiple SPV-EVCS integrated distribution network is developed with the intention of power management study.

The research work is mainly conducted in two phases. In the first phase, four case studies are performed for optimal allocation of EVCSs in distribution networks, considering two different mode of power flow, namely, load point mode and power injection mode. In *Case Study 1*, investigation is done on the voltage profile of the EVCS integrated IEEE 15-bus system under load point mode of operation. In *Case Study 2*, investigation is carried out on the bi-directional SPV-EVCS integration with IEEE 69-bus system for voltage profile upgradation at power injection mode. In *Case Study 3* investigation is done on bi-directional RE-EVCS integration with IEEE 15-bus system aiming to improvement in voltage profile and minimization of line losses in power injection mode of operation. In *Case Study* 4, investigation is conducted on RE-EVCS integration with IEEE 33-bus system for voltage profile improvement and line loss minimization in power injection mode. The voltage sensitivity analysis and

loss sensitivity analysis are also performed in different case studies. The reason behind the sensitivity analysis is to verify the suitability of nodes for integration. The results of the case studies signify that the strategic integration of EVCSs into the power distribution network can improve the system voltage profile while minimizing the system line loss. The EVCSs operating in load point mode in an integrated system, may degrade the voltage profile. Thus, to maintain the voltage profile and power loss within the allowable limits, both the EVCS capacity and location selection are important.

The second phase of the work is accomplished in two fragments. In first fragment, a simulation model of a multiple SPV-EVCS integrated distribution network is developed, and power flow management study is conducted disregarding the ESU and EV changing. In the second fragment of the work, the power flow management study is comprehended by incorporating the ESU and EV charging. The voltages, currents, and powers at different points of the integrated network are examined and the results are found permitting power flow between EVCSs and power distribution network satisfactorily.

All investigated results in connection with the optimum allocation of EVCSs and power flow management are presented. From the entire work, it can be concluded that the multiple RE-EVCS integrated distribution network can manage power transfer coordinately. At adverse conditions, one can support the other thus avoiding peak loading support and high-capacity battery back-up.

5.2 Future Scope

The present research work proposes the optimum allocation of EVCSs in a distribution network and power management of the integrated system. More future works can be suggested as follows:

- Activity based behavior of vehicle drivers can be accounted in the optimization model.
- EVCS integrated system with G2V and V2G enabled power transfer for net profit maximization can be modeled and investigated.

- In the power management study of the present work, the power flow only from EVCSs to distribution network is considered. However, the work can be extended to realize an advanced controller to efficiently control power flow providing G2V, V2G and V2V functionalities.
- To enable the combined economic and technical management or the coordination of diversified EVCSs; aggregator supported EV charging realization can be focused.

Appendices:

Table I: IEEE 15-bus line and load data

Line No.	**Start Node**	**End Node**	**Length (m)**	***R*/Length (Ω)**	***X*/Length (Ω)**	**P_L in end node (kW)**	**Q_L in end node (kVAR)**
1	1	2	1	1.35309	1.32349	44.1	44.99
2	2	3	1	1.17024	1.14464	70	71.41
3	3	4	1	0.84111	0.82271	140	142.82
4	4	5	1	1.52348	1.0276	44.1	44.99
8	2	9	1	2.01317	1.3579	70	71.44
9	9	10	1	1.68671	1.1377	44.1	44.99
5	2	6	1	2.55727	1.7249	140	142.82
7	6	7	1	1.0882	0.734	140	142.82
6	6	8	1	1.25143	0.8441	70	71.41
10	3	11	1	1.79553	1.2111	140	142.82
11	11	12	1	2.44845	1.6515	70	71.41
12	12	13	1	2.01317	1.3579	44.1	44.29
14	4	14	1	2.23081	1.5047	70	71.414

Table II: IEEE 33-bus line and load data

Line No.	Start Node	End Node	Length (m)	*R*/Length (Ω)	*X*/Length (Ω)	P_L in end node (kW)	Q_L in end node (kVAR)
1	1	2	1	0.0922	0.0477	100	60
2	2	3	1	0.4930	0.2511	90	40
3	3	4	1	0.3661	0.1864	120	80
4	4	5	1	0.3811	0.1941	60	30
5	5	6	1	0.8190	0.7070	60	20
6	6	7	1	0.1872	0.6188	200	100
7	7	8	1	0.7115	0.2351	200	100
8	8	9	1	1.0299	0.7400	60	20
9	9	10	1	1.0440	0.7400	60	20
10	10	11	1	0.1967	0.0651	45	30
11	11	12	1	0.3744	0.1298	60	35
12	12	13	1	1.4680	1.1549	60	35
13	13	14	1	0.5416	0.7129	120	80
14	14	15	1	0.5909	0.5260	60	10
15	15	16	1	0.7462	0.5449	60	20
16	16	17	1	1.2889	1.7210	60	20
17	17	18	1	0.7320	0.5739	90	40
18	2	19	1	0.1640	0.1565	90	40
19	19	20	1	1.5042	1.3555	90	40
20	20	21	1	0.4095	0.4784	90	40
21	21	22	1	0.7089	0.9373	90	40
22	3	23	1	0.4512	0.3084	90	50
23	23	24	1	0.8980	0.7091	420	200
24	24	25	1	0.8959	0.7071	420	200
25	6	26	1	0.2031	0.1034	60	25

26	26	27	1	0.2842	0.1447	60	25
27	27	28	1	1.0589	0.9338	60	20
28	28	29	1	0.8043	0.7006	120	70
29	29	30	1	0.5074	0.2585	200	600
30	30	31	1	0.9745	0.9629	150	70
31	31	32	1	0.3105	0.3619	210	100
32	32	33	1	0.3411	0.5302	60	40

Table III: IEEE 69-bus line and load data

Line No.	**Start Node**	**End Node**	**Length (m)**	***R*/Length (Ω)**	***X*/Length (Ω)**	**P_L in end node (kW)**	**Q_L in end node (kVAR)**
1	1	2	1	0.0005	0.0012	0	0
2	2	3	1	0.0005	0.0012	0	0
3	3	4	1	0.0015	0.0036	0	0
4	4	5	1	0.0251	0.0294	0	0
5	5	6	1	0.366	0.1864	2.6	2.2
6	6	7	1	0.381	0.1941	40.4	30
7	7	8	1	0.0922	0.047	75	54
8	8	9	1	0.0493	0.0251	30	22
9	9	10	1	0.819	0.2707	28	19
10	10	11	1	0.1872	0.0619	145	104
11	11	12	1	0.7114	0.2351	145	104
12	12	13	1	1.03	0.34	8	5
13	13	14	1	1.044	0.345	8	5.5
14	14	15	1	1.058	0.3496	0	0
15	15	16	1	0.1966	0.065	45.5	30
16	16	17	1	0.3744	0.1238	60	35
17	17	18	1	0.0047	0.0016	60	35

18	2	19	1	0.3276	0.1083	0	0
19	19	20	1	0.2106	0.069	1	0.6
20	20	21	1	0.3416	0.1129	114	81
21	21	22	1	0.014	0.0046	5	3.5
22	3	23	1	0.1591	0.0526	0	0
23	23	24	1	0.3463	0.1145	28	20
24	24	25	1	0.7488	0.2475	0	0
25	25	26	1	0.3089	0.1021	14	10
26	26	27	1	0.1732	0.0572	14	10
27	3	28	1	0.0044	0.0108	26	18.6
28	28	29	1	0.064	0.1565	26	18.6
29	29	30	1	0.3978	0.1315	0	0
30	30	31	1	0.0702	0.0232	0	0
31	31	32	1	0.351	0.116	0	0
32	32	33	1	0.839	0.2816	14	10
33	33	34	1	1.708	0.5646	19.5	14
34	34	35	1	1.474	0.4873	6	4
35	3	36	1	0.0044	0.0108	26	18.55
36	36	37	1	0.064	0.1565	26	18.55
37	37	38	1	0.1053	0.123	0	0
38	38	39	1	0.0304	0.0355	24	17
39	39	40	1	0.0018	0.0021	24	17
40	40	41	1	0.7283	0.8509	1.2	1
41	41	42	1	0.31	0.3623	0	0
42	42	43	1	0.041	0.0478	6	4.3
43	43	44	1	0.0092	0.0116	0	0
44	44	45	1	0.1089	0.1373	39.22	26.3
45	45	46	1	0.0009	0.0012	39.22	26.3
46	4	47	1	0.0034	0.0084	0	0
47	47	48	1	0.0851	0.2083	79	56.4

48	48	49	1	0.2898	0.7091	384.7	274.5
49	49	50	1	0.0822	0.2011	384.7	274.5
50	8	51	1	0.0928	0.0473	40.5	28.3
51	51	52	1	0.3319	0.1114	3.6	2.7
52	9	53	1	0.174	0.0886	4.35	3.5
53	53	54	1	0.203	0.1034	26.4	19
54	54	55	1	0.2842	0.1447	24	17.2
55	55	56	1	0.2813	0.1433	0	0
56	56	57	1	1.59	0.5337	0	0
57	57	58	1	0.7837	0.263	0	0
58	58	59	1	0.3042	0.1006	100	72
59	59	60	1	0.3861	0.1172	0	0
60	60	61	1	0.5075	0.2585	1244	888
61	61	62	1	0.0974	0.0496	32	23
62	62	63	1	0.145	0.0738	0	0
63	63	64	1	0.7105	0.3619	227	162
64	64	65	1	1.041	0.5302	59	42
65	11	66	1	0.2012	0.0611	18	13
66	66	67	1	0.0047	0.0014	18	13
67	12	68	1	0.7394	0.2444	28	20
68	68	69	1	0.0047	0.0016	28	20

REFERENCES

Ahmad, A., Khan, Z. A., Saad Alam, M., and Khateeb, S. (2018). A review of the electric vehicle charging techniques, standards, progression, and evolution of EV technologies in Germany. *Smart Science*, 6(1), 36-53.

Alonso, M., Amaris, H., and Alvarez-Ortega, C. (2012). Integration of renewable energy sources in smart grids by means of evolutionary optimization algorithms. *Expert Systems with Applications*, 39(5), 5513-5522.

Al-Shetwi, A. Q., Hannan, M. A., Jern, K. P., Mansur, M., and Mahlia, T. M. I. (2020). Grid-connected renewable energy sources: Review of the recent integration requirements and control methods. *Journal of Cleaner Production*, 253, 119831.

Amin, A., Altinoz, B., and Dogan, E. (2020). Analyzing the determinants of carbon emissions from transportation in European countries: the role of renewable energy and urbanization. *Clean Technologies and Environmental Policy*, 22(8), 1725-1734.

Asadi, M. R., and Kouhsari, S. M. (2009, March). Optimal overcurrent relays coordination using particle-swarm-optimization algorithm. In *2009 IEEE/PES Power Systems Conference and Exposition* (pp. 1-7). IEEE.

Baran, M., and Wu, F. F. (1989). Optimal sizing of capacitors placed on a radial distribution system. *IEEE Transactions on Power Delivery*, 4(1), 735-743.

Berthold, F., Ravey, A., Blunier, B., Bouquain, D., Williamson, S., and Miraoui, A. (2015). Design and development of a smart control strategy for plug-in hybrid vehicles including vehicle-to-home functionality. *IEEE Transactions on Transportation Electrification*, 1(2), 168-177.

Celik, A. N. (2003). Techno-economic analysis of autonomous PV-wind hybrid energy systems using different sizing methods. *Energy Conversion and Management*, 44(12), 1951-1968.

Chakrabarti, A., Kothari, D. P., and De, A. (2010*). An introduction to reactive power control and voltage stability in power transmission systems*. PHI Learning Pvt. Ltd., New Delhi, 1st edition.

Cowell, R., Bristow, G., and Munday, M. (2011). Acceptance, acceptability, and environmental justice: the role of community benefits in wind energy development. *Journal of Environmental Planning and Management*, 54(4), 539-557.

Datta, A., Bhattacharya, G., Mukherjee, D., and Saha, H. (2014). An efficient technique for controlling power flow in a single stage grid-connected photovoltaic system. *Scientia Iranica*, 21(3), 885-897.

Datta, A., Bhattacharya, G., Mukherjee, D., and Saha, H. (2016). Modelling and simulation-based performance study of a transformer less single-stage grid-connected photovoltaic system in Indian ambient conditions. *International Journal of Ambient Energy*, 37(2), 172-183.

Deilami, S., Masoum, A. S., Moses, P. S., and Masoum, M. A. (2011). Real-time coordination of plug-in electric vehicle charging in smart grids to minimize power losses and improve voltage profile. *IEEE Transactions on Smart Grid*, 2(3), 456-467.

Di Giorgio, A., Liberati, F., and Canale, S. (2014). Electric vehicles charging control in a smart grid: A model predictive control approach. *Control Engineering Practice*, 22, 147-162.

Diaf, S., Diaf, D., Belhamel, M., Haddadi, M., and Louche, A. (2007). A methodology for optimal sizing of autonomous hybrid PV/wind system. *Energy Policy*, 35(11), 5708-5718.

Díaz, G., Gómez-Aleixandre, J., and Coto, J. (2015). Direct backward/forward sweep algorithm for solving load power flows in AC droop-regulated microgrids. *IEEE Transactions on Smart Grid*, 7(5), 2208-2217.

Du, J., Ouyang, M., and Chen, J. (2017). Prospects for Chinese electric vehicle technologies in 2016–2020: Ambition and rationality. *Energy*, 120, 584-596.

El-Fergany, A. (2015). Optimal allocation of multi-type distributed generators using backtracking search optimization algorithm. *International Journal of Electrical Power & Energy Systems*, 64, 1197-1205.

Faddel, S., Elsayed, A. T., and Mohammed, O. A. (2018). Bilayer multi-objective optimal allocation and sizing of electric vehicle parking garage. *IEEE Transactions on Industry Applications*, 54(3), 1992-2001.

Faisal, M., Hannan, M. A., Ker, P. J., Hussain, A., Mansor, M. B., and Blaabjerg, F. (2018). Review of energy storage system technologies in microgrid applications: Issues and challenges. *IEEE Access*, 6, 35143-35164.

Fathabadi, H. (2017). Novel solar powered electric vehicle charging station with the capability of vehicle-to-grid. *Solar Energy*, 142, 136-143.

Fattori, F., Anglani, N., and Muliere, G. (2014). Combining photovoltaic energy with electric vehicles, smart charging and vehicle-to-grid. *Solar Energy*, 110, 438-451.

García-Villalobos, J., Zamora, I., San Martín, J. I., Asensio, F. J., and Aperribay, V. (2014). Plug-in electric vehicles in electric distribution networks: A review of smart charging approaches. *Renewable and Sustainable Energy Reviews*, 38, 717-731.

Georgilakis, P. S., and Hatziargyriou, N. D. (2013). Optimal distributed generation placement in power distribution networks: models, methods, and future research. *IEEE Transactions on Power Systems*, 28(3), 3420-3428.

Ghanbari, N., Golzari, H., Mokhtari, H., and Poshtan, M. (2017, November). Optimum location for operation of small size distributed generators. In 2017 *IEEE 6th International Conference on Renewable Energy Research and Applications (ICRERA)* (pp. 300-303). IEEE.

Ghosh, S., and Sherpa, K. S. (2008). An efficient method for load− flow solution of radial distribution networks. *International Journal of Electrical and Computer Engineering*, 2(9), 2094-2101.

Gielen, D., Boshell, F., Saygin, D., Bazilian, M. D., Wagner, N., and Gorini, R. (2019). The role of renewable energy in the global energy transformation. *Energy Strategy Reviews*, 24, 38-50.

Goel, S., Sharma, R., and Rathore, A. K. (2021). A review on barrier and challenges of electric vehicle in India and vehicle to grid optimization. *Transportation Engineering*, 100057.

Goli, P., and Shireen, W. (2014). PV powered smart charging station for PHEVs. *Renewable Energy*, 66, 280-287.

Gong, D., Tang, M., Buchmeister, B., and Zhang, H. (2019). Solving location problem for electric vehicle charging Stations—A sharing charging model. *IEEE Access*, 7, 138391-138402.

Grainger, J. J., and Lee, S. H. (1982). Capacity release by shunt capacitor placement on distribution feeders: A new voltage-dependent model. *IEEE Transactions on Power Apparatus and Systems*, (5), 1236-1244.

Gupta, V., Konda, S. R., Kumar, R., and Panigrahi, B. K. (2020). Collaborative multi-aggregator electric vehicle charge scheduling with PV-assisted charging stations under variable solar profiles. *IET Smart Grid*, 3(3), 287-299.

He, T., Zhu, J., Zhang, J., and Zheng, L. (2018). An optimal charging/discharging strategy for smart electrical car parks. *Chinese Journal of Electrical Engineering*, 4(2), 28-35.

Ji, D., Lv, M., Yang, J., and Yi, W. (2020). Optimizing the locations and sizes of solar assisted electric vehicle charging stations in an urban area. *IEEE Access*, 8, 112772-112782.

Jian, L., Zhu, X., Shao, Z., Niu, S., and Chan, C. C. (2014). A scenario of vehicle-to-grid implementation and its double-layer optimal charging strategy for minimizing load variance within regional smart grids. *Energy Conversion and Management*, 78, 508-517.

Jiang, C., Jing, Z., Ji, T., and Wu, Q. (2018). Optimal location of PEVCSs using MAS and ER approach. *IET Generation, Transmission & Distribution*, 12(20), 4377-4387.

Kaabeche, A., Belhamel, M., and Ibtiouen, R. (2011). Techno-economic valuation and optimization of integrated photovoltaic/wind energy conversion system. *Solar Energy*, 85(10), 2407-2420.

Kang, J., Duncan, S. J., and Mavris, D. N. (2013). Real-time scheduling techniques for electric vehicle charging in support of frequency regulation. *Procedia Computer Science*, 16, 767-775.

Karfopoulos, E. L., and Hatziargyriou, N. D. (2012). A multi-agent system for controlled charging of a large population of electric vehicles. *IEEE Transactions on Power Systems*, 28(2), 1196-1204.

Karmaker, A. K., Ahmed, M. R., Hossain, M. A., and Sikder, M. M. (2018). Feasibility assessment & design of hybrid renewable energy based electric vehicle charging station in Bangladesh. *Sustainable Cities and Society*, 39, 189-202.

Katoch, S., Chauhan, S. S., and Kumar, V. (2020). A review on genetic algorithm: past, present, and future. *Multimedia Tools and Applications*, 1-36.

Kaushal, P. K., &Tomar, M. (2017, August). Real and reactive power loss minimization of IEEE-33 bus by optimal DG placement using LSO in RDS. In *2017 International Conference on Energy, Communication, Data Analytics and Soft Computing* (ICECDS) (pp. 1841-1844). IEEE.

Keskin, I., and Soykan, G. (2017, November). Reduction of peak power consumption by using photovoltaic panels in Turkey. In *2017 IEEE 6th International Conference on Renewable Energy Research and Applications (ICRERA)* (pp. 886-890). IEEE.

Khatod, D. K., Pant, V., and Sharma, J. (2012). Evolutionary programming based optimal placement of renewable distributed generators. *IEEE Transactions on Power Systems*, 28(2), 683-695.

Lam, A. Y., Leung, Y. W., and Chu, X. (2014). Electric vehicle charging station placement: Formulation, complexity, and solutions. *IEEE Transactions on Smart Grid*, 5(6), 2846-2856.

Leung, D. Y., and Yang, Y. (2012). Wind energy development and its environmental impact: A review. *Renewable and Sustainable Energy Reviews*, 16(1), 1031-1039.

Liu, H. C., Yang, M., Zhou, M., and Tian, G. (2018). An integrated multi-criteria decision-making approach to location planning of electric vehicle charging stations. *IEEE Transactions on Intelligent Transportation Systems*, 20(1), 362-373.

Liu, Z. F., Zhang, W., Ji, X., and Li, K. (2012, May). Optimal planning of charging station for electric vehicle based on particle swarm optimization. In *IEEE PES Innovative Smart Grid Technologies* (pp. 1-5). IEEE.

Luo, L., Wu, Z., Gu, W., Huang, H., Gao, S., and Han, J. (2020). Coordinated allocation of distributed generation resources and electric vehicle charging stations in distribution systems with vehicle-to-grid interaction. *Energy*, 192, 116631.

McCall, J. (2005). Genetic algorithms for modelling and optimization. *Journal of Computational and Applied Mathematics*, 184(1), 205-222.

Mehrjerdi, H. (2020). Dynamic and multi-stage capacity expansion planning in microgrid integrated with electric vehicle charging station. *Journal of Energy Storage*, 29, 101351.

Mirjalili, S. (2019). Genetic algorithm. *In Evolutionary algorithms and neural networks* (pp. 43-55). Springer, Cham.

Mishra, S., Verma, S., Chowdhury, S., Gaur, A., Mohapatra, S., Dwivedi, G., and Verma, P. (2021). A comprehensive review on developments in electric vehicle charging station infrastructure and present scenario of India. *Sustainability*, 13(4), 2396.

Moghaddam, Z., Ahmad, I., Habibi, D., and Phung, Q. V. (2017). Smart charging strategy for electric vehicle charging stations. *IEEE Transactions on Transportation Electrification*, 4(1), 76-88.

Mohtasham, J. (2015). Renewable energies. *Energy Procedia*, 74, 1289-1297.

Moradi, M. H., Abedini, M., Tousi, S. R., and Hosseinian, S. M. (2015). Optimal siting and sizing of renewable energy sources and charging stations simultaneously based on differential evolution algorithm. *International Journal of Electrical Power & Energy Systems*, 73, 1015-1024.

Motyka, D., Kajanova, M., and Bracinik, P. (2018, October). The Impact of Embedded Generation on Distribution Grid Operation. In *2018 7th International Conference on Renewable Energy Research and Applications (ICRERA)* (pp. 360-364). IEEE.

Mozafar, M. R., Moradi, M. H., and Amini, M. H. (2017). A simultaneous approach for optimal allocation of renewable energy sources and electric vehicle charging stations in smart grids based on improved GA-PSO algorithm. *Sustainable Cities and Society*, 32, 627-637.

Mumtaz, S., Ali, S., Ahmad, S., Khan, L., Hassan, S. Z., and Kamal, T. (2017). Energy management and control of plug-in hybrid electric vehicle charging stations in a grid-connected hybrid power system. *Energies*, 10(11), 1923.

Muñoz-Aguilar, R. S., Candela, I., Rocabert, J., and Rodríguez, P. (2017, November). Grid resonance attenuation in long lines by using renewable energy sources. In 2017 IEEE 6th International Conference on Renewable Energy Research and Applications (ICRERA) (pp. 429-434). IEEE.

Narang, N., Sharma, E., and Dhillon, J. S. (2017). Combined heat and power economic dispatch using integrated civilized swarm optimization and Powell's pattern search method. *Applied Soft Computing*, 52, 190-202.

Nezamabadi-pour, H., Rostami-Shahrbabaki, M., and Maghfoori-Farsangi, M. (2008). Binary particle swarm optimization: challenges and new solutions. *CSI Journal of Computer Science and Engineering*, 6(1), 21-32.

Nguyen, H. K., and Song, J. B. (2012). Optimal charging and discharging for multiple PHEVs with demand side management in vehicle-to-building. *Journal of Communications and Networks*, 14(6), 662-671.

Oliveira, D. Q., De Souza, A. Z., and Delboni, L. F. N. (2013). Optimal plug-in hybrid electric vehicles recharge in distribution power systems. *Electric Power Systems Research*, 98, 77-85.

Pal, A., Bhattacharya, A., and Chakraborty, A. K. (2021). Allocation of electric vehicle charging station considering uncertainties. *Sustainable Energy, Grids and Networks*, 25, 100422.

Ponnam, V. K. B., and Swarnasri, K. (2020). Multi-objective optimal allocation of electric vehicle charging stations and distributed generators in radial distribution systems using metaheuristic optimization algorithms. *Engineering, Technology & Applied Science Research*, 10(3), 5837-5844.

Popović, D. H., Greatbanks, J. A., Begović, M., and Pregelj, A. (2005). Placement of distributed generators and reclosers for distribution network security and reliability. *International Journal of Electrical Power & Energy Systems*, 27(5-6), 398-408.

Qian, Y., Wang, C., Wang, H., and Wang, Z. (2007, August). The optimization design of urban traffic signal control based on three swarm's cooperative-particle swarm optimization. In *2007 IEEE International Conference on Automation and Logistics* (pp. 512-515). IEEE.

Qu, B., Li, C., Liang, J., Yan, L., Yu, K., and Zhu, Y. (2020). A self-organized speciation based multi-objective particle swarm optimizer for multimodal multi-objective problems. *Applied Soft Computing*, 86, 105886.

Ren, G., Ma, G., and Cong, N. (2015). Review of electrical energy storage system for vehicular applications. *Renewable and Sustainable Energy Reviews*, 41, 225-236.

Rodrigues, Y. R., de Souza, A. Z., and Ribeiro, P. F. (2018). An inclusive methodology for Plug-in electrical vehicle operation with G2V and V2G in smart microgrid environments. *International Journal of Electrical Power & Energy Systems*, 102, 312-323.

Roy, P., and Das, P. K. (2013). Reactive power sensitivity index-based voltage stability analysis to a real system (400 kV system of WBSEB). *International Journal of Electronics & Communication Technology*, 4 (Spl-1), 167-169.

Sadeghi-Barzani, P., Rajabi-Ghahnavieh, A., and Kazemi-Karegar, H. (2014). Optimal fast charging station placing and sizing. *Applied Energy*, 125, 289-299.

Sanjay, R., Jayabarathi, T., Raghunathan, T., Ramesh, V., and Mithulananthan, N. (2017). Optimal allocation of distributed generation using hybrid grey wolf optimizer. *IEEE Access*, 5, 14807-14818.

Savić, A., and Đurišić, Ž. (2014). Optimal sizing and location of SVC devices for improvement of voltage profile in distribution network with dispersed photovoltaic and wind power plants. *Applied Energy*, 134, 114-124.

Shirmohammadi, D., Hong, H. W., Semlyen, A., and Luo, G. X. (1988). A compensation-based power flow method for weakly meshed distribution and transmission networks. *IEEE Transactions on Power Systems*, 3(2), 753-762.

Singh, M., Kumar, P., and Kar, I. (2013). A multi charging station for electric vehicles and its utilization for load management and the grid support. *IEEE Transactions on Smart Grid*, 4(2), 1026-1037.

Singh, R. K., and Goswami, S. K. (2011). Multi-objective optimization of distributed generation planning using impact indices and trade-off technique. *Electric Power Components and Systems*, 39(11), 1175-1190.

Soares, F. J., Almeida, P. R., and Lopes, J. P. (2014). Quasi-real-time management of Electric Vehicles charging. *Electric Power Systems Research*, 108, 293-303.

Soltech 1STH-215-P PV Datasheet (S1PVD). (2021). http://www.solarhub.com/product-catalog/pv-modules/5623-1STH-215-P-1Soltech (Accessed January 2021)

Sortomme, E., and El-Sharkawi, M. A. (2010). Optimal charging strategies for unidirectional vehicle-to-grid. *IEEE Transactions on Smart Grid*, 2(1), 131-138.

Sortomme, E., Hindi, M. M., MacPherson, S. J., and Venkata, S. S. (2010). Coordinated charging of plug-in hybrid electric vehicles to minimize distribution system losses. *IEEE Transactions on Smart Grid*, 2(1), 198-205.

Sousa, T. J., Monteiro, V., Fernandes, J. A., Couto, C., Meléndez, A. A. N., & Afonso, J. L. (2018, October). New perspectives for vehicle-to-vehicle (V2V) power transfer. In IECON 2018-44th Annual Conference of the IEEE Industrial Electronics Society (pp. 5183-5188). IEEE.

Srivastava, S. P., & Srivastava, S. P. (2013). Solar energy and its future role in Indian economy. *International Journal of Environmental Science: Development and Monitoring*, 4(3), 81-88.

Strzalka, A., Alam, N., Duminil, E., Coors, V., and Eicker, U. (2012). Large scale integration of photovoltaics in cities. *Applied Energy*, 93, 413-421.

Su, S. Y., Lu, C. N., Chang, R. F., and Gutierrez-Alcaraz, G. (2011). Distributed generation interconnection planning: A wind power case study. *IEEE Transactions on Smart Grid*, 2(1), 181-189.

Sudabattula, S. K., and Kowsalya, M. (2016). Optimal allocation of solar based distributed generators in distribution system using Bat algorithm. *Perspectives in Science*, 8, 270-272.

Tan, J., and Wang, L. (2015). Real-time charging navigation of electric vehicles to fast charging stations: A hierarchical game approach. *IEEE Transactions on Smart Grid*, 8(2), 846-856.

Teng, J. H., and Chang, C. Y. (2007). Backward/forward sweep-based harmonic analysis method for distribution systems. *IEEE Transactions on Power Delivery*, 22(3), 1665-1672.

Vagropoulos, S. I., Kyriazidis, D. K., and Bakirtzis, A. G. (2015). Real-time charging management framework for electric vehicle aggregators in a market environment. *IEEE Transactions on Smart Grid*, 7(2), 948-957.

Valentine, K., Temple, W. G., and Zhang, K. M. (2011). Intelligent electric vehicle charging: Rethinking the valley-fill. *Journal of Power Sources*, 196(24), 10717-10726.

Van Der Kam, M., and van Sark, W. (2015). Smart charging of electric vehicles with photovoltaic power and vehicle-to-grid technology in a microgrid; A case study. *Applied Energy*, 152, 20-30.

Vaya, M. G., and Andersson, G. (2012, July). Centralized and decentralized approaches to smart charging of plug-in vehicles. In *2012 IEEE power and energy society general meeting* (pp. 1-8). IEEE.

Vidhi, R., and Shrivastava, P. (2018). A review of electric vehicle lifecycle emissions and policy recommendations to increase EV penetration in India. *Energies*, 11(3), 483.

Viral, R., & Khatod, D. K. (2012). Optimal planning of distributed generation systems in distribution system: A review. *Renewable and Sustainable Energy Reviews*, 16(7), 5146-5165.

Wang, S., Dong, Z. Y., Luo, F., Meng, K., and Zhang, Y. (2017). Stochastic collaborative planning of electric vehicle charging stations and power distribution system. *IEEE Transactions on Industrial Informatics*, 14(1), 321-331.

Wang, Y., Wang, X., Shao, C., and Gong, N. (2020). Distributed energy trading for an integrated energy system and electric vehicle charging stations: A nash bargaining game approach. *Renewable Energy*, 155, 513-530.

Wirasingha, S. G., Schofield, N., and Emadi, A. (2008, September). Plug-in hybrid electric vehicle developments in the US: Trends, barriers, and economic feasibility. In *2008 IEEE vehicle power and propulsion conference* (pp. 1-8). IEEE.

Wu, D., Aliprantis, D. C., and Ying, L. (2011). Load scheduling and dispatch for aggregators of plug-in electric vehicles. *IEEE Transactions on Smart Grid*, 3(1), 368-376.

Xiong, Y., Gan, J., An, B., Miao, C., and Bazzan, A. L. (2017). Optimal electric vehicle fast charging station placement based on game theoretical framework. *IEEE Transactions on Intelligent Transportation Systems*, 19(8), 2493-2504.

Xu, X., Yao, L., Zeng, P., Liu, Y., and Cai, T. (2015). Architecture and performance analysis of a smart battery charging and swapping operation service network for electric vehicles in China. *Journal of Modern Power Systems and Clean Energy*, 3(2), 259-268.

Yang, G., Zhou, F., Ma, Y., Yu, Z., Zhang, Y., and He, J. (2017). Identifying lightning channel-base current function parameters by powell particle swarm optimization method. *IEEE Transactions on Electromagnetic Compatibility*, 60(1), 182-187.

Yang, H., Lu, L., and Zhou, W. (2007). A novel optimization sizing model for hybrid solar-wind power generation system. *Solar energy*, 81(1), 76-84.

Yang, X. S. (2020). *Nature-inspired optimization algorithms*. Academic Press.

Yao, W., Zhao, J., Wen, F., Dong, Z., Xue, Y., Xu, Y., and Meng, K. (2014). A multi-objective collaborative planning strategy for integrated power distribution and electric vehicle charging systems. *IEEE Transactions on Power Systems*, 29(4), 1811-1821.

Yazdi, L., Ahadi, R., and Rezaee, B. (2019, January). Optimal electric vehicle charging station placing with integration of renewable energy. In *2019 15th Iran International Industrial Engineering Conference (IIIEC)* (pp. 47-51). IEEE.

Zakariazadeh, A., Jadid, S., and Siano, P. (2014). Multi-objective scheduling of electric vehicles in smart distribution system. *Energy Conversion and Management*, 79, 43-53.

Zhang, C., Wei, Y. L., Cao, P. F., and Lin, M. C. (2018). Energy storage system: Current studies on batteries and power condition system. *Renewable and Sustainable Energy Reviews*, 82, 3091-3106.

Zhang, K., Mao, Y., Leng, S., He, Y., Maharjan, S., Gjessing, S., Zhang, Y. and Tsang, D. H. (2018). Optimal charging schemes for electric vehicles in smart grid: A contract theoretic approach. *IEEE Transactions on Intelligent Transportation Systems*, 19(9), 3046-3058.

Zhao, H., and Li, N. (2016). Optimal siting of charging stations for electric vehicles based on fuzzy Delphi and hybrid multi-criteria decision-making approaches from an extended sustainability perspective. *Energies*, 9(4), 270.

Zhou, J., Wu, Y., Wu, C., He, F., Zhang, B., and Liu, F. (2020). A geographical information system based multi-criteria decision-making approach for location analysis and evaluation of urban photovoltaic charging station: A case study in Beijing. *Energy Conversion and Management*, 205, 112340.

Zhou, W., Lou, C., Li, Z., Lu, L., and Yang, H. (2010). Current status of research on optimum sizing of stand-alone hybrid solar–wind power generation systems. *Applied Energy*, 87(2), 380-389.

Brief Biodata of the Candidate

1. **Name:** DEBAPARNA SENGUPTA

2. **Father's Name:** Late Sri Debabrata Sengupta

3. **Mother's Name:** Late Smt. Aparna Deb (Sengupta)

4. **Address:** Saptarshi Appt., Flat 2, 2 Green Row, Ganguly bagan, Kolkata-700084

5. **Designation:** Assistant Professor, Techno International New Town

6. **Date of Birth:** 20/08/1978

7. **Educational qualification:**

Degree	Year	University/ Board	Division	Subjects taken
Madhyamik (10^{th}) exam	1995	T.B.S. E	First	Science, Mathematics, Geography, History, Bengali, English, Additional Mathematics.
HS (+2) Exam	1997	T.B.S. E	First	Physics, Mathematics, Chemistry, Biology, English, Bengali.
B.E in Electrical Engineering	2001	Tripura University	First, Ranked First in Electrical Engineering	Electrical Machine, Power Electronics, Power System, Control System, Circuit Theory, Measurement, Basic

				Electrical, Analog & Digital Electronics, Field Theory etc.
M.E in Electrical Engineering	2007	Jadavpur University	First	Control System Specialization in Electrical Engineering

8. **Teaching Experience:** 13 Years (Under Techno Group, working as an Assistant Professor**)**

9. **Research Experience:** 6.5 years (3 years self-research + 3.5 years Ph.D. related)

10. **Area of research interest:** Effective allocation of electric vehicle charging stations and power management in a distribution network, Control System, Power System, Power Electronics.

11. **Publication related to Ph.D.:** Journal Papers-3
Conference Papers- 3

12. **Other Publications:** Conference Papers -6

13. **Conferences (other than Ph.D. related)/ workshops/ FDPs/ courses attended:** 28

The information provided above is true to the best of my knowledge and belief.

(Signature)

List of Research Publications

Journal Publications:

1. Sengupta, D., and Datta, A. (2021). Validation of optimal electric vehicle charging station allotment on IEEE 15-bus system. *Electrical Engineering & Electromechanics,* (3), 68-73, ISSN 2074-272X (Print), ISSN 2309-3404 (Online), https://doi.org/10.20998/2074-272X.2021.3.11

2. Sengupta, D., and Datta, A. (2021). Voltage profile improvement in power distribution network: effective deployment of solar powered electric vehicle charging stations, *International Journal of Electrical Engineering and Technology (IJEET)*, 12(3), 6-16. ISSN Print: 0976-6545, ISSN Online: 0976-6553. https://scopedatabase.com/Entry/both/13628

3. Sengupta, D., and Datta, A. (2021). Renewable Energy Supported Bi-directional Electric-Vehicle Charging Station Allocation in Distribution Network using INBPSO Technique. *International Journal of Renewable Energy Research* (IJRER), 11(2), 750-761. Online ISSN: 1309-0127. https://www.ijrer.org/ijrer/index.php/ijrer/article/view/11978

4. Sengupta, D., and Datta, A. (2022). Voltage Profile Improvement by Solar PV Powered EVCS Integration with the Distribution Network– A Power Management Study on IEEE 15-Bus System. *Journal of Electrical Engineering and Technology*, (Communicated).

Conferences Presented:

1. Sengupta, D., and Datta, A. (2021). Backward Forward Sweep Method for Distributed Generation Unit Integration with Radial Distribution Network. In *International conference on new scientific creations in engineering and technology (ICNSCET21).* Paper ID: ICNSCET21-09. http://www.ijsred.com/icnscet21-part1.html

2. Sengupta, D., and Datta, A. (2021). An Efficient, Fast and Versatile Power Flow Analysis Method for Radial Distribution Network. In *International conference on new scientific creations in engineering and technology (ICNSCET21).* Paper ID: ICNSCET21-11. http://www.ijsred.com/icnscet21-part1.html

3. Sengupta, D., Sinha, V., Kumari, I., and Datta, A. (2021). Renewable Energy Based Electric Vehicle Charging Station for Greenhouse Gas Emission Reduction. In *First virtual international conference on green energy and smart technologies in engineering (GEST 2021).*

Other Publications:

1. Kumar, R., Anand P., Sengupta, D. and Datta M. (In press. Pub. Month: February 2022) Agro Nutrition Alert (ANA). In *Advances in Data Science and Computing Technology*, Methodology and Applications. Apple academic Press. URL: https://www.appleacademicpress.com/advances-in-data-science-and-computing-technology-methodology-and-applications/9781774639979

2. Singh, R.K., Prasad, Rahul Singh, R.K., Ashish, A., Sengupta, D., Sarker, R., and Datta, M. (In press. Pub. Month: February 2022) A Classy Fuzzy MPPT Controller for Standalone PV System. In *Advances in Data Science and Computing Technology, Methodology and Applications*. Apple academic Press. URL: https://www.appleacademicpress.com/advances-in-data-science-and-computing-technology-methodology-and-applications/9781774639979

3. Sarker, R., Sengupta, D., and Datta, A. (2021). PWM Control Technique for Switched Reluctance Generator in Variable Speed Applications. In *Recent Advances in Power Electronics and Drives* (pp. 339-350). Springer, Singapore.

4. Sarker, R., Sengupta, D., Bhattacharya, S. K., and Datta, A. (2018). An Implicit Approach to Minimize the Reactive Power of a 765 kV Interconnected Bus System in India. In *Advances in Communication, Devices and Networking* (pp. 151-157). Springer, Singapore.

5. Das, A., Samanta, S., Alam, S., Kumar, S., Sengupta, D., Bose, R., and Chatterjee, S. (2017, August). Recognition of power system transients based on higher order statistical moments using empirical mode decomposition. In *2017 IEEE International Conference on Smart Technologies and Management for Computing, Communication, Controls, Energy and Materials (ICSTM)* (pp. 12-17). IEEE.

6. Das, S., Ganguly, S., Ghosh, S., Sarker, R., & Sengupta, D. (2016, October). A bluetooth based sophisticated home automation system using smartphone. In *2016 International Conference on Intelligent Control Power and Instrumentation (ICICPI)* (pp. 236-240). IEEE.

Conferences/ Workshops/ FDPs/ Courses Attended:

1. Completed one week FDP on Energy Engineering organized by 'Mizoram University' form 23rd - 27th August 2021.
2. Completed a short course on "Learn to Design Your Own Solar Home System" on 17th August 2020 organized by the 'Energy Swaraj Foundation in association' with 'Mizoram University' as a part of Energy Literacy Drive.
3. Completed 5 Days e-FDP on "Enhancement of New Learning Tools In Management Education Through Case Studies" organized by 'Department of Business and Management studies', Meerut Institute of Engineering and Technology. 8th August to 10th August 2020.
4. Short Term Training Program through ICT Mode on "Fundamental and Applications of Nanomaterials" organized by 'NITTTR' from 27th July 2020 to 31st July 2020 [duration: 1 Week]
5. Completed an AICTE sponsored STTP on "Human Values, Ethics, Moral, Behavioral Sciences and Attitudes" organized by 'Sagar Institute of Research and Technology Pharmacy', Bhopal from 20th July 2020 to 25th July,2020.
6. Completed Coursera course on "Introduction to Data Analytics for Business" by 'University of Colorado' on 21stJuly 2020
7. Completed 5 Days International FDP on "Emerging Trends in Sensors, Security and Smart Automation Systems (ETSSSAS 2020)" organized by 'University of Colorado', from 8thto 12th July 2020.

8. Completed the Workshop on “Best Practices for Teaching Online” organized by ‘Surendranath College for Woman in association with ABP Education’, 4th July,2020.
9. Completed Coursera course on “Welcome to Game Theory” organized by ‘The University of Tokyo’ on 26th June 2020.
10. Participated in 5 days workshop on “Machine Learning and R “organized by ‘Department of Information Technology, Techno International New Town’, from 15th July 2019 to 19th July 2019.
11. Participated in 10 days FDP on “Dissemination Methodology in ES-EE 101” Organized by ‘EE Department, Netaji Subhash Engineering College’, from 3rd July 2019 to 12th July 2019.
12. Participated in 5 days FDP in “Advanced Control Systems and Power Electronics (ACSPI 2k19)" organized by ‘EE Department, TINT’, held on 4th to 8th February 2019.
13. Completed 12 weeks’ online course in “Electromagnetic Theory”, from January to April 2018, from NPTEL organized by ‘IIT Kanpur’ and achieved “ELITE” category.
14. Participated in one day Faculty Development Program on “Cyber Security" held on 29th January 2018 organized by ‘MSIT, Kolkata’.
15. Participated in One day seminar on "Smart Grid in smart City" held on 12th November 2017, organized by ‘TICT, Kolkata’.
16. Participated in two weeks’ ISTE STTP on "Electric Power System" organized by ‘IIT, Kharagpur’ from 12thJune 2017 to 15thJuly 2017.
17. Participated in one day seminar on “Application of Soft Computing Techniques in Control System Application” organized by ‘Department of Electrical Engineering, TICT, Rajarhat’ on 22nd December 2016.
18. Participated in one day seminar on “Application of Soft Computing Techniques in Power System Optimization” organized by ‘Department of Electrical Engineering, TICT, Rajarhat’ on 21st December 2016.
19. Participated in 2016 International Conference on “Intelligent Control, Power and Instrumentation (ICICPI)” organized by ‘Department of EE and AEIE (jointly), RCC Institute of Information Technology, Beliaghata’ on 21st to 23rd October 2016.

20. Participated in "5 Day's Workshop on MATLAB, Simulink and LATEX" organized by 'Department of Information Technology, TICT, Rajarhat' from 25th to 29th January 2016.
21. Participated and successfully completed the "AICTE Approved Four-week Faculty Development Program (FDP) on Use of ICT in Education for Online and Blended Learning" organized by 'Indian Institute of Technology, Bombay' from 2nd May 2016 to 10th July 2016.
22. Participated and successfully completed the "Basic Pedagogy Training: Objective and Outcome Based Education System- Transforming Engineering Education to Match Global Needs" organized by 'EQUATE, New Delhi' from 30th November 2015 to 4th December 2015.
23. Participated in "One-week FDP on Electrical Engineering" organized by 'Department of Electrical Engineering, NSEC, Garia' from 7th to 13th January 2015.
24. Participated in a workshop on "Electrical Machines and Design" in 'CIEM' in 2014.
25. Completed a short-term course on "**Programmable Logic Controllers**" from '**College of Lake County', Illinois, USA in 2012 and achieved highest grade on that.**
26. Participated in Short Term/In-house Training Program on "Analysis of Nonlinear Control Systems" organized by 'National Institute of Technical Teachers' Training and Research, Kolkata', (Established by Ministry of HRD, Govt. of India) from 4th January 2010 to 8th January 2010.
27. Participated in AICTE sponsored Short Term Course on "Electric Power—Quality and Control" organized by 'Department of Applied Electronics & Instrumentation Engineering and Department of Electrical Engineering, Netaji Subhash Engineering College, Techno city, Garia, Kolkata' from 12th February 2010 to 25th February 2010
28. Attended a workshop on "Teaching Methodologies" conducted by 'US consolidate, The American Centre' in collaboration with 'Techno India College of Technology' in 2008.

Other Academic Credentials:

1. M.E Project named "Survey on Handoff Mechanisms in Wireless Cellular Networks", under the guidance of Dr. Madhubanti Maitra and Prof. Samar Bhattacharya, Jadavpur University, Kolkata, India in June 2007.The project work aimed at the introduction of 1G, 2G, 3G and 4G wireless communication systems and a survey/study on the handoff mechanisms used in these systems.
2. "Certificate course in Programming with C and C++" from CMC Ltd in the year 2001.
3. Final year B.E project on "Speed Control of DC Servomotor using Microprocessor" under the Guidance of Prof. Arup Das Choudhury, Tripura Engineering College (Presently known as NIT, Tripura) in the year 2001. The aim of the project was to interface all the hardware components like servo motor, microprocessor etc. to design the whole plant and to control the speed of the servomotor by 8085 microprocessor using Assembly Language.
4. Vocational training at Salt Lake 132/33 KV Transmission Distribution Substation under West Bengal State Electricity Board (W.B.S.E.B), Kolkata in the year 2000.
5. Software exposure to tools like MS Word, MS Excel, MS Power point and languages like C, C++.

Other Achievements:

1. Reviewer of a Book on "Electromagnetic Field Theory" published by 'Tata McGraw-Hill Publications'.
2. Worked as Examiner/ Evaluator of B. Tech examination conducted by 'MAKAUT (formerly known as West Bengal University of Technology' several times.

PARTICULARS OF THE CANDIDATE

NAME OF THE CANDIDATE: DEBAPARNA SENGUPTA
DEGREE: DOCTOR OF PHYLOSOPHY (Ph.D.)

DEPARTMENT: Electrical Engineering

TITLE OF THESIS: Effective Allocation of Electric Vehicle Charging Stations and Power Management in a Distribution Network

DATE OF ADMISSION: 08/08/2018

APPROVAL OF RESEARCH PROPOSAL:

1. DRC: 04/04/2019

2. BOS: 25/04/2019

3. SCHOOL BOARD: 30/04/2019

MZU REGISTRATION NO: 1800055

Ph.D. REGISTRATION NO. & DATE: MZU/Ph.D./1294 of 08.08.2018

EXTENTION (IF ANY): N/A

Head

Department of Electrical Engineering

Mizoram University

ABSTRACT

EFFECTIVE ALLOCATION OF ELECTRIC VEHICLE CHARGING STATIONS AND POWER MANAGEMENT IN A DISTRIBUTION NETWORK

A THESIS SUBMITTED IN PARTIAL FULFILLMENT OF THE REQUIREMENTS FOR THE DEGREE OF DOCTOR OF PHILOSOPHY

DEBAPARNA SENGUPTA
MZU REGN. NO. 1800055
PH.D. REGN. NO. MZU/PH.D./1294 OF 08.08.2018

DEPARTMENT OF ELECTRICAL ENGINEERING
SCHOOL OF ENGINEERING AND TECHNOLOGY
FEBRUARY 2022

EFFECTIVE ALLOCATION OF ELECTRIC VEHICLE CHARGING STATIONS AND POWER MANAGEMENT IN A DISTRIBUTION NETWORK

DEBAPARNA SENGUPTA
Department of Electrical Engineering

Supervisor: Prof. Asim Datta

Submitted

In partial fulfillment of the requirement of the Degree of Doctor of Philosophy in Electrical Engineering of Mizoram University, Aizawl

Abstract:

Due to the rapid depletion, price inflation and detrimental environmental effects of conventional energy reserves, the development of efficient renewable energy harnessing techniques is one of the most important considerations of recent energy policies of developed and developing countries. The power generation and transportation sectors are rapidly evolving with the development of renewable energy resources (RERs). With the proliferation of electric vehicles (EVs) and their increased charging needs, researchers have proposed to integrate electric vehicle charging stations (EVCSs) into the power distribution networks. However, the active integration of EVCSs with the power distribution networks is a delicate matter. If this is not done wisely, the voltage profile of the network may degrade with the increase in system losses. Consequently, the overall performance of the integrated network may be degraded. Moreover, integration of the EVCSs at inappropriate buses may lead to the system instability. Thus, appropriate allocation of EVCSs in an existing power distribution network is a matter of pronounced significance. The research work aims to achieve certain goals in this domain. The work is mainly conducted in two phases.

In the first phase of the research work, allocation of EVCSs in power distribution network is considered as optimization problem. Two objective functions are articulated. The first objective function aims to maintain the distribution network voltage profile, whereas the second one is for minimization of node voltage errors along with the total line loss. Four case studies are carried out. In *Case Study* 1, particle swarm optimization (PSO) collaborated with an efficient power flow analysis technique is applied for optimum EVCS allocation in the IEEE 15-bus radial distribution network with the intention of optimum power flow and voltage profile analysis. The EVCSs are considered as load points (taking power from the distributed network). *Case Study* 2 employs an upgraded version of PSO technique named Powell's PSO (PPSO) collaborated with the backward forward sweep method (BFSM). The optimum allocation of solar photovoltaic powered EVCSs (SPV-EVCSs) in the IEEE 69-bus distribution network is accomplished considering power injection mode (injecting power into the distribution network).

The effect of optimally placed EVCSs on the network profile under load point mode is investigated. In *Case Study* 3, optimum allocation of bi-directional renewable energy powered EVCSs (RE-EVCSs) is carried out to upgrade voltage profile and reduce the total line loss in power injection mode of operation. An improved new binary particle swarm optimization (INBPSO) method collaborated with BFSM is utilized for selecting the optimum locations of the optimal number of EVCSs possessing optimal sizes. The IEEE 15-bus system is chosen as a test bed system to substantiate the effectiveness of the anticipated technique. In *Case Study* 4, optimum allocation of RE-EVCSs in the IEEE 33-bus system is done using genetic algorithm (GA) collaborated with BFSM. The RE-EVCSs are considered in power injection mode. The results of all case studies are presented. The results signify that the strategic integration of EVCSs into the power distribution network improves the system voltage profile while minimizing the system line loss. However, the EVCSs operating in load point mode in an integrated system, may degrade the voltage profile. Thus, to maintain the voltage profile and power loss within the allowable limits, both the EVCS capacity and location selection are performed optimally. The voltage sensitivity analysis and loss sensitivity analysis are also performed in different case studies. The reason behind the sensitivity analysis is to verify the power injection/extraction suitability of network nodes.

The second phase of the work is accomplished in two fragments. In first fragment, a simulation model of a multiple SPV-EVCS integrated distribution network is developed, and power flow management study is conducted disregarding the ESU and EV changing. In the second fragment of the work, the power flow management study is comprehended by introducing the ESU and EV charging. The voltages, currents, and powers at different points of the integrated network are examined and the results are found showing power flow between EVCSs and power distribution network acceptably.

All investigated results in connection with the optimum allocation of EVCSs and power flow management are presented. From the entire work, it can be concluded that an effective allocation of RE-EVCSs into power distribution

network can manage power transfer coordinately. It avoids the peak loading support and high-capacity battery back-up.